

*Department of Civil and
Environmental Engineering,
University College Cork.*



***An Investigation of Flood Forecasting using a
Physically-Based Rainfall-Runoff Model***

By

Emmanuel Steinmann

*A Thesis submitted for the
Degree of Master of Engineering Science*

October 2005

To My Parents

Acknowledgements

The author wishes to express his thanks to the following people:

Prof. Ger Kiely, my supervisor, for his guidance and his encouragement.

Prof. J.P.J. O’Kane, for the use of the facilities of the Department of Civil and Environmental Engineering, U.C.C.

Dr. Micheal Creed, for his warm welcoming and administrative support.

Cecile Delolme, for help and encouragement to come to Ireland.

Dara Entekhabi, for his help in the provision of tRIBS.

Enrique Vivoni, for his helpful advices on tRIBS.

Kieran Commins of Met Eireann for his help on radar data.

Helen Bradley of the Department of Geography for her support on GIS.

The Environmental Protection Agency

The Office of Public Work

The Staff of Cork County Council in Mallow

Paul Leahy, for his patience and his grateful help throughout the year.

Gearoid Corcoran, for his help and previous work on flooding of the Blackwater River.

Matteo Sottocornola, for his friendship and support throughout the year.

Marie Berthier, Anna Laine, Delphine Lawton, Vesna Jaksic, Ken Byrne, Viacheslav Voronovich, Adrian Birkby, Jean-Baptiste Gobert, Julien Gillet, Paul Guero and Javier Ordoñez Muñoz for their help and their friendship.

Abstract

The town of Mallow on the river Blackwater experiences flooding on an annual basis leading to traffic disturbances and sometimes severe economic losses. A web-based flood warning system monitors the river in real-time at different stations upstream of Mallow and sends out warnings when predefined thresholds are broken.

Adding a flood forecasting model to this warning system would be of great benefit for the local community as it would provide more time to respond to the flood event.

This project applied a physically-based fully-distributed rainfall runoff model developed in the Ralph Parson Laboratory at the Massachusetts Institute of Technology (MIT), the TIN-based Real-time Integrated Basin Simulator (tRIBS), to assess its potential as a flood forecasting model. tRIBS takes advantage of the new developments in rainfall measurements by using radar rainfall data, and simulates the hydrologic processes taking place in the catchment given the inputs of the topography, the soil and land use characteristics.

GIS and hydrometeorological data were collected and transformed to create the model inputs. The model was calibrated and then tested on 5 flood events between January 2002 and January 2005. The results showed that the present calibrated model could have predicted accurately 1 out of the 5 flood events, underestimating the 4 others so that 2 of them would have been missed by the warning system. Issues were raised about the calibration parameters and the measurements of rainfall and streamflow discharges. The model is promising and could lead to better predictions with further work on the input characteristics.

Table of Contents

Acknowledgements	iii
Abstract	iv
Table of Contents	v
Chapter 1 Introduction	1
<i>1.1 Introduction</i>	2
<i>1.2 Flooding of the Munster Blackwater</i>	3
1.2.1 History of flooding	3
1.2.2 Flood warning system.....	4
<i>1.3 Previous work</i>	4
<i>1.4 Objectives</i>	5
<i>1.5 Layout of the thesis</i>	5
Chapter 2 Literature Review	6
<i>2.1 The modelling of the rainfall-runoff process</i>	7
<i>2.2 Different types of models</i>	7
2.2.1 Metric models.....	8
2.2.2 Metric models.....	8
2.2.3 Mechanistic models.....	9
<i>2.3 The current state of the art</i>	10
Chapter 3 Methods: tRIBS Model	11
<i>3.1 Model overview</i>	12
3.1.1 Modelling approach.....	12
3.1.2 Topographic representation	14
3.1.3 Computational element.....	15
<i>3.2 The hydrologic modelling approach</i>	17
3.2.1 Rainfall interception	17
3.2.2 Energy balance and surface fluxes	17
3.2.2.1 Short and longwave radiation.....	18
3.2.2.2 Latent heat flux	18

3.2.2.3	Sensible heat flux	19
3.2.2.4	Ground heat flux	19
3.2.3	Evapotranspiration.....	19
3.2.4	Infiltration scheme.....	21
3.2.4.1	Basic assumptions	21
3.2.4.2	Ponded infiltration.....	23
3.2.4.3	Infiltration under unsaturated conditions.....	24
3.2.4.4	Evolution of fronts	26
3.2.4.5	Basic soil moisture states and runoff generation potentials	27
3.2.4.6	Subsurface flow exchange in the vadose zone	28
3.2.4.7	Soil water redistribution during interstorm periods.....	28
3.2.4.8	Initialization of the water table depth and soil moisture distribution	29
3.2.5	Groundwater model	30
3.2.6	Runoff generation scheme	31
3.2.7	Runoff routing	32
3.2.7.1	Hydrologic routing.....	32
3.2.7.2	Hydraulic routing	33
3.3	<i>Model inputs</i>	35
3.3.1	Input parameters	35
3.3.2	GIS based inputs.....	36
3.3.2.1	Topographic mesh (TIN).....	36
3.3.2.2	Soil and land use input	37
3.3.2.3	Groundwater input	38
3.3.2.4	Rainfall input.....	38
3.3.2.5	Meteorological data input.....	39
3.4	<i>Model outputs</i>	41
3.4.1	Outlet hydrograph.....	41
3.4.2	Spatially lumped variables.....	41
3.4.3	Spatially distributed state variables	41
3.4.4	Spatially distributed time-integrated variables	42
Chapter 4	Model Application	44
4.1	<i>Site description</i>	45
4.1.1	Catchment location.....	45
4.1.2	Topography	46
4.1.3	Soils.....	47
4.1.4	Land use	51

4.1.5 Climate	52
<i>4.2 Model input description</i>	<i>54</i>
4.2.1 GIS data	54
4.2.1.1 Topography	54
4.2.1.2 Soils.....	56
4.2.1.3 Land use	57
4.2.1.4 Groundwater table.....	58
4.2.2 Weather data.....	60
4.2.2.1 Rainfall.....	60
4.2.2.2 Meteorological data.....	71
4.2.3 Streamflow data.....	71
4.2.3.1 River heights	71
4.2.3.2 River flows.....	72
Chapter 5 Results: Calibration and Validation	74
<i>5.1 Model calibration</i>	<i>75</i>
5.1.1 Model sensivity	75
5.1.1.1 Soil hydraulic properties	75
5.1.1.2 Land use parameters.....	77
5.1.1.3 Routing parameters	77
5.1.2 Calibration strategy	78
5.1.2.1 Calibration period.....	78
5.1.2.2 Soil parameters.....	79
5.1.2.3 Vegetation parameters.....	80
5.1.2.4 Routing parameters	81
5.1.3 Calibration results.....	81
<i>5.2 Model evaluation -Water Balance</i>	<i>84</i>
5.2.1 Water balance equation	84
5.2.2 Precipitation.....	84
5.2.3 Stream runoff.....	84
5.2.4 Evapotranspiration.....	85
5.2.5 Soil moisture status.....	85
5.2.6 Groundwater	85
5.2.7 Results	86
<i>5.3 Model assessment for flood forecasting</i>	<i>87</i>
5.3.1 Model validation on flood event.....	87

5.3.1.1 Flood events	87
5.3.1.2 Simulation results.....	88
5.3.1.3 Discussion	91
5.3.2 Radar – raingauges comparison.....	92
5.3.2.1 Simulations.....	92
5.3.2.2 Discussion	94
5.3.3 Potential warning time.....	95
5.3.3.1 Simulation	95
5.3.3.2 Discussion	98
Chapter 6 Conclusion.....	99
6.1 Conclusion.....	100
6.2 Recommendation for further research	100
References.....	102
Appendix A Example of a tRIBS input file.....	108
Appendix B Matlab Code for creating tRIBS radar rainfall input files.....	115

Chapter 1

Introduction

1.1 Introduction

Flooding occurs when water overtops the banks of the river due to an excess rainfall that cannot be stocked in the soils or discharged fast enough by the stream network. Contrary to its current connotation, flood can have great benefits. The Egyptian civilisation was well known for taking advantage of the Nile's waters that regularly covered their lands and deposited fertile sediments. But nowadays, flooding is rather seen as a natural disaster. Agriculture is not at the centre of our society any more, urbanisation has concentrated population and economic activity, often near big rivers and in the river beds. Therefore damage resulting from floods became more important than its benefits. While in some poor rural countries, like in Bangladesh in 1998 or Venezuela in 1999, extreme events cause the death of thousands of people, in developed countries consequences of floods are, hopefully, mostly counted in euros worth of damage. In 1993, the worst flood in history of the Mississippi River in the USA, caused the death of 50 people and damaged 56,000 homes and the economic losses were estimated to about \$10 billions (Mississippi River Flood, 1998). More recently in Europe, the Elbe River in Germany flooded to its highest ever recorded level in 2002, causing approximately €23 billions worth of damage (Corcoran, 2004), and Hurricane Katrina flooded New Orleans in August 2005 causing about 950 casualties and damage worth \$200 billions.

Concerns about flooding issues have been rising in the last decade as their frequency and their magnitude seem to be increasing continuously. Climate change is often seen as responsible for changes in storm patterns and the use of land for accelerating the runoff process. Another element that appears obvious is that the vulnerability of the catchments has increased. Urbanisation tends to concentrate population and economic activity around cities which for most of them have historically been built along rivers (for reasons of arable lands, transportation or water supply). This development often takes advantage of virgin floodplains to expand and thus enhances the risk of flooding.

Solutions exist to mitigate the risk. They are usually divided into structural and non-structural solutions. Structural solutions are mainly preventative and focusing on curtailing the magnitude of floods using different methods such as dams, dikes, compound channels, widening of river beds, etc. These solutions could however have adverse environmental, hydrologic, ecologic or economic consequences. Non-structural solutions mainly focus on lowering the vulnerability of an area. They include regulation on land use (forbidding construction in floodplains, etc.), and flood warning systems.

Flood warning does not prevent floods but often constitutes a complement of structural response as the latter cannot prevent the disaster completely. It allows population to protect themselves by building up temporary defences or evacuating areas before the flood wave hits. Warnings can prove very useful if they can be provided a long time enough ahead and if they are accurate. That is where flood forecasting plays an important role.

Flooding is indeed one of the most predictable of the natural disasters, contrary to earthquakes or volcanic eruptions. It is driven by two main factors, which are rainfall and the catchment characteristics. The prediction of the first constitutes the task of meteorologist. Knowing how much water will fall on the catchment is the first step of the prediction process which is particularly important for flash flood events. Knowing the amount of rain, it is then the task of the hydrologist to assess how it will be drained to the stream network, considering the characteristics of the catchment. This aspect is particularly important in the case slow floods which the most common type of floods occurring in Ireland. The expansion of scientific knowledge and computational tools allows more and more accurate forecasting models to be developed. The US National Weather Service uses forecast models in its local units. Bangladesh, where flooding is a very important issue, has set up a flood forecasting and warning centre with forecasted river levels available on the Internet. In France, the flood warning units have been reorganised and will deliver flow forecast in the beginning of 2006.

This could apply to the Munster Blackwater River where flooding is recurrent in the town of Mallow. This project applies a rainfall-runoff model to the Blackwater catchment with the aim of forecasting flood flows in Mallow to improve the existent flood warning system.

1.2 Flooding of the Munster Blackwater

1.2.1 History of flooding

The Munster Blackwater catchment suffers from regular flooding in the towns of Mallow and Fermoy. These towns experienced major floods in 1853, 1875, 1916, 1946, 1948, 1969 and 1980. The most disastrous of them, in 1853, washed away the old bridge of Mallow and left the lowest streets of the town under 3.6m of water. The latest of the major flood occurred on November 2nd 1980. This event, with an estimated return period of 30 years (Corcoran, 2004) occasioned damage and losses estimated at over £2.5 million (Doheny, 1997).

The Town Park and the Park Road flood on more regular basis, almost once every year or more. It has, for instance, been flooded 3 times in the space of four months, in October and

December 2004, and January 2005, with the worst of them happening in October 2004 with the flood level extending to Bridge Street. The inundation of the Park Road causes major traffic disturbance in the town of Mallow as it is one of its main streets, and can be dangerous as at least two mishaps have occurred in the past decade (Corcoran, 2004). To prevent accidents, both ends of the road are closed when a flood has been detected. Flood warning is therefore vital to prevent fatalities at places like this.

1.2.2 Flood warning system

A flood warning system was set up for Mallow in 1982, as a consequence of the 1980 flood. However, this system failed due to lack of expertise and maintenance (Steinmann, 2004). The warnings were then only issued by an engineer of the Cork County Council, Mr Martin Corcoran, who has been observing the river level near Millstreet, 40 km upstream of Mallow, since 1975. In 2003, in collaboration with Ott-Hydrometry and UCC, Cork County Council installed two new automatic river level monitoring devices, reviving the 1982 automatic warning system (Corcoran, 2004). The system is set up such that engineers of the County Council receive warning message from the station when the river reaches a critical level. Steinmann (2004) however showed that this method does not always provide a long enough warning for the authorities to respond. Studies have been carried out by UCC hydromet research group to develop a forecasting tool to predict floods. A web site has also been created (irishfloodwarning.com) that allows anyone to know what the river level is at two location by simply logging onto the web. The web page is frequently visited during flood events.

1.3 Previous work

Different methods for flood warning have been studied by the UCC Hydromet research group, leading to a forecasting model using the Artificial Neural Networks (ANN) approach. The ANN model is a so called black-box model as it does not consider any of the characteristics of the catchment but only data (here river stage). The transfer function that is established by training the network on several years of data doesn't necessarily have a physical interpretation. The model merely learns to recognise patterns so as to anticipate what the output is at the next time step.

This forecasting model is able to predict river levels ten hours ahead with good accuracy. The ANN model used is remarkable in the simplicity of its inputs which are only river levels at

three different stations on the river at different times. This fact leads me to believe there is a possibility to increase the forecasting time by considering rainfall.

1.4 Objectives

The objective of the project is to calibrate the physically-based distributed tRIBS rainfall runoff model to the Blackwater catchment and assess its possible implementation as a flow forecasting tool for the existing flood warning system. This consists in:

- The collection of the necessary input data to run the model.
- The calibration of the parameters of the model and their validation.
- The assessment of the potential use of the model for flood forecasting on the Blackwater River.

1.5 Layout of the thesis.

Chapter 2 of this thesis presents a literature review of the state of art in rainfall runoff modelling for flood forecasting. The modelling method used for this research is described in chapter 3. Chapter 4 describes the characteristics of the catchment and details the inputs used for the modelling. The results of calibration and the assessment of the implementation of the model as flood forecasting tool are presented in chapter 5. Chapter 6 sums the conclusions and details recommendation for further work.

Chapter 2

Literature Review

2.1 The modelling of the rainfall-runoff process

There is a long history of rainfall-runoff modelling, for different purposes. One of the first modelling of flood peak was the equation published by the Irish engineer Thomas James Mulvaney, which related the hydrograph peak discharge Q_p to the catchment area A , a maximum rainfall areal average R and an empirical parameter C in $Q_p = CAR$. This kind of estimation for Q_p is often all that is needed for engineering hydrologists to design a bridge or a culvert. This model has become known as the “rational method”, and many variations have been published since and are still in use today.

Rainfall-runoff modelling has developed since then as hydrologic knowledge spread alongside with computational tools. But the hydrological processes involved are not yet perfectly known, and as Shertzer et al (2002) puts it, the understanding of the dynamics of the rainfall-runoff process constitutes one of the most important and challenging problems in hydrology.

The main reason for modelling hydrological processes is the limitation of hydrological measurements (Beven, 2001). Models are therefore means of extrapolating from those available measurements in both space and time. Modelling is carried out for pure research to develop scientific knowledge about hydrological systems but the ultimate aim of prediction using models must be to improve decision-making about hydrological problems. Flood forecasting is one of these applications of rainfall-runoff modelling in predicting stream flows at the outlet of the catchment from rainfall input.

2.2 Different types of models

A large number of rainfall runoff models have been developed and implemented into software since the early 1960s (Wagener, 2004). Todini (1988) gives a historical review of rainfall-runoff modelling. These models use different kind of approaches and structures. There exist different ways of classifying the variety of model encountered. One of the most common classifications refers to Wheater et al (1993) which distinguishes three classes:

- Metric models, also called statistical, stochastic, probabilistic or black box models.
- Parametric models, also referred to as conceptual or grey box models.
- Mechanistic models, also mentioned as physically based or white box models.

2.2.1 Metric models

Metric or statistical models use time series of data available to derive both model structure and parameters (Wagener, 2004). They are purely based on the information contained in the data and do not require any previous knowledge of the catchment. They therefore only apply to gauged catchments. These models are usually spatially lumped, i.e., they treat the catchment as a single unit. The established transfer functions are characteristic of the basin and are not necessarily have a physical interpretation. Statistical models generally require a dataset of past observations sufficiently large to allow the system to be adequately parameterized (Porporato and Ridolfi, 2001)

Among the most popular models of this type are Artificial Neural Networks (ANN). ANN simulates biological neural systems and the human way of thinking and learning (Elshorogaby et al, 2000). They are computational tools with the ability to represent non-linear systems. ANN combine nonlinear functions of variables presented as inputs in order to model a prescribed output. The combination of functions is optimised via a process known as training the network in order to best match the output of the network with the desired or target value (Wasserman, 1989). ANN modelling has been applied to the Blackwater catchment (Corcoran, 2004; Leahy, 2005). Other models of this type are Auto-Regressive Moving Average (ARMA) (Kisi, 2004), Transfer Functions (Young, 1992), or Nonlinear Prediction (Tamea et al, 2005).

2.2.2 Metric models.

Metric or conceptual models use storage elements as the main building component (Wagener et al, 2004). These storages are filled through fluxes such as rainfall, infiltration or emptied through evapotranspiration, drainage or runoff. In contrast to stochastic models, the modelling structure is defined according to the modeller's understanding of the hydrological system. These models use parametric equations to describe the storage variations or the fluxes and therefore still rely on time series of data to calibrate the various parameters. These parameters mostly have a direct physical interpretation but often cannot be derived from field measurements as a number of processes are often aggregated (in space and time) into a single parameter. Conceptual models usually try to find a trade off between complexity of the modelling approach and output accuracy. Indeed, more complexity means more parameters, more parameters mean more calibration problems, and more calibration problems mean more uncertainty in predictions (Beven, 2001). Conceptual models consider the basin as a single unit, however some of them use a so-called semi-distributed approach which considers a segmentation of the catchment into

smaller sub-catchments (Wagener, 2004) to account for the spatial variation of the catchment characteristics.

One of the most known models of this category is TOPMODEL (Beven and Kirby, 1979). TOPMODEL is a conceptual but spatially distributed model which implements an index of hydrological similarity known as the topographic index (Kirby, 1975). It has been originally developed to simulate small catchments in the UK (Beven, et al, 1984), but has been applied to several different basins throughout the world (Beven, 2001). Other conceptual models include the Soil Moisture Accounting model (SAC-SMA) used by the US National Weather Service River Forecast Centers (Vieux et al, 2004) or GR4J developed by the French Cemagref.

2.2.3 Mechanistic models

Mechanistic models are based on the conservation of mass, momentum and energy (Wagener et al, 2004). They use a spatial discretization based on grids, hillslopes or some type of hydrologic response unit. They are therefore particularly appropriate when a high level of resolution is required. This kind of model became practically applicable in the 1980s, as a result of improvements in computer power. It requires a large amount of data to be run. The physical realism sought by these models makes it possible to relate their parameters to measurable characteristics of the catchment, thus, in theory, eliminating the need for calibration. Therefore the potential for physically based distributed models to be used in locations where no stream gauge exists is a major motivation this approach (Vieux et al, 2004). The spatial distribution of the data also allows accounting for the spatial variations of the catchment characteristics and rainfall. However, the extreme data demand, the scale related problems and the over parameterization has the consequence that the model parameters often cannot be derived through measurements (Wagener et al, 2004). Therefore, mechanistic models are often applied in a way that is similar to lumped conceptual models (Beven, 1989).

The Systeme Hydrologique Europeen (SHE) (Abbott et al, 1986) model originally developed as a joint collaboration between the Institute of Hydrology in the UK, the Danish Institute of Hydraulics and SOGREAH in France was one of the first models of this kind to be developed. It is a grid based model coupling hydrological processes involved in rainfall-runoff process and subsurface and groundwater flows. Other examples of physically based include tRIBS (Ivanov et al, 2004) used in this study, or r.water.fea (Vieux, 2004).

2.3 The current state of the art

Conceptual models make up the majority of models used in practical applications (Wagener et al, 2004). The metric and mechanistic approaches have recently improved due to increase in computational power. But despite the high degree of accuracy by now attained, discharge forecasts performed by conceptual models, are still affected by errors, which, in some cases, are shown to be considerable (Toth, 1998). The main reason is that the conceptualisation of the physical phenomena is often not detailed enough: on one hand in order not to increase the complexity of the model structure, on the other hand because the physical phenomena involved are not yet completely known. Both metric and mechanistic methods have evolved in the recent years. Combinations of metric and parametric approaches have been studied (Toth, 1998). The statistical approach allows an estimation of prediction uncertainty (Kryztofowicz, 2001), the value of which has been realized by decision makers (Siccardi et al, 2005).

Comparisons between different types of models have been conducted (WMO, 1992; Moore et al, 2000). While the utility of distributed models to predict interior hydrologic processes is well know, few studies have specifically addressed the improvement of distributed models over lumped models for the predicting basin outflow hydrographs of the type useful to flood forecasting (Smith et al, 2004). As a consequence, the hypothesis that distributed modelling using higher resolution data will lead to more accurate outlet hydrograph simulation remains largely untested. The recent Distributed Model Intercomparison Project (DMIP) carried out by the US National Weather Service (Reed at al, 2004) showed that although the lumped model used as reference outperformed distributed models in more cases that the distributed models outperformed the lumped model, some calibrated distributed models can perform at a level comparable to or better than a calibrated lumped model. The wide range of accuracies among model results suggest factors such as model formulation, parameterization and the skill pf the modeller can have a bigger impact on simulation than simply whether or not the model is lumped or distributed. But as the computers will continue to improve and with the proliferation of high resolution data sets and GIS capabilities, there is no doubt that distributed hydrological models will get more detailed (Beven, 2001).

Chapter 3

Methods: tRIBS Model

3.1 Model overview

The model used for this research is the TIN-based Real-time Integrated Basin Simulator (tRIBS) model developed at the Ralph M. Parsons Laboratory, Massachusetts Institute of Technology. It is a physically based distributed model designed for real time, continuous hydrologic forecasting (Ivanov et al 2004).

tRIBS is a development of the former Real-time Integrated Basin Simulator (RIBS) (Garrote and Bras, 1995) which was a raster based model implementing an event-based scheme for rainfall-runoff analysis. It has inherited the functionality of the latter while adding the hydrology necessary for continuous operation (Ivanov et al 2004). It inherited the Triangulated Irregular Network architecture (TIN), which constitutes another major development from the RIBS model, from the CHILD model framework (Tucker et al, 2001).

The main motivations for the application of this model to the Blackwater catchment were the size of the catchment (1200km²) which implies important spatial variations in catchment characteristics and rainfall distribution, and the use of the new radar rainfall data available in Ireland. Moreover the model was tested on a catchment of similar size in the United States (Ivanov et al, 2004).

3.1.1 Modelling approach

tRIBS couples the different hydrological processes of rainfall interception, evapotranspiration, infiltration, subsurface flows, runoff generation, and channel routing to account for a continuous simulation of the hydrologic characteristics of the catchment.. Figure 3-1 is a schematic representation of the coupled hydrologic processes used in tRIBS. Table 3-1 lists the hydrologic components of the model which are detailed in 3.2 .

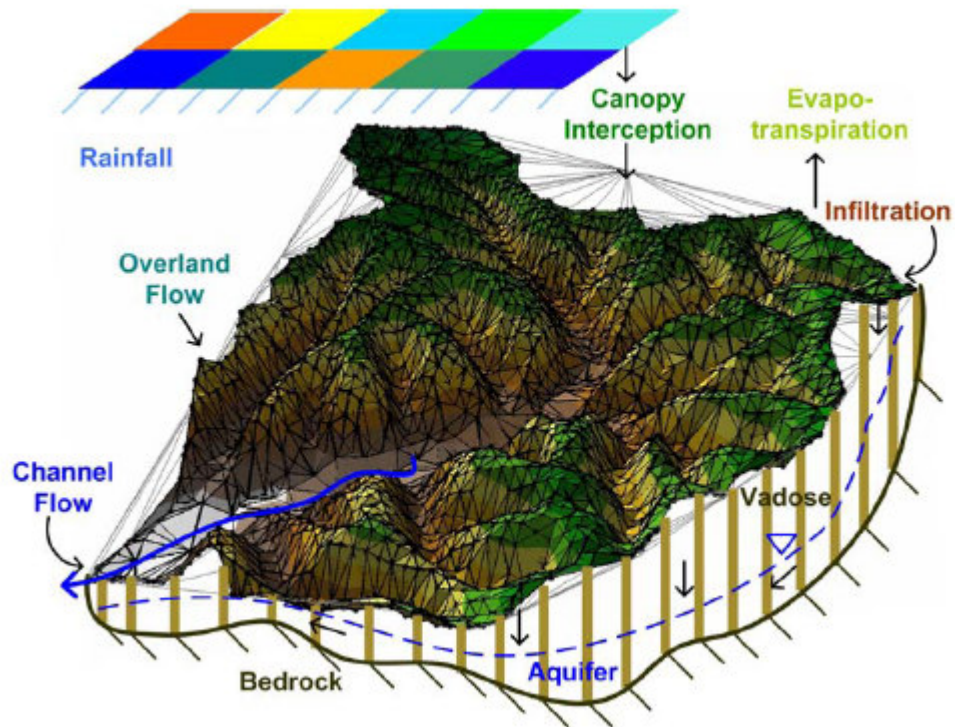


Figure 3-1 Schematic representation of the coupled hydrological processes in the tRIBS model (from tRIBS user manual)

Table 3-1 Components of the tRIBS distributed hydrologic model (from tRIBS user manual)

Model Process	Description
Rainfall Interception	Canopy water balance model
Surface Energy Balance	Combination equation (IE), Gradient method (H) and Force restore equation (G)
Surface radiation Model	Short-wave and long-wave components accounting for terrain variability
Evapotranspiration	Bare soil evaporation, transpiration and evaporation from wet canopy
Infiltration	Kinematic approximation with capillarity effects; unsaturated, saturated and perched conditions; top and wetting infiltration fronts
Lateral Vadose Flow	Topography-driven lateral unsaturated and saturated vadose flow
Runoff Production	Infiltration-excess, saturation excess, perched return flow and groundwater exfiltration
Groundwater Flow	Two dimensional flow in multiple directions, dynamic water table
Overland Flow	Non linear routing
Channel Flow	Kinematic wave hydraulic routing

tRIBS uses GIS based data such as the topography, soils and land use data to characterize the catchment, water table depth to initialise soil moisture, radar rainfall as precipitation input, and meteorological station data for interstorm periods modelling. For every computation step it calculates the dynamic state variables of the catchment (water table depth, soil moisture, etc.) and the river flows at the specified points. Figure 3-2 is a schematic of the framework of the model.

tRIBS is a fully distributed hydrologic model able to simulate the complete hydrologic state of a catchment. Although our main focus is on flood forecasting, the model can also be used for other hydrologic purposes, such as water resources management, etc.

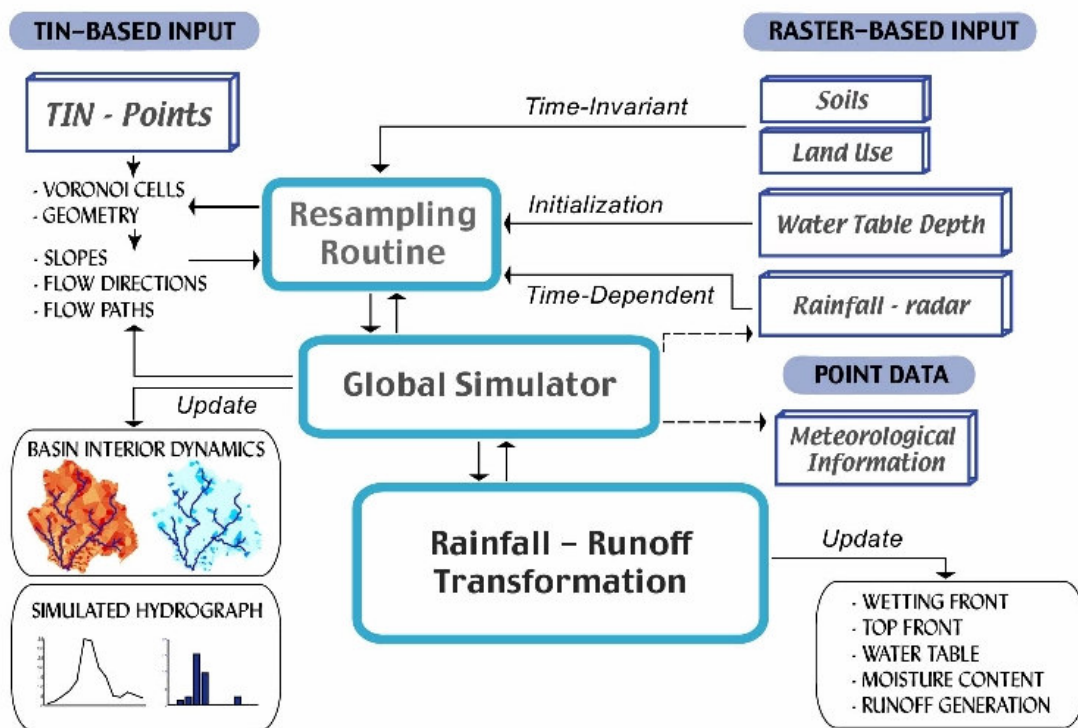


Figure 3-2 General Framework of the tRIBS model (from tRIBS user manual)

3.1.2 Topographic representation

tRIBS assumes that the topography of the catchment plays a significant role in the runoff generation of a catchment in a watershed model, there are different ways of representing the topography, among which are contour lines, Digital Elevation Models (DEM), or Triangulated Irregular Networks (TIN), which are used in the tRIBS model.

TINs are a piecewise linear representation of a surface defined by triangular elements of varying size. They are composed of nodes, which represent points of the surface defined by their

coordinates x , y and z , and triangles linking the nodes and representing the slope of the surface. The primary motivation for the use of TINs by the model developers is the multiple resolutions offered by the irregular domain (Ivanov et al 2004). Where a raster grid represents a surface using a regular grid, a TIN can adapt its resolution to the variability of the terrain. Thus a uniform plateau can be represented with less detail (in numbers of nodes and triangles) than a complex irregular mountainous surface. This translates to computational savings as the number of nodes can be significantly reduced.

Another advantage of TINs is that the linear features can be preserved as the mesh can mimic terrain breaklines, stream networks, and boundaries between heterogeneous regions (Ivanov et al 2004).

3.1.3 Computational element

A finite difference control volume approach is used in used to estimate the state of the dynamic hydrological variables. As a result of using a TIN as topographic input, the computational framework is irregular as well and consists in Voronoi polygons. A Voronoi polygon (or cell) associated with a specific node is the polygon whose interior consists of all points in the plane which are closer to a particular node than to any other (same as a Thiessen polygon). A Voronoi cell is defined for each node of the TIN mesh as shown in Figure 3-3. The dashed lines define the edges that connect TIN nodes, while the solid lines depict boundaries of Voronoi regions associated with the TIN nodes.

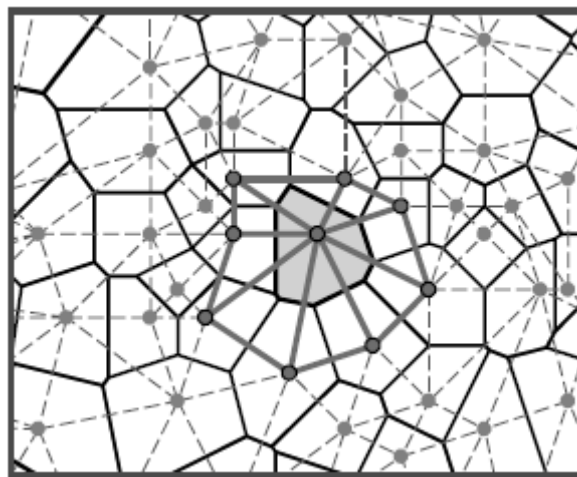


Figure 3-3 Example of a Voronoi diagram constructed for a TIN (Ivanov et al, 2004)

A reference system is defined for each cell by the axes n and p where n follows the direction normal to the plane of cell and p follows the direction of the maximum slope of that plane. Figure 3-4 shows the 3-dimensional geometry of a Voronoi region: the shaded triangles depict TIN facets and the polygon inside is the constructed Voronoi cell sloped along the steepest direction.

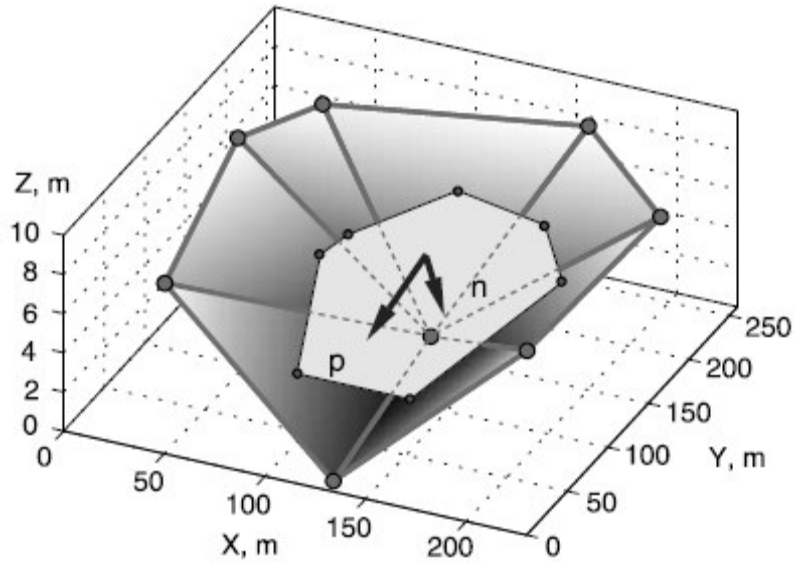


Figure 3-4 Geometry of a Voronoi cell in three dimensions (Ivanov et al, 2004)

3.2 The hydrologic modelling approach

The description of the hydrologic components of the modelling detailed in 3.2 refers to Ivanov (2002) and Ivanov et al (2004).

3.2.1 Rainfall interception

The canopy water balance model (Rutter et al., 1971) provides a method for modelling rainfall interception. It relates changes in the canopy storage C to the rainfall rate R , canopy drainage D , and potential evaporation rate E_p in the form:

$$\frac{dC}{dt} = (1 - p)R - D - \frac{C}{S} E_p \quad (1)$$

where parameters S and p are the canopy capacity and free throughfall coefficient. While the rainfall is prescribed from observations, the potential evaporation is computed based on meteorological and surface conditions.

The canopy drainage, accounting for water losses from leaf dripping and stemflow, is modelled as (Shuttleworth, 1979)

$$D = K e^{g(C-S)} \quad (2)$$

where K and g are the drainage rate coefficient and exponential decay parameter.

3.2.2 Energy balance and surface fluxes

Current meteorological conditions and the antecedent soil moisture state define the amount of energy going into evaporation moisture loss. The surface energy balance describes the partitioning of net radiation R_n into sensible H , latent λE , and ground G heat fluxes at the soil surface:

$$R_n - G = \lambda E + H \quad (3)$$

Since each term can be expressed as a function of the soil surface temperature, an iterative scheme is used to solve each component for given meteorological conditions.

3.2.2.1 Short and longwave radiation

The net radiation component R_n is composed of net incoming short wave radiation R_{si} , incoming longwave radiation R_{li} , and outgoing longwave radiation R_{lo} : $R_n = R_{si} + R_{li} - R_{lo}$. Parameterizations detailed in Bras (1990) are utilized for each radiative flux component. The incoming short wave radiation is a combination of various inputs resulting in its significant spatial variability:

$$R_{si} = (1 - a)K_t \left[(1 - 0.65N^2)(R_{dirs} + R_{difs}) + R_{refs} \right] \quad (4)$$

where a is the albedo, K_t is the optical transmission coefficient, N is the cloud cover. R_{dirs} and R_{difs} are the direct and diffuse solar radiation fluxes. These variables account for the geographic location, time of year, aspect of the element surface and its slope (Bras, 1990). R_{refs} is the radiation component which accounts for the reflected radiation from other sloping surfaces (Wilson and Gallant, 2000). The incoming longwave radiation is modelled using grey body theory:

$$R_{li} = \sigma K_c E_a T_a^4 \quad (5)$$

where σ is the Stefan-Boltzman constant, K_c is a function of cloud cover, E_a is the atmospheric thermal emissivity and T_a is the air temperature. Similarly, the outgoing longwave radiation is

$$R_{lo} = \sigma E_s T_s^4 \quad (6)$$

where E_s is the surface emissivity and T_s is the soil surface temperature.

3.2.2.2 Latent heat flux

The Penman-Monteith approach (Penman, 1948; Monteith, 1965) combines the energy and mass transfer techniques as a tool for estimating the surface latent heat flux λE :

$$\lambda E = \frac{\Delta(R_n - G) + \gamma \frac{\rho_m \lambda_v \delta q_a}{r_a}}{\Delta + \gamma \left(1 + \frac{r_s}{r_a} \right)} \quad (7)$$

where Δ is the slope of Clausius-Clayperon relationship, γ is the psychometric constant, ρ_m is the moist air density, λ_n is the latent heat of vaporization, δq_a is specific humidity deficit, r_a is the aerodynamic resistance, and r_s is the stomatal resistance. The state variables are calculated using standard meteorological relationships described in Rogers and Yau (1989) and Bras (1990). The resistance terms are computed utilizing methods described in Shuttleworth (1992).

3.2.2.3 Sensible heat flux

The sensible heat flux component H of the surface energy balance is computed from the gradient of the surface T_s and air temperature T_a using an aerodynamic surface resistance approach (C_p is the specific heat capacity of dry air):

$$H = \frac{\rho_m C_p}{r_a} (T_s - T_a) \quad (8)$$

3.2.2.4 Ground heat flux

The ground heat flux G is determined using the force-restore model as described by Lin (1980) and Hu and Islam (1995). This method is based on solving the heat diffusion equation between a soil surface layer and a deeper soil profile. Both the surface T_s and the deep soil T_d temperatures are obtained. The flux G is obtained from Lin (1980) as:

$$G = \frac{1}{2} C_s d_1 \left(\xi \frac{dT_s}{dt} + \omega (T_s - T_d) \right) \quad (9)$$

where C_s is soil heat capacity, w is daily frequency of oscillation, $d_1 \sqrt{2k/\omega}$ is the soil heat wave damping depth, $k = k_s/C_s$ is the soil diffusivity, and k_s is the soil heat conductivity. The parameter ξ is computed using the Hu and Islam (1995) parameterization.

3.2.3 Evapotranspiration

Following Wigmosta et al. (1994), three evaporation components are estimated: evaporation from wet canopy E_{wc} , canopy transpiration E_{dc} , and bare soil evaporation E_s . The latent heat flux, computed from the energy balance at the surface, provides an estimate for the

actual evaporation E_a , while the potential evaporation rate E_p is obtained as (Wigmosta et al., 1994):

$$E_p = E_a \frac{\Delta + \gamma \left(1 + \frac{r_a}{r_s}\right)}{\Delta + \gamma} \quad (10)$$

A vegetative fraction, v , for each computational element determines the proportion undergoing canopy and bare soil evaporation or transpiration. These processes are controlled by the amount of moisture available in the upper soil layer.

The bare soil evaporation is (Deardorff, 1978)

$$E_s = (1-v)\beta_e E_p \quad (11)$$

where β_e is determined from the saturation soil moisture θ_s and the soil moisture in the top 100 mm of the soil column θ_{100}

$$\beta_e = \min\left(1, \frac{\theta_{100}}{0.75\theta_s}\right) \quad (12)$$

For the vegetation fraction, evaporation has two components: evaporation from the canopy E_{wc} and transpiration E_{dc} which are related in the following way (Eltahir and Bras, 1993):

$$\begin{aligned} E_{wc} &= vE_p, \quad E_{dc} = 0, \quad C \geq S \\ E_{wc} &= \frac{C}{S}vE_p, \quad E_{dc} > 0, \quad 0 \leq C \leq S \end{aligned} \quad (13)$$

Transpiration occurs at a rate

$$E_{dc} = \beta_t v (E_p - E_{wc}) \left[\frac{\Delta + \gamma}{\Delta + \gamma \left(1 + \frac{r_a}{rs}\right)} \right] \quad (14)$$

where β_t accounts for the current soil moisture stress which limits the root water uptake. A simplified approach is used to parameterize this factor:

$$\beta_t = \min\left(1, \frac{\theta_{top} - \theta_r}{0.75\theta_s - \theta_r}\right) \quad (15)$$

where θ_{top} is the soil moisture content in the top meter of the soil column and θ_r is the residual moisture content (Brooks and Corey, 1964). Of the three evapotranspiration components, only transpiration E_{dc} and bare soil evaporation E_s contribute to the depletion of the surface soil moisture. The wet canopy evaporation, E_{wc} , plays an important role in reducing canopy interception storage.

3.2.4 Infiltration scheme

3.2.4.1 Basic assumptions

The reference system is defined by the axes n and p introduced in the previous section (Figure 3-4). The model considers a soil column of heterogeneous, anisotropic, and sloped soil in which the saturated hydraulic conductivity decreases with normal depth. The properties are assumed constant on a plane perpendicular to the (n, p) plane of a grid cell. The spatial variability in the domain is considered by the elements of the grid. Besides accounting for the large scale heterogeneity in the two-dimensional plane, soils in the model also exhibit non-uniformity with depth. The changes in the hydraulic conductivity are represented by a continuous function of depth (Beven 1982, 1984). The assumed relationship is the exponential decay of the saturated conductivity with normal depth:

$$\begin{aligned} K_{Sn} &= K_{0n} e^{-fn} \\ K_{Sp} &= K_{0p} e^{-fp} \end{aligned} \quad (16)$$

where $K_{Sn}(n)$ and $K_{Sp}(n)$ are the saturated conductivities at the depth n perpendicular to the land surface, K_{0n} and K_{0p} are the saturated conductivities in the directions n and p at the land surface, f is the decay parameter, controlling the decay of conductivity, and n is the normal depth. Beven (1982, 1984) has argued that a relationship of this form could be used to describe the characteristics of a number of soil types. Soil anisotropy is introduced (Cabral et al., 1992) as the dimensionless ratio of the saturated hydraulic conductivities in the directions n and p :

$$a_r = \frac{K_{0p}}{K_{0n}} \quad (17)$$

This relationship is assumed to be valid for all depths. The Brooks-Corey (1964) parameterization scheme is used to relate the unsaturated hydraulic conductivity and the pore pressure with moisture content. The Brooks-Corey (1964) model uses Burdine's theory (Burdine, 1953) to relate hydraulic conductivity and the moisture content:

$$K(S_e) = K_s S_e \frac{\left(\int_0^{S_e} \frac{1}{\psi^2(S)} dS \right)}{\left(\int_0^1 \frac{1}{\psi^2(S)} dS \right)} \quad (18)$$

where $\psi(S)$ is the soil water retention curve and S_e is the effective saturation:

$$S_e = \frac{(\theta - \theta_r)}{(\theta_s - \theta_r)} \quad (19)$$

where θ_s is the saturated moisture content, and θ_r is the residual moisture content, defined as is the amount of soil water that cannot be removed from the soil by drainage or evapotranspiration. Brooks-Corey (1964) used Burdine's theory assuming the empirical model for soil water retention curve:

$$\psi(S_e) = \psi_b S_e^{-\frac{1}{\lambda}} \quad (20)$$

where ψ_b is the air entry bubbling pressure and λ is the pore-size distribution index, to get the expression relating unsaturated conductivity and the soil moisture content:

$$K_n(S_e) = K_s S_e^{\frac{2+3\lambda}{\lambda}} = K_s \frac{(\theta - \theta_r)^{\frac{2+3\lambda}{\lambda}}}{(\theta_s - \theta_r)^{\frac{2+3\lambda}{\lambda}}} \quad (21)$$

Substitution of equations (16) for the saturated conductivities in the directions n and p into equation (21) yields:

$$\begin{aligned} K_n(\theta, n) &= K_{0n} e^{-fn} S_e^{\frac{2+3\lambda}{\lambda}} = K_{0n} e^{-fn} \left(\frac{\theta - \theta_r}{\theta_s - \theta_r} \right)^{\frac{2+3\lambda}{\lambda}} \\ K_p(\theta, n) &= K_{0p} e^{-fn} S_e^{\frac{2+3\lambda}{\lambda}} = K_{0p} e^{-fn} \left(\frac{\theta - \theta_r}{\theta_s - \theta_r} \right)^{\frac{2+3\lambda}{\lambda}} \end{aligned} \quad (22)$$

where K_n and K_p are the unsaturated conductivities in the directions n and p at moisture content θ and depth n . Therefore, given the soil parameters and the distribution of moisture content (or matric potential) in the vadose zone, the unsaturated conductivity is obtained from equation (22). It is worth noting that K_{0n} , θ_s , and θ_r are measurable parameters and thus have physical meaning. Parameter λ has more or less obvious physical sense either being small for media having a wide range of pore sizes or large for media with a relatively uniform pore size. The parameterization has a limitation: it is applicable only for the range of ψ satisfying $\psi > \psi_b$. It is necessary to note that though the Brooks-Corey model was developed for isotropic media (drainage cycle, hysteresis neglected) it appears feasible to apply the model (22) for nonuniform soils.

3.2.4.2 Pondered infiltration

The standard Green-Ampt model of pondered infiltration (Green and Ampt, 1911; Morel-Seytoux and Khanji, 1974; Neuman, 1976) follows from assuming that for a moisture wave infiltrating into a semi-infinite soil with a uniform initial volumetric water content, there exists a sharply defined wetting front for which the water pressure head h_f remains constant with time and position. A modified formulation of the model presented by Childs and Bybordi (1969) and Beven (1984) for layered soils is used:

$$q_n(N_f) = -K_{eff} \left[\frac{h_f(N_f)}{N_f} - 1 \right] \quad (23)$$

where $q_n(N_f)$ is the normal component of the flow vector, N_f is the wetting front depth, and K_{eff} is the harmonic mean of conductivities over the saturated depth. For the surface saturated conductivity K_{0n} exponentially decaying with depth at the rate f , K_{eff} can be expressed as:

$$K_{eff}(N_f) = K_{0n} \frac{fN_f}{e^{fN_f} - 1} \quad (24)$$

The effective wetting front capillary pressure which explicitly accounts for changes in the soil moisture and conductivity with depth is parameterized as (Ivanov, 2002)

$$h_f(N_f) = \psi_b \frac{1 - S_{ei}^{3 + \frac{1}{\lambda(N_f)}}}{3\lambda(N_f) + 1} \quad (25)$$

Where $S_{ei}(N_f) = (\theta_i(N_f) - \theta_r) / (\theta_s - \theta_r)$ and $\lambda(N_f) = \lambda_0 e^{\frac{N_f}{2}}$, ψ_b is the air entry bubbling pressure, λ_0 is the pore-size distribution index, and $\theta_i(N_f)$ is the moisture content at the depth N_f of the initial moisture profile. Taking into account the change in the gravity gradient with slope of the soil element, equation (23) can be rewritten in the following form:

$$q_n(N_f) = K_{eff}(N_f) \cos \alpha + \Psi_{is}(N_f) \quad (26)$$

where α is the slope of the soil column and the term $\Psi_{is}(N_f) = -K_{eff} \left(\frac{h_f(N_f)}{N_f} \right)$ represents the flux rate due to capillary forces in the soil. The index “is” denotes the soil moisture range $\theta_i(N_f)$ to θ_s for which the term is evaluated. Equation (26) constitutes the basis for modelling saturated infiltration when the rainfall rate is higher or equal to the q_n .

3.2.4.3 Infiltration under unsaturated conditions

At the onset of an infiltration event, if the rainfall rate is lower than the infiltration capacity of the soil, the movement of water in the soil occurs under unsaturated conditions. This phase includes the development of a wetted unsaturated wedge and, if the rainfall intensity is sufficiently high, the formation of a perched zone may follow. A schematic soil moisture profile in Figure 3-5, simulated in the tRIBS model, depicts the wetting and the top front. The wetting front separates the infiltrated rainfall from the initial soil moisture profile in a discontinuous fashion. The top front represents the ascent of the “shock wave” caused by the formation of the perched saturation zone. The normal depths to the wetting and the top front, N_f and N_t correspondingly, coincide if there is no perched layer (Figure 3-5b).

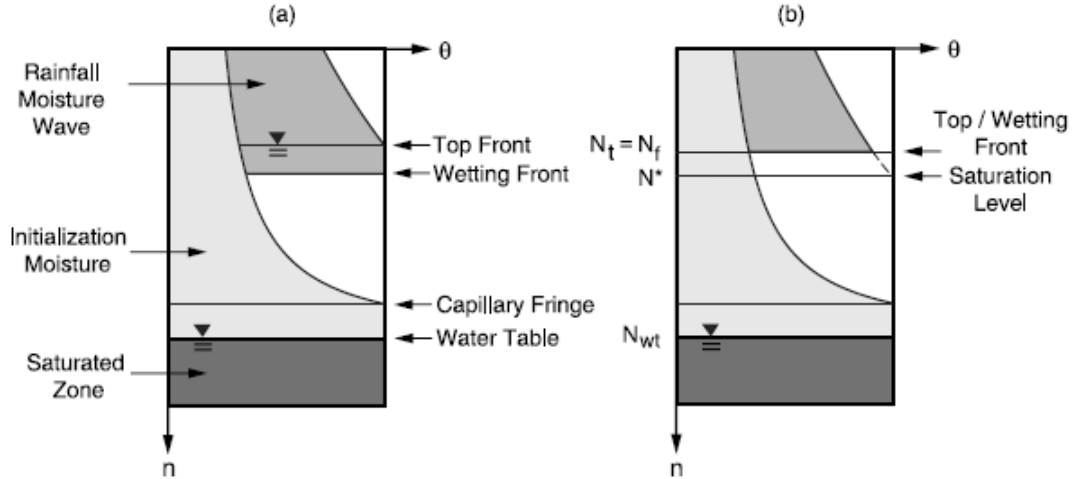


Figure 3-5 Schematic of the basic computational element. (a) Vertical structure. (b) Unsaturated state (Ivanov et al, 2004)

Wetted wedge dynamics: unsaturated phase

One of the key assumptions made in the infiltration model is that while recognizing the importance of the capillary forces, gravity is considered to be the dominant component in the infiltration process (Cabral et al., 1992). Capillarity effects are accounted in a simple way by an analogy with (26). The redistribution flux in the normal to the surface direction is formulated for the unsaturated wetted wedge as:

$$q_n(N_f) = R_e \cos \alpha + \Psi_{ie}(N_f) \quad (27)$$

where R_e is an “equivalent” rainfall rate defined as the value that leads to the same moisture content above the wetting front as from a constant rainfall at rate R_e under equilibrium conditions (Garrote and Bras, 1995) and $\Psi_{ie}(N_f)$ is the capillary drive across the wetting front in the unsaturated conditions. For the discontinuous profile as in Figure 3-5b, $\Psi_{ie}(N_f)$ is evaluated for the range of values $[\theta_e(R_e, N_f), \theta_i(N_f)]$, where $\theta_e(R_e, N_f)$ is the maximum moisture value in the wedge. For an unsaturated form of Darcy’s law (Smith et al., 1993), $\Psi_{ie}(N_f)$ is:

$$\Psi_{ie}(N_f, \theta_i, \theta_e) = -K_{Sn}(N_f) \frac{h_f(N_f, \theta_i, \theta_e)}{N_f} \quad (28)$$

where $K_{Sn}(N_f)$ is the saturated conductivity at the depth N_f and $h_f(N_f, \theta_i, \theta_e)$ is the effective unsaturated capillary pressure evaluated for an arbitrary moisture range in soils with decaying

saturated conductivity. This term is approximated by generalizing (25) (similar to Smith et al. (1993)):

$$h_f(N_f, \theta_i, \theta_e) = \psi_b \frac{S_{ee}^{3+\frac{1}{\lambda(N_f)}} - S_{ei}^{3+\frac{1}{\lambda(N_f)}}}{3\lambda(N_f)+1} \quad (29)$$

where $S_{ee}(N_f) = \frac{(\theta_e(R_e, N_f) - \theta_r)}{(\theta_s - \theta_r)}$.

Wetted wedge dynamics: perched zone formation

Given that the saturated conductivity decreases with normal depth, the saturation may develop at some depth N^* . If the moisture influx above the wetting front is high enough, water accumulates above N^* and perched saturation develops (Figure 3a). An analogous expression to (26) for the normal flux can be written as:

$$q_n(N_f, N_t) = K_{eff}(N_f, N_t) \cos \alpha + \Psi_{ie}(N_f) \quad (30)$$

where K_{eff} is as previously the harmonic mean of the conductivities over the saturated thickness:

$$K_{eff}(N_f, N_t) = K_{0n} \frac{f(N_f - N_t)}{e^{-fN_n} - e^{-fN_t}} \quad (31)$$

3.2.4.4 Evolution of fronts

The formulation of the wetting and top front evolution for unsaturated and surface saturated state (Figure 3-6b and Figure 3-6d) is similar to the one described by Cabral et al. (1992) and Garrote and Bras (1995). For the perched saturated state (Figure 3-6c), it is assumed that at any instantaneous time the top front depth represents the saturation level of the steady state profile corresponding to some constant rainfall rate R_e , determined by the moisture content above the wetting front.

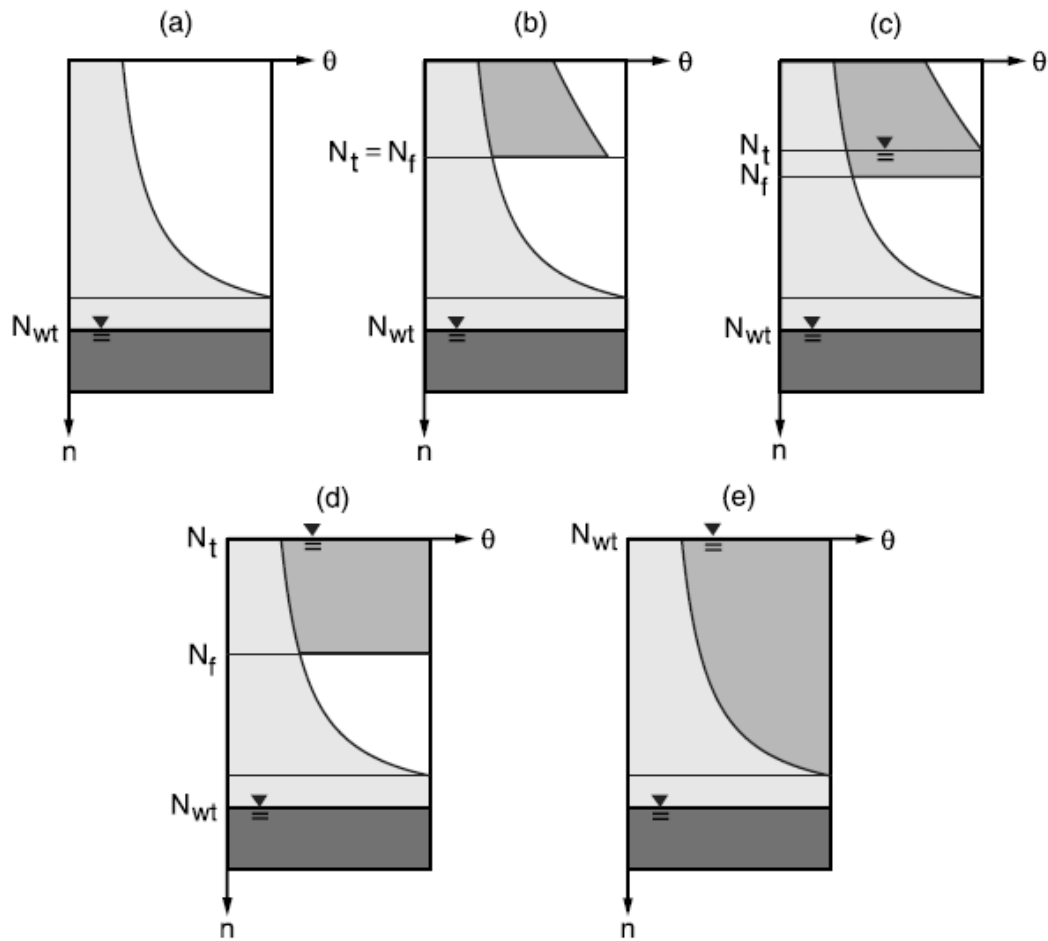


Figure 3-6 Basic vadose zone states: (a) initial, (b) unsaturated, (c) perched saturated, (d) surface saturated, (e) fully saturated (Ivanov et al, 2004)

3.2.4.5 Basic soil moisture states and runoff generation potentials

Five distinct cell states are considered, each defined by the dynamic variables describing the moisture state of the soil column (Figure 3-6). These states have different potentials for runoff generation among the four mechanisms considered by the rainfall-runoff scheme.

For the first three states: initial, unsaturated, and perched saturated state (Figure 3-6a-c), the soil infiltration capacity is not constrained by the surface conductivity unless the top of the soil column reaches immediate saturation. In the surface saturated state (Figure 3-6d), the infiltration capacity is constrained by the conductivity at the bottom of the saturated profile. Depending on soil parameters and rainfall intensity, infiltration excess runoff may be produced. Within the model, runoff is considered to be of infiltration excess type when the redistribution rate of the top saturated layer is lower than the rainfall intensity, irrespective of the preceding

infiltration history. In the context of literature definitions (e.g., Freeze, 1974; Bras, 1990; Beven, 2001), this is a mixture of ‘‘Hortonian’’ runoff type, occurring when soil becomes saturated from above by a high-intensity rainfall, and saturation from below runoff occurring due to the development of perched groundwater (e.g., Beven (2001) also refers to the latter mechanism as of infiltration excess type). Perched subsurface stormflow may also occur at an element in this state if the outflux from the vadose zone of an upslope cell discharges onto the surface of the element. The fully saturated state implies that the wetting front has reached the water table and the top front is at the soil surface (Figure 3-6e). The cell infiltration capacity in this state is zero and if rainfall persists, the element produces saturation excess runoff. Lateral redistribution fluxes in the phreatic aquifer may result in groundwater runoff production. Perched subsurface stormflow may also be produced at an element in this state.

3.2.4.6 Subsurface flow exchange in the vadose zone

A simplified scheme is adopted to account for the moisture transfers in the vadose zone between contiguous elements based on the formulation provided by Cabral et al (1992). The spatial orientation of flows entering a cell is assumed to be parallel to the line of maximum terrain slope, the direction p , irrespective of the orientation of triangular facets of the TIN that compose the surface of the Voronoi cell (Figure 3-4) as well as discontinuities at the cell boundaries associated with slopes in adjacent elements.

3.2.4.7 Soil water redistribution during interstorm periods

Adequate representation of the soil water redistribution and dynamic adjustments of the moisture profile during evapotranspiration are required for continuous model operation. Interstorm conditions are modelled using various state transitions detailed in Ivanov (2002) and are briefly outlined below.

The first transition describes the water table drop from the soil surface as a result of evaporation conditions applied to the computational element. A hydraulic equilibrium profile (section 3.2.4.8) is assumed to be attained in the unsaturated zone and a mass conservative scheme is used to define the new groundwater level. The second transition deals with evaporation conditions applied to elements having water table located at some depth below the land surface. The implemented scheme subtracts moisture from the whole unsaturated profile resulting in the drop of the groundwater level and reinitialization of the soil water profile. Adjustments of the

moisture profile are also made during simulation of rainfall of decreasing intensity, rainfall hiatus, or interstorm periods when a wedge of infiltrated water exists in the soil. The moisture wedge may transit to various states depending on the prior cell state, the soil parameters and the intensity of evaporative demand. The principal transitions are illustrated in Figure 3-7.

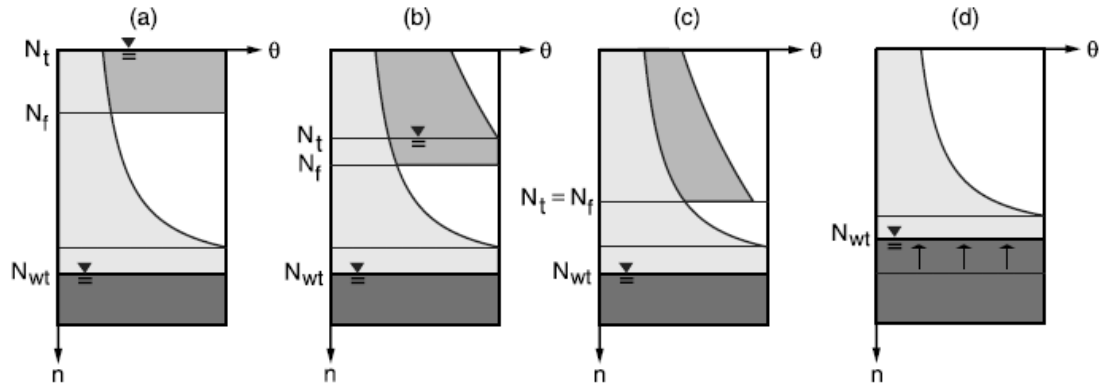


Figure 3-7 Principal phases of drying cycle in the computational element (Ivanov et al, 2004)

It is assumed that after a given time with no rainfall the interstorm period begins. This marks the time at which redistribution of moisture excess in the unsaturated zone occurs and the resulting soil moisture will be the initial state or any subsequent storm. The characteristic time that marks the beginning of an interstorm period is assumed to be climatically dictated and varies for different regions, commonly to be in the range 1-3 days (Restrepo-Posada and Eagleson, 1982).

3.2.4.8 Initialization of the water table depth and soil moisture distribution

Catchment initial conditions, required for modeling the rainfall-runoff response, involve two distinct but interconnected aspects: the initial water table depth and the initial moisture profile in the vadose zone. The former represents a measure of the storage capacity of a basin while the latter determines the moisture deficit and the infiltration characteristics. Spatial information for both states is not usually available and, consequently, reasonable approximations have to be made. It is important to point out, however, that the effect of initial conditions has less influence on the simulation results in the case of continuous modelling. The influence of the initial state diminishes with the simulation time as storm and interstorm periods redistribute soil moisture in the watershed in vertical and lateral directions. The long-term continuous modelling is therefore suitable for elucidating the inherent catchment dynamics.

Specifying the initial moisture state of the catchment is a common problem in rainfall-runoff modeling (Salvucci, 1993; Salvucci and Entekhabi, 1994). It is assumed that the depth to the water table significantly controls wetness conditions in the basin and therefore defines the

soil's initial infiltration capacity. The implemented approach assumes hydrostatic equilibrium for the vertical distribution of pressure head which corresponds to zero initial flux in the unsaturated zone: $\partial y/\partial n = 1$ (Sivapalan et al., 1987; Famiglietti and Wood, 1991; Troch et al., 1993; Coles et al., 1997). The suction head at any depth $N < (N_{wt} + \psi_b)$ is given as $\psi_y(n) = N_{wt} - n$. Using the Brooks-Corey parameterization and Miller scaling (Miller and Miller, 1956), the soil moisture profile can be expressed as :

$$\theta(n) = \theta_r + (\theta_s - \theta_r) \left[\frac{\psi_b}{n - N_{wt}} \right]^{\lambda(n)} \quad (32)$$

where $\lambda(n)$ accounts for changes in pore size with depth of the form: $\lambda(n) = \lambda_0 e^{fn/2}$ (Selker et al., 1999). However, a computationally convenient assumption is to use (32) with the exponent approximated by the surface pore-size distribution $\lambda(n) \approx \lambda_0$ (Ivanov, 2002).

3.2.5 Groundwater model

A quasi three-dimensional ‘‘cascade’’ groundwater model is utilized. An explicit cell to cell approach is used to route the lateral saturated subsurface flow. For each direction of a TIN edge j , the total groundwater flow from a Voronoi cell is:

$$\sum_j Q_{Soutj} = \sum_j -TW_j \tan \beta_j \quad (33)$$

where Q_{Sout} is the outflux from a saturated layer of width W along the negative hydraulic gradient, approximated as a local gradient of the water table, $\tan(\beta)$, where β is the local slope of the groundwater level. The index j refers to values of the width and hydraulic gradient defined in the j^{th} direction. The aquifer transmissivity, T , nonlinearly depends on the groundwater depth N_{wt} and bedrock depth h_0 due to the exponential decay of the saturated conductivity:

$$T = \frac{a_r K_{0n}}{f} \left(e^{-fN_{wt}} - e^{-fh_0} \right) \quad (34)$$

where a_r is the soil anisotropy ratio. The total influx nQ_{Sinj} for any given Voronoi cell is obtained by summing the outfluxes from elements that contribute to that cell. The corresponding changes in depth to the water table are modelled as:

$$S_y \frac{dN_{wt}}{dt} = \frac{\sum_j Q_{Sout_j} - \sum_j Q_{Sin_j}}{A} \quad (35)$$

where A is the Voronoi cell area. From a computational standpoint, the treatment of the specific yield S_y in equation (35) is inconvenient, especially when moisture fronts are present in the vadose zone. An approach with an “implicit” computation of the specific yield based on mass conservation in the element is used instead (Ivanov, 2002). Various possible transitions allow simulation of the subsurface saturated exchanges and couple the subtraction/addition of water from/to the groundwater with the corresponding adjustments of the soil moisture profile in the vadose zone.

3.2.6 Runoff generation scheme

The actual infiltration I, rainfall R, infiltration capacity f_c , and runoff R_f can be related as

$$\begin{aligned} I = R, \quad R_f = 0 & \quad \text{if} \quad N_t > 0, \quad N_f < N_{wt} \\ I = f_c, \quad R_f = R - f_c & \quad \text{if} \quad N_t = 0, \quad N_f < N_{wt}, \quad R > f_c \\ I = 0, \quad R_f = R & \quad \text{if} \quad N_t = 0, \quad N_f = N_{wt} \end{aligned}$$

Return flow is the result of lateral subsurface exchange and is produced under similar conditions:

$$I = f_c, \quad R_f = \sum Q_U = f_c \quad \text{if} \quad N_t = 0, \quad N_f < N_{wt}, \quad \sum Q_U < f_c$$

where $\sum Q_U$ is the net sum of subsurface lateral inflows and outflows in the unsaturated zone. The runoff generation due to groundwater corresponds to the following conditional expression:

$$I = 0, \quad R_f = \sum Q_S - f_c \quad \text{if} \quad N_t = 0, \quad N_f = N_{wt}$$

where $\sum Q_S$ is the net positive sum of fluxes in the saturated zone. The total surface flow generated in the element is the sum of all runoff types produced under the described conditions. A reinfiltration scheme is not considered and runoff produced in a cell is assumed to contribute to streamflow at the catchment outlet.

3.2.7 Runoff routing

The chosen methodology for routing runoff represents a trade-off between exploiting the efficient TIN structure and the complexity of the routing problem over the TIN surface. Runoff is assumed to follow TIN edges in accordance with the consecutive drainage directions. The total runoff travel path l_t consists of a hillslope fraction l_h and a stream fraction l_s : $l_t = l_h + l_s$ (Figure 3-8). Two different routing models are applied for these path fractions.

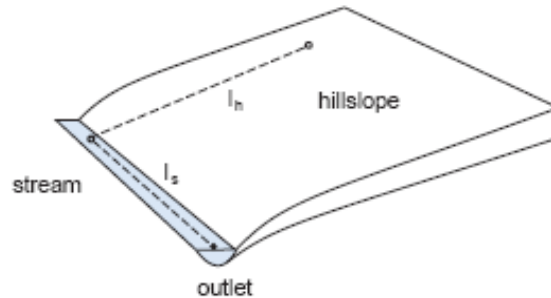


Figure 3-8 Schematic representation of a flow path for a hillslope node (Ivanov, 2002)

3.2.7.1 Hydrologic routing

For every hillslope path, the bulk transport of water is assumed to be the dominant factor in runoff routing. The effect of dispersion is introduced in a simplified manner that keeps the model parameters to a minimum and leads to high computational efficiency. Each hillslope node is assigned an “outlet” stream node to which it contributes flow via consecutive drainage paths of the TIN. The travel time t_τ of runoff between a hillslope node and its “outlet” can be defined as: $t_\tau = l_h/v_h(\tau)$, where $v_h(\tau)$ is the hillslope velocity at time τ . This velocity is allowed to vary in space and time as

$$v_h(\tau) = c_v \left[\frac{Q(\tau)}{A_c} \right]^r \quad (36)$$

where $Q(\tau)$ is the discharge at the “outlet” stream node at time τ , A_c is the surface contributing area of the “outlet” node, and c_v and r are uniform parameters for a given basin. Assuming steady state flow conditions, the relationship $Q(\tau)/A_c$ for any given point in the stream network is constant (Leopold and Maddock, 1953; Rodriguez-Iturbe and Valdes, 1979) and therefore the latter parameters can be roughly approximated through an analysis of various flow regimes.

The uniform surface velocity approximation allows for a simple computation of the hydrograph at the basin outlet. Thus at time τ the instantaneous response function of the basin element located at (x, y) would be the Dirac delta function given by:

$$h_{\tau}(x, y, t) = \delta\left(\frac{t - l_h}{v_h(\tau)}\right) \quad (37)$$

An incremental basin response is estimated independently for every time step for the runoff generated at every pixel:

$$q_{\tau}(t) = \sum_{(x,y \in \text{Catchment})} R_{f\tau}(x, y) h_{\tau}(x, y, t) \Delta x \Delta y \quad (38)$$

where $R_{f\tau}(x,y)$ is the runoff rate generated in a cell at location (x,y) at time τ and $\Delta x \Delta y$ is the area of that element. The total basin response at time T is obtained by adding the incremental response since the beginning of the storm:

$$Q_h(t)|_T = \sum_{\tau=0}^{\tau=T} q_{\tau}(t) \quad (39)$$

3.2.7.2 Hydraulic routing

Hillslope hydrographs, from equation (39), in the stream nodes represent lateral inflow into the channel network of the basin. A kinematic wave routing model is used to simulate transport of water in the channel network (e.g., Goodrich et al., 1991; Singh, 1996). The one-dimensional continuity equation for unsteady free surface flow is:

$$\frac{\partial F}{\partial t} + \frac{\partial Q}{\partial x} = R_b \quad (40)$$

where F is the cross-sectional area, Q is the discharge along the x axis, R_b is the lateral influx of water into the channel per unit length. If the channel cross section is approximated by a rectangle and Manning's equation is used to parameterize the unsteady flow velocity:

$$Q = \frac{\sqrt{i_0}}{n_e} H^{5/3} b \quad (41)$$

where H is the depth, i_0 is the channel slope, n_e is the channel roughness, and b is the channel width. The channel width b is obtained using the relationship $b = \alpha A^{\beta}$ (Orlandini and Rosso, 1998)

where A is the contributing catchment area and α and β respectively channel width-area coefficient and exponent.

A union of connected segments without tributaries constitutes a stream reach which serves as a basic one dimensional finite element domain for the routing model. Using piecewise polynomial basis functions, $F(x,t)$ and $Q(x,t)$ can be approximated continuously within each channel reach (Kuchment et al., 1983). The Galerkin method is used to minimize the errors of the approximation. An implicit numerical scheme results in a system of nonlinear equations which is solved using Newton-Raphson iteration method combined with line searches and backtracking (Press et al., 1999).

3.3 Model inputs

The tRIBS program runs with reading a text file which contains the run period and run options details, the data input files directory and routing parameters. An example of a tRIBS run file is shown in appendix A. GIS data and GIS based parameters inputs are created separately and read by the program using the main input text file.

3.3.1 Input parameters

From the modelling equations detailed in 3.2 , 25 direct parameters can be listed as inputs to the model. The other parameters are either built in the model as constants (such as γ , the psychometric constant in equation (7)) or calculated from other built-in models not detailed here. Table 3-2 lists these parameters in 3 different categories: parameters related to the soils, parameters related to the vegetation and land use, and parameters related to the river channel.

Table 3-2 tRIBS model parameters

Parameter Symbol	Description	Units
Vegetation Properties		
p	Free throughfall coefficient	mm
S	Canopy capacity	mm/h
K	Canopy drainage rate coefficient	mm ⁻¹
g	Canopy drainage exponent	
a	Surface albedo	
H _v	Vegetation height	m
K _t	Optical transmission coefficient	
r _s	Average canopy stomatal resistance	s/m
v	Vegetation fraction	
Soil Hydraulic and Thermal Properties		
K _{0n}	Saturated hydraulic conductivity	mm/h
θ _s	Saturation soil moisture content	
θ _r	Residual soil moisture content	
λ ₀	Pore distribution index	
ψ _b	Air entry bubbling pressure	m
f	Conductivity decay parameter	m ⁻¹
a _s	Saturated anisotropy ratio	
a _u	Unsaturated anisotropy ratio	
n	Total porosity	
k _s	Volumetric heat conductivity	J/msK
C _s	Soil heat capacity	J/m ³ K

Channel and Hillslope Routing Parameters

n_c	Channel roughness coefficient
α_B	Channel width-area coefficient
β_B	Channel width-area exponent
c_v	Hillslope velocity coefficient
r	Hillslope velocity exponent

Channel and hillslope routing parameters are introduced to the model through its main input file along with time period parameters and the directories of the other input files. Vegetation and soil parameters are introduced to the model along with the land use and soil maps developed with GIS tools (see section 3.3.2).

3.3.2 GIS based inputs

3.3.2.1 Topographic mesh (TIN)

Topographic data is inputted to the model as *.points files during the initial model construction (first model run for a given catchment). After a successful tRIBS run, the model outputs a set of files (*.nodes, *.edges, *.tri, *.z) describing the TIN mesh in greater details that can be used for other runs, accelerating the process of mesh construction.

A *.points file is a simple text file containing a listing of point coordinates (x,y,z) and boundary code (0 for interior nodes – 1 for boundary nodes – 2 for the outlet – 3 for stream nodes), with a header indicating the number of points.

7			
405	120	25	1
505	135	14	1
235	385	13	1
450	490	7	0
465	205	2	3
630	150	12	1
580	640	0	2

Figure 3-9 Example of a tRIBS *.points file

A *.points file is elaborated by tRIBS from various sets of input data exported from ArcInfo (GIS software) such as a *.net file or a set of *.pnt and *.lin files. While running with this kind of input, tRIBS only constructs the TIN mesh and outputs a *.points file, but runs no hydrologic simulation.

3.3.2.2 Soil and land use input

Soil texture and land use cover are inputted in the form of ASCII grids of a particular soil or land use code. ASCII grids files are text files with a header containing spatial information and a grid containing the data.

The header contains the number of columns and rows (`ncols`, `nrows`) of the grid, the coordinates of the lower left corner (`xllcorner`, `yllcorner`), the size of a grid cell in the coordinate system (`cellsize`) and the value that considered as no data in the grid (`NODATA_value`). Figure 3-10 below gives an example of an ASCII grid file.

```

ncols      6
nrows      6
xllcorner  110000
yllcorner  80000
cellsize   10000
NODATA_value -9999
-9999      -9999   1       2       3       1
-9999      1       1       2       2       2
1          1       1       1       2       2
1          1       1       1       2       2
1          1       1       1       -9999  2
-9999      3       3       -9999  -9999  -9999

```

Figure 3-10 Example of ASCII grid for soil and land use data

The soil and land use parameters described in section 3.3.1 are inputted through 2 other text files. Each soil or land use code mentioned in the ASCII grid is assigned a set of parameters, which are gathered in a soil reclassification table that is used as input. Figure 3-12 and Figure 3-13 give the structure of soil and land use reclassification files. The description of the parameter symbols is detailed in Table 3-2. Note that some parameters, as A and b1 for the land use table are not mentioned in the parameters list above. Those parameters are used in other interception models (canopy storage model) which can also be used with tRIBS. Figure 3-12 Example of soil data input file Figure 3-12 and Figure 3-14 show examples of soil and land use input file.

#Types	#Params										
ID	K_s	θ_s	θ_R	λ_0	Ψ_B	f	a_s	a_u	n	k_s	C_s

Figure 3-11 Soil reclassification table structure

```

3 12
1 10 0.4 0.04 0.35 -100 0.001 800 600 0.45 0.5 1200000
2 10 0.4 0.04 0.35 -100 0.010 800 600 0.45 0.5 1200000
3 0.1 0.4 0.04 0.35 -100 0.005 500 400 0.45 0.5 1200000

```

Figure 3-12 Example of soil data input file

```

#Types  #Params
ID      A      b      P      S      K      g      a      Hv  Kt  Rs  v

```

Figure 3-13 Land Use reclassification structure

```

3 12
1 0.1 0.2 0.1 0.1 0.45 3.2 0.05 0.15 0.65 50 0.0
2 0.1 0.2 0.5 1.0 0.175 4.0 0.05 0.15 0.65 100 0.9
3 0.1 0.2 0.45 0.6 0.175 4.0 0.05 0.15 0.65 70 0.6

```

Figure 3-14 Example of a land use data input file

3.3.2.3 Groundwater input

The groundwater table is inputted through an ASCII grid file similar to Figure 3-10. The data in the grid represents the depth of the water table below the soil in millimetres.

3.3.2.4 Rainfall input

There are two types of rainfall data that can be presented to the tRIBS model: either radar-rainfall data, or rain gauge data. In the case of radar-rainfall, ASCII grids similar to Figure 3-10 are used as input. The grid data is then representing the rainfall intensities for each cell of the mesh. In case of rain gauge data, other text files are used as inputs. Every station is assigned a data file containing the rainfall intensities time series and a station file gathering the information about the stations is used as direct input to the model. Figure 3-15 shows an example of a rain gauge time series file with a header indicating the format of the following data (Year, Month, Day, Hour, Rainfall intensity)

```

Y M D H R
2003 1 1 0 0.0
2003 1 1 1 0.6
2003 1 1 2 1.0
2003 1 1 3 2.4
2003 1 1 4 0.8
2003 1 1 5 0.0

```

Figure 3-15 Example of rain gauge data file

Figure 3-16 below shows an example of a rain gauge station file with a header indicating the number of stations and the number of parameters in the current file. The 6 parameters in the file indicate respectively the station ID, the pathname for the time series files, the latitude and the longitude in the coordinate system, the length of the time series and the number of parameters in the times series files.

```

5 6
1 rain\gauges\Lyre.mdf 92500 141500 4344 5
2 rain\gauges\Millstreet.mdf 90600 127400 4344 5
3 rain\gauges\Ballydesmond.mdf 104000 114900 4344 5
4 rain\gauges\Ballinatona.mdf 112300 128300 4344 5
5 rain\gauges\Castlemagner.mdf 103900 144500 4344 5

```

Figure 3-16 Exemple of a rain gauge station file

3.3.2.5 Meteorological data input

As for rainfall data, meteorological data can be inputted either in the form of grids or weather stations.

In the case of weather station, the input format is similar to the rain gauges, with a weather station file containing the station information and data file for each station. The meteorological parameters used by the model are listed in Table 3-3 below.

Table 3-3 Meteorological parameters

Symbol	Description	Unit
PA	Atmospheric Pressure	[mb]
TD	Dew Point Temperature	[C]
XR	Relative Humidity	[%]
VP	Vapor Pressure	[mb]
XC	Sky Cover	[tenths]
US	Wind Speed	[m/s]
TA	Air Temperature	[C]
TS	Surface Temperature	[C]
NR	Net Radiation	[W/m2]

Figure 3-17 and Figure 3-18 respectively show the structure of a meteorological station file with a header and the list of parameters, and an example of a station file. Figure 3-19 and Figure 3-20 respectively show the structure of a meteorological data file and an example of it.

```
#Stations  #Params
StationID  FilePath  AbsLat  RefLat  AbsLong  RefLong  GMT  RecordLength  #WeatherParams  Other
```

Figure 3-17 Meteorological station file structure

```
1 10
1 weather\donoughmore.mdf 51.92 148370 -8.75 74289 0 30495 11 0
```

Figure 3-18 Example of a meteorological station file

```
Y    M    D    H    PA    TD/XR/VP  XC    US    TA    TS    NR
```

Figure 3-19 Meteorological data file structure

```
Y M D H PA XR XC US TA TS NR
2004 1 1 0 986.20 79.15 7 5.10 6.75 5.16 -61.46
2004 1 1 1 985.70 78.26 5 6.23 7.52 6.01 -59.67
2004 1 1 2 985.4 78.45 5 10.30 7.97 6.31 -71.58
```

Figure 3-20 Example of a meteorological data file

3.4 Model outputs

tRIBS creates different types output files for all the variables that are computed during the simulation run.

3.4.1 Outlet hydrograph

The main output is the outlet hydrograph, which is a file (*.qout file) containing the stream flow time series at the outlet of the catchment at the time step defined in the main input file. The program can also generate hydrograph files for interior stream node.

3.4.2 Spatially lumped variables

The program generates an .mrf output file containing time series of spatially lumped variables. These variables are given in Table 3-4.

Table 3-4 Spatially lumped variables in the .mrf output file

Variable	Unit
Time Step	hrs
Discharge at the catchment outlet using the hydrologic routing model	m ³ /s
Mean areal precipitation	mm/hr
Maximum rainfall value	mm/hr
Minimum rainfall value	mm/hr
Forecast state	-
Mean areal moisture content in the top 10 cm	-
Mean areal moisture content in the top 1m (root zone)	-
Mean areal moisture content in the unsaturated zone	-
Mean water table depth	mm
Fraction of the basin that has reach surface saturation	%
Fraction of the basin that has non-zero rainfall	%

3.4.3 Spatially distributed state variables

The tRIBS program outputs _00d data files at the beginning and at the end of the simulation containing the values of spatially distributed state variables. These files can also be generated for any time step specified in the main input file. The variables written in these files are listed in Table 3-5.

Table 3-5 Spatially distributed state variables outputted in _00d files

Variables	Units
Element (TIN node) ID number	-
Node elevation	m
Slope of the element	-
Contributing area	m ²
Water table depth	mm
Total moisture content in the unsaturated zone	mm
Initialization profile soil moisture content	mm
Wetting front depth	mm
Top front depth	mm
Lateral subsurface outflux from the unsaturated zone	mm/hr
Lateral subsurface influx from the unsaturated zone	mm/hr
Runoff production	mm
Rainfall intensity	mm/hr
Soil moisture content in the top 10 cm	-
Soil moisture content in the top 1m (root zone)	-
Canopy moisture storage	mm
Total evapotranspiration	mm/hr
Evaporation from soil	mm/hr
Transpiration	mm/hr
Ground heat flux	W/m ²
Sensible heat flux	W/m ²
Latent heat flux	W/m ²
Discharge (non-void if the node is a stream node)	m ³ /s
Water level (non-void if the node is a stream node)	m
Flow velocity	m/s
Soil index (only for file outputted at time 0)	-
Land use index (only for file outputted at time 0)	-

3.4.4 Spatially distributed time-integrated variables

The tRIBS program writes at the beginning and at the end of the simulation _00i data file that contain spatially distributed time-integrated (over simulation time) variables. These variables are listed in Table 3-6.

Table 3-6 Spatially distributed time-integrated variables outputted in _00i files

Variables	Units
Element (TIN node) ID number	-
Boundary code	-
Node elevation	m
Contributing area of the element	km ²
Slope of the element	-
Aspect of the element from North	rad
Mean soil moisture in the top 10 cm	mm
Mean soil moisture in the top 1 m (root zone)	mm
Occurrence of the infiltration excess runoff type	#
Mean rate if the infiltration excess runoff type	mm/hr
Occurrence of the saturation from below runoff type	#
Mean rate if the saturation from below runoff type	mm/hr
Occurrence of the perched subsurface stormflow runoff type	#
Mean rate if the perched subsurface stormflow runoff type	mm/hr
Occurrence of the groundwater runoff type	#
Mean rate if the groundwater runoff type	mm/hr
Net groundwater exchange	mm/hr
Mean evapotranspiration	mm/hr
Mean evaporative fraction	-

Chapter 4

Model Application

4.1 Site description

4.1.1 Catchment location

The Munster Blackwater catchment is located in the southwest of Ireland (Figure 4-1). The catchment is primarily within North West County Cork, Mid Cork and East Cork. The total area of the catchment is 3324km² which is almost 4% of the total land area of Ireland (Doheny, J. 1997). The Munster Blackwater catchment drains most of the Northern Division of County Cork and a large part of east County Waterford.

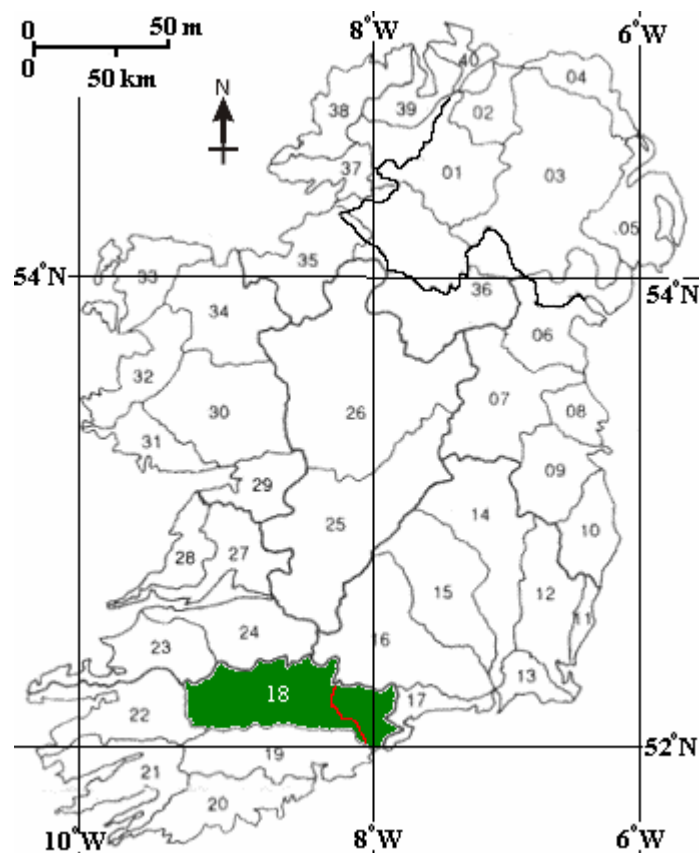


Figure 4-1 The Munster Blackwater Catchment is shown shaded and given a catchment No.18 by the Office of Public Work (OPW)

The project's interest is in flooding of Mallow, which is located about midway on the West-East line of the catchment (Figure 4-2). The Blackwater catchment to Mallow represents about 1/3 of the catchment with an area of 1180 km².

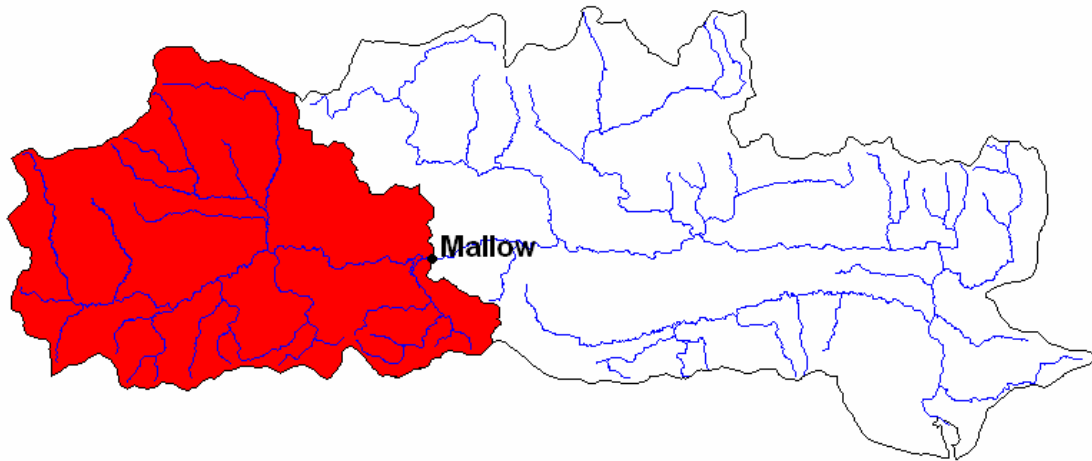


Figure 4-2 The Munster Blackwater catchment to Mallow

4.1.2 Topography

The Muster Blackwater rises in the foothills of the Mullaghareirk Mountains at Knocknafune in County Kerry and flows East to Mallow through a broad valley bounded by the Derrynasaggart and Boggeragh mountains in the South and the Mullagahreirk Mountains in the North (Figure 4-3). The highest point of the catchment is located in the South-West ranges of the Derrynasaggart Mountains at an altitude of 681m AOD, while Mallow, the lowest part of the catchment is at an altitude of 50m AOD. The Blackwater runs for 75km to Mallow with an average slope of 2.1% (Corcoran, 2004).

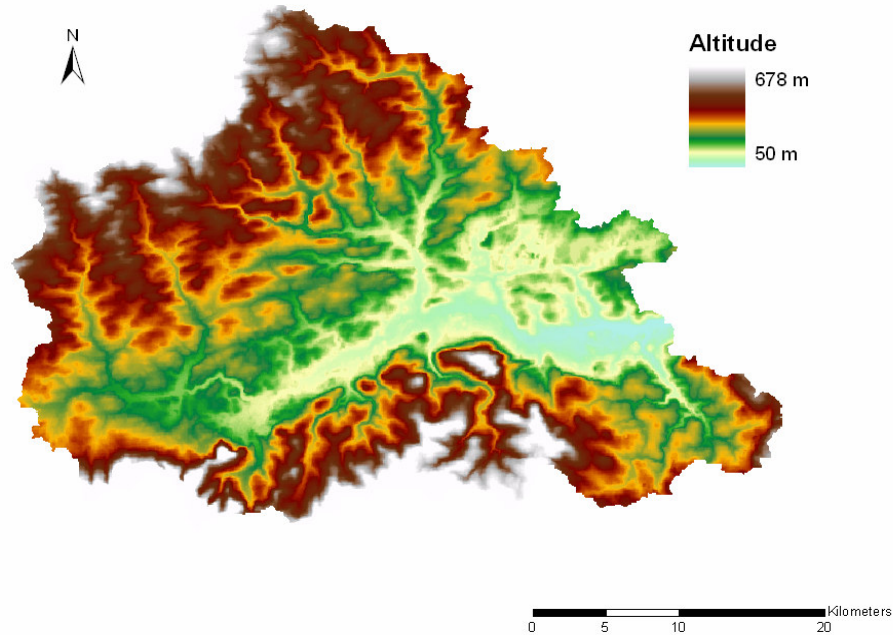


Figure 4-3 Topography map of the catchment from a digital elevation model (DEM)

4.1.3 Soils

The Environmental Protection Agency (EPA) is currently undertaking a Soil Survey for Ireland under the Water Frame Directory, completing the Forest Inventory and Planning System (FIPS) project, which had already mapped 44% of Ireland. This data is available for most of the Blackwater catchment to Mallow, except for a small area in the North (see Figure 4-4). Soil classification is described according to the Irish Forest Soils (IFS) classification which give qualitative, however not quantitative, information about the soils hydraulic properties. This classification divides soils into 6 main groups: deep well drained minerals, shallow well drained minerals, deep poorly drained minerals, poorly drained minerals with peaty topsoils, alluvium and peats.

The map of Figure 4-4 shows most of the basin is covered with deep well drained mineral soils (60%). Poorly drained mineral soils appear in patches all over the catchment (13.8% of the surface), blanket peat lands are found on the mountainous areas bordering the catchment and alluviums cover the main river beds and floodplains. The percentage of soil categories are detailed in Table 4-1.

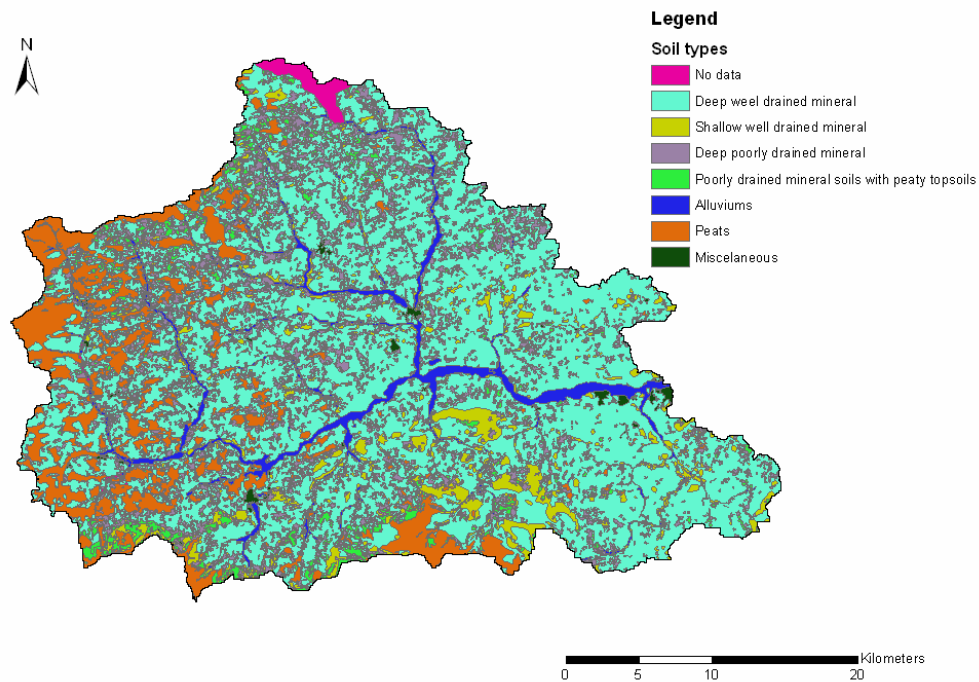


Figure 4-4 Catchment soils types

Table 4-1 Soil types repartition

IFS Soil Classification			Percentage	
Description	IFS Code	IFS Attribute	Level 1	Level 2
No Data	0			0.79%
Deep well drained mineral	1			59.98%
Derived from mainly acidic parent materials	11	AminDW	59.91%	
Derived from mainly basic parent materials	12	BminDW	0.06%	
Shallow well drained mineral	2			6.00%
Derived from mainly acidic parent materials	21	AminSW	6.00%	
Deep poorly drained mineral	3			13.80%
Derived from mainly acidic parent materials	31	AminPW	13.79%	
Derived from mainly basic parent materials	32	BminPW	0.01%	
Poorly drained mineral soils with peaty topsoil	4			3.57%
Derived from mainly acidic parent materials	41	AminPDPT	2.57%	
Mineral podsolised soils and peaty top soil with occasional iron pan layer	43	PodPDPT	0.99%	

Alluviums	5			4.14%
Mineral alluvium	51	AlluvMIN	4.07%	
Peaty alluvium	52	AlluvPT	0.06%	
Lacustrine alluviums	56	AlluvLk	0.01%	
Peat	6			11.18%
Mountain blanket peat	63	BkPt	11.09%	
Cutaway blanket peat	65	Cut	0.08%	
Miscellaneous	7			0.56%
Made	74	Made	0.55%	
Water	76	Water	0.01%	

More information about soils can be obtained from the parents materials (also called subsoils) which is the mineral from which the soil is formed. Parent materials are divided in tills (diamictons), glaciofluvial sands and gravels, esker sands and gravels, glaciolacustrine deposits, alluvium, peat, marine deposits, miscellaneous materials, and bedrock at or close to the surface.

Figure 4-5 and Table 4-2 show that most of the soils (75%) are originate from tills (TDSs, TLs, and TNSSs) which are sediments deposited by glacier ice. The other important parent materials are peat (11.1%), bedrock at surface (8.8%) and Alluviums (4.1%).

Tills are diamicton (nonlithified, nonsorted or poorly sorted sediments that contain a wide range of particle sizes) deposited by or from glacier ice. They correspond to the well drained and poorly drained mineral soils. The association of soils and subsoils allows reference to the general soil map classification and thus give more details about the nature of the soil. Indeed acidic well drained minerals from tills can be associated, in that area with Brown Podzolics which are gravelly loams. In the same way acidic poorly drained minerals from tills mostly refer to Gleys which are clay loams, and acidic shallow well drained minerals to Lithosols which are sandy laoms.

Peat is a post-glacial deposit, consisting mostly of vegetation which has only partially decomposed. Alluvium is a post-glacial deposit and may consist of gravel, sand, silt or clay in a variety of mixes and usually consists of a fairly high percentage of organic carbon (10%-30%). Rocks close to the surface are often associated with shallow well drained areas.

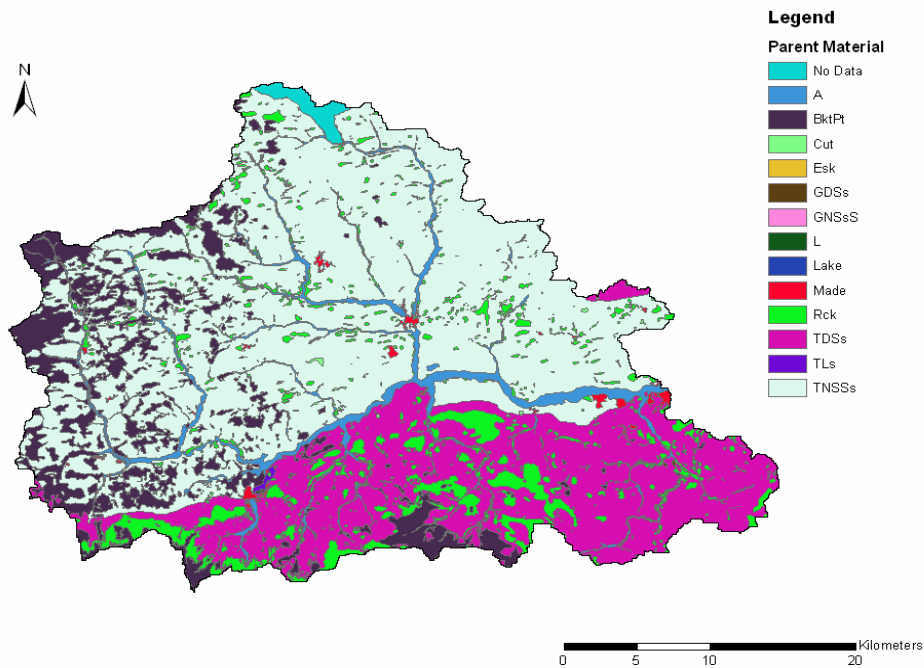


Figure 4-5 Catchment subsoils

Table 4-2 Subsoils repartition

Subsoil types	Map code	Percentage of area	
Tills			75.22%
Sandstone dominated till (Devonian)	TDSs	23.60%	
Limestone dominated till (Carboniferous)	TLs	0.07%	
Shales and sandstones dominated till (Namurian)	TNSSs	51.55%	
Glaciofluvial sands and gravels			0.01%
Sandstone sands and gravels (Devonian)	GDSs	0.01%	
Shales and sandstones sands and gravels (Namurian)	GNSsS	0.005%	
Glaciolacustrine deposits			0.02%
Lake sediments undifferentiated	L	0.01%	
Lake sediments	Lake	0.01%	
Alluvium			4.16%
Gravelly Alluviums	A	4.16%	
Peat			11.14%
Blanket Peat	BkPt	11.05%	
Cutover peat	Cut	0.08%	
Esker sands and gravels	Esk	0.003%	
Other categories			9.45%
Made ground	Made	0.55%	
Bedrock at surface	Rck	8.18%	
Miscellaneous materials		0.71%	

4.1.4 Land use

Land use information is available through the Corine (for Co-ORDination of INFORMATION on the Environment) Land Cover database elaborated by the EPA. This database covers the whole catchment with up to 3 levels of information describing 44 different land use categories.

As can be seen on Figure 4-6, agriculture is the dominant land use with almost 80% of the catchment area with approximately 80% of agricultural land under pasture. Forests and semi-natural areas are the second main land use with 12.8%. Wetlands cover 6.6% of the land, mainly in the mountainous region bordering the catchment. Artificial areas such as urban areas, industrial or commercial units use only a small part of the land (0.6%). Table 4-3 summarizes the partition of land use in the catchment.

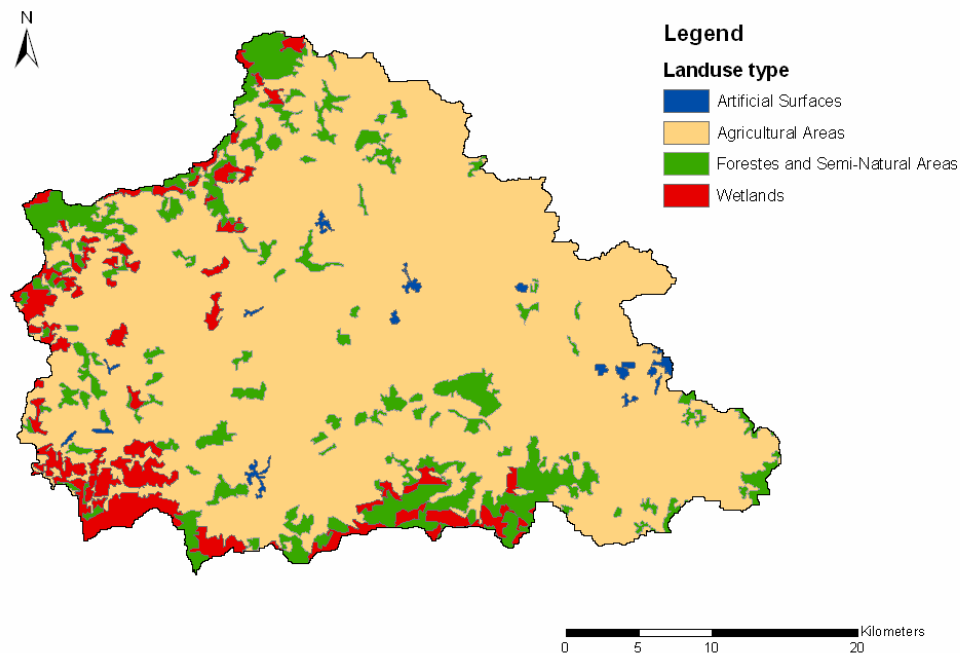


Figure 4-6 Catchment land use

Table 4-3 Land use repartition

Corine Landuse classification		Percentage	
Description	Code	Level 2	Level 1
Artificial Surfaces	1		0.7%
Urban fabric	11	0.49%	
Industrial, commercial and transport units	12	0.11%	
Mines, dumps and construction sites	13	0.03%	
Artificial non-vegetated areas	14	0.07%	
Agricultural areas	2		79.9%
Arable land	21	7.23%	
Pastures	23	65.14%	
Heterogeneous	24	7.58%	
Forest and semi-natural areas	3		12.8%
Forest	31	6.52%	
Scrub and/or vegetation associations	32	6.23%	
Wetlands	4		6.6%
Inland wetlands	41	6.61%	

4.1.5 Climate

The climate is mild and humid due to the influence of the warm Gulf Stream. Daily air temperature have a small range of variation during the year, going from a maximum of 20°C to a minimum of 0°C, with an average of 15°C in summer and 5°C in winter (Jaksic, 2004).

The annual average rainfall is about 1200mm with about 300 to 400 mm of evapotranspiration (Corcoran, 2004). However, the south and western part of the catchment gets more rain due to the mountainous topography, than in the floodplains and Mallow. During the period 2000 to 2004 averages of 1770mm and 1480mm precipitation have been recorded at the station of Ballydesmond, at the Cork/Kerry border, and Banteer in the South of the catchment, while an average of only 960mm has been recorded in Mallow. The rainfall regime is characterized throughout the year by long duration events of low hourly intensity. Short duration events of high intensity are more seldom and mostly occur in the summer. Figure 4-7 shows daily rainfall depth for Mallow for year 2004.

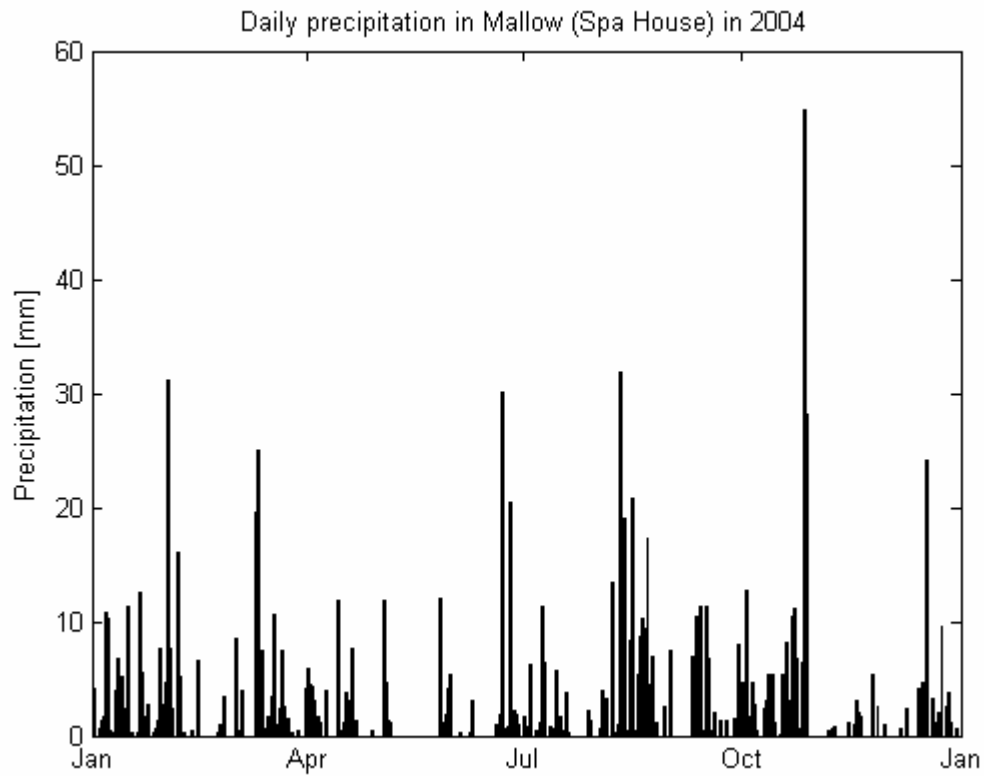


Figure 4-7 Daily rainfall precipitation for the year 2004 at Mallow

4.2 Model input description

4.2.1 GIS data

4.2.1.1 Topography

Although the topographic inputs for tRIBS are TINs, these are not currently available but constructed from other topographic sources. A digital elevation model (DEM) has been used to elaborate a TIN mesh.

Digital Elevation Model (DEM)

A 73.23m cell resolution DEM of the area is used to delineate the watershed and the stream network, and elaborate the TIN used as model input. These operations are undertaken with the ArcInfo GIS software and a set of aml (ArcInfo Macro Language) scripts.

To delineate the watershed, the direction of flow is first to be computed. Each cell is assigned a flow direction number between 1 and 128 according to the direction of the steepest drop. If the surrounding cells are all higher or if more than one cell can be defined as the steepest drop, some sets of tools are built in the ArcInfo commands to assign a flow direction to that cell.

The flow accumulation can then be computed for each cell as the total number of 'upstream' cells flowing into that given cell. Streams are then defined with a threshold of flow accumulation (cells receiving flows from more than 1000 'upstream' cells, for example). The watershed is delineated for a point of the stream network, defined as all the cells flowing into the outlet cell.

Figure 4-8 shows the flow accumulation computed for the Blackwater catchment to Mallow. Values of flow accumulation vary from 0 (black) to 219416 (white). The high values (from grey to white) reveal the stream network of the catchment.

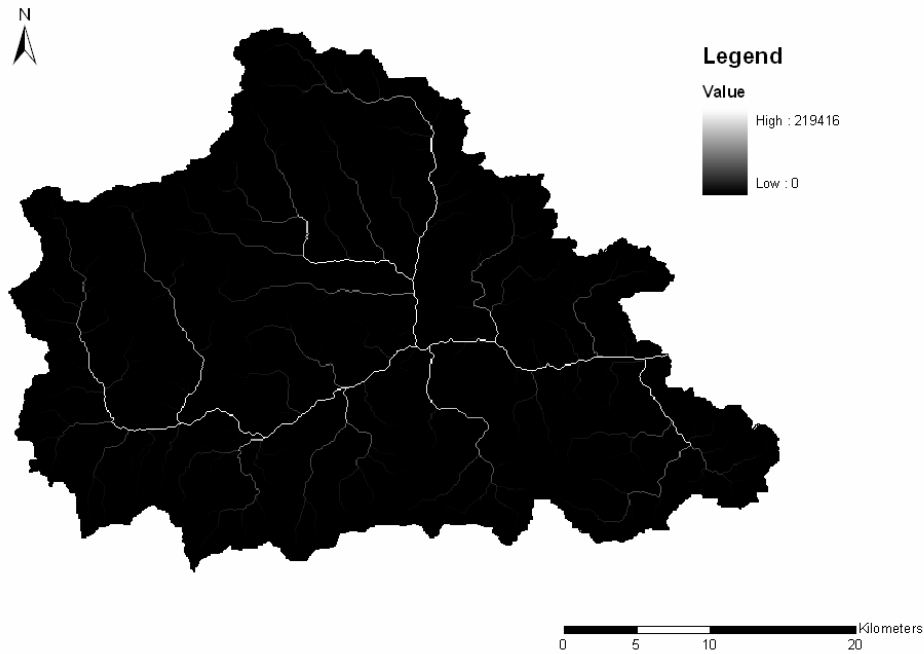


Figure 4-8 Flow accumulation computed for the Blackwater catchment

Triangulated Irregular Network (TIN)

The model input TIN is created from the delineated watershed DEM using the TIN Index Analysis Package (TIAP), a set of aml (ArcInfo Macro Language) scripts developed by E. Vivoni (developer of the tRIBS). This package facilitates the elaboration of the TIN utilizing different methods. These methods allow to extract floodplains and consider topographic features known as Hydrologic Response Units (HRU) (terrain method), or derive a TIN using grid parameters (index method). Our main limitation for the beginning of this study was computational efficiency. It was therefore decided to generate a TIN using the index method, using the Proximal Distance method. The reader is referred to Vivoni et al (2004) for further details on TIN generation.

The resulting TIN consists of 8220 nodes and 15500 triangles, elaborated from an original DEM containing 219417 cells. The data ratio of TIN nodes over DEM points is therefore of 3.7%.

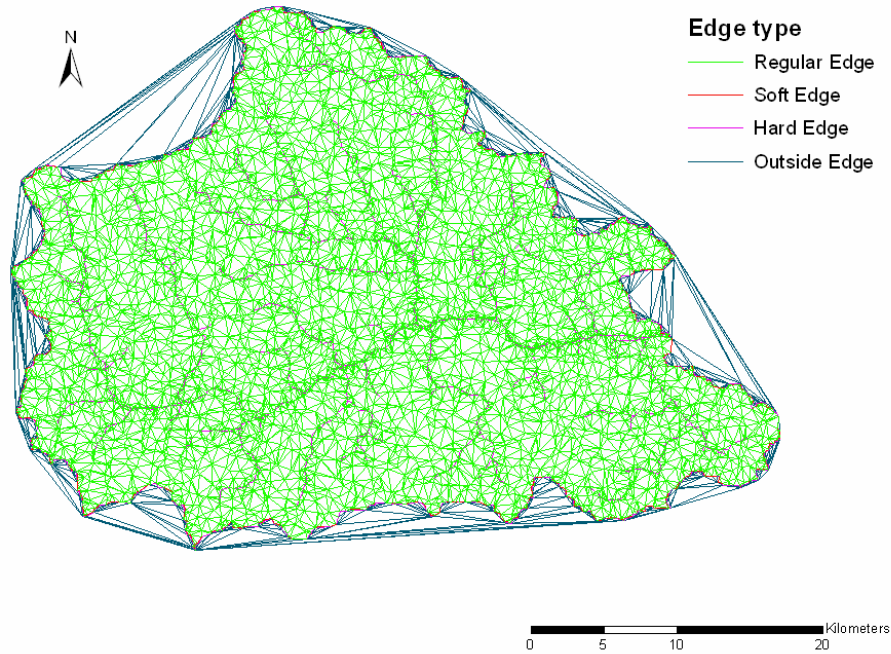


Figure 4-9 Triangular Irregular Network developed with TIAP for the Blackwater catchment

4.2.1.2 Soils

The soils map shown in Figure 4-4 has been resampled into a 200m resolution grid for the model input (see Figure 4-10). The 500m resolution appears as a trade off between the large scale data available and the resolution of the TIN mesh. The soil categories described in are regrouped into 5 groups representing the 5 main soil categories mentioned in 4.1.3 : deep well drained minerals considered as gravely loam, shallow well drained mineral considered sandy loam, poorly drained minerals (regrouping category 3 and 4) considered as clay loam, alluviums and peat.

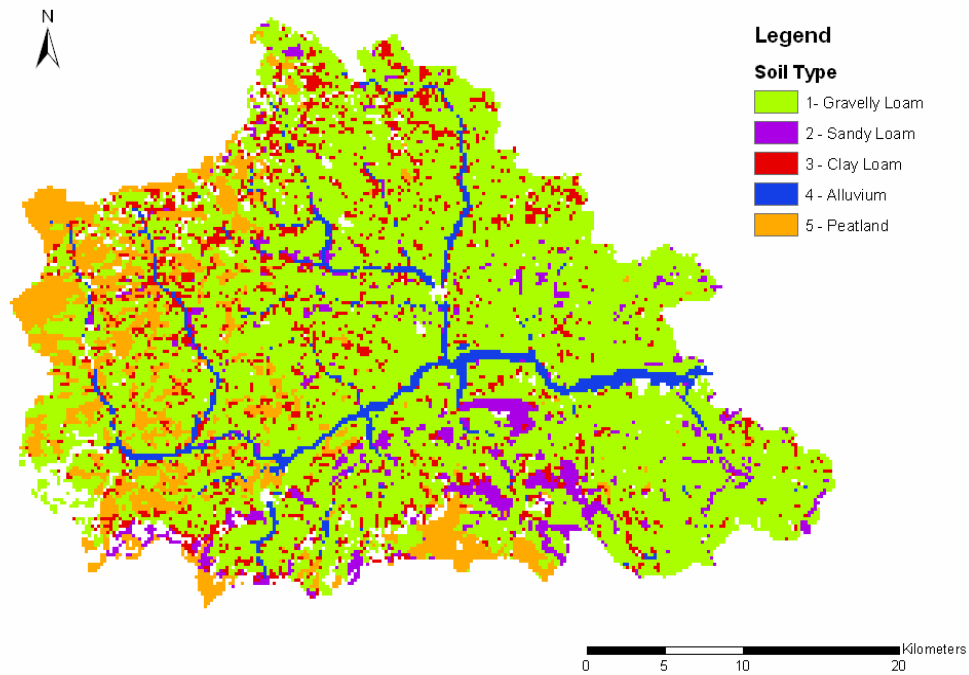


Figure 4-10 Map of the soil classification input grid

4.2.1.3 Land use

The land use map shown in Figure 4-6 is resampled into a 200m grid for the model input (see Figure 4-11). The 500m resolution is again a trade off between the large scale data available and the resolution of the TIN mesh. Four land use categories are used to describe the spatial variation of the land use in the catchment, corresponding to the four Corine land cover categories of level 1 (see Table 4-3).

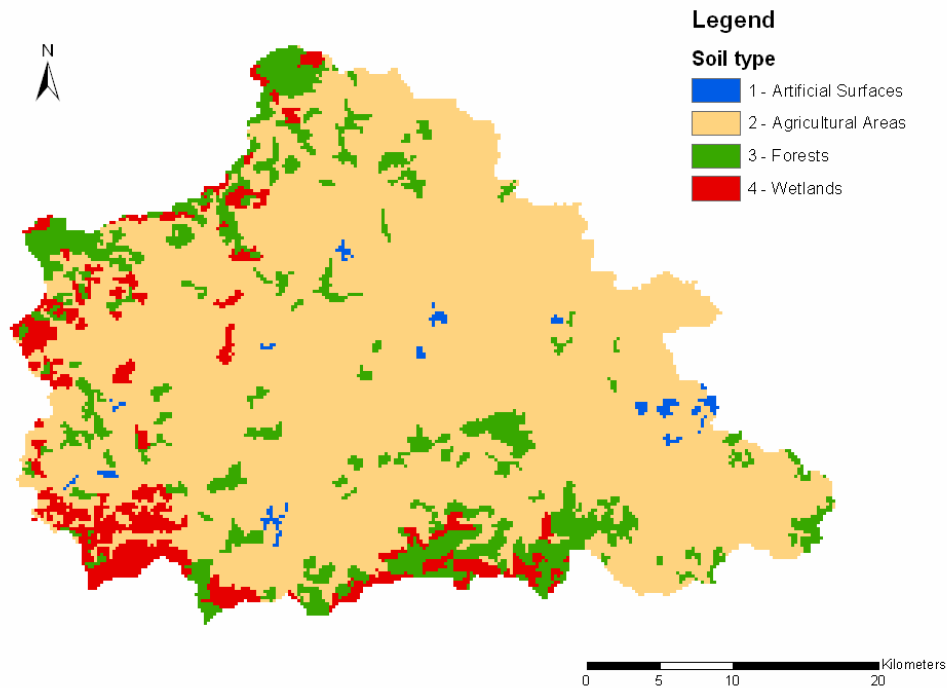


Figure 4-11 Map of the land use classification input grid

4.2.1.4 Groundwater table

The water table depth is the boundary condition that determines the initial soil moisture and therefore influences particularly the infiltration potential of the catchment. There is no data available about the depth of the groundwater, another way is therefore used to set up this input.

The method used here is considers the baseflow of the river as an indicator of the level of the groundwater table. The basin is drained until the outlet discharge corresponds to the pre-event baseflow. The topography of the groundwater table at this time is used as initialisation guess. tRIBS indeed outputs the depth of the water table at each node for any specified time of the simulation. These point values are sampled and interpolated into a grid dataset that is then used as model input for the groundwater topography (Figure 4-12).

This method is advantageous for its easy implementation. However, this method doesn't give a unique solution for the water table profile as significantly different water table level distributions may correspond to a same stream flow value. These different solutions correspond to various parameter sets that influence the release of water by the groundwater system (hydraulic conductivity K_s , decay parameters f , anisotropy ratio a_r) This method therefore poses some

problems during the calibration process as these parameters are not yet fully determined. To limit this problem the groundwater table depth is recomputed for every step of the calibration process. Other difficulties arise from assigning an initial uniform depth for the drainage simulation which introduces a lot of noises in the groundwater topography. It therefore requires some computational effort to reach a steady flow condition. Other methods for initialising the groundwater table depth are described in Ivanov (2002).

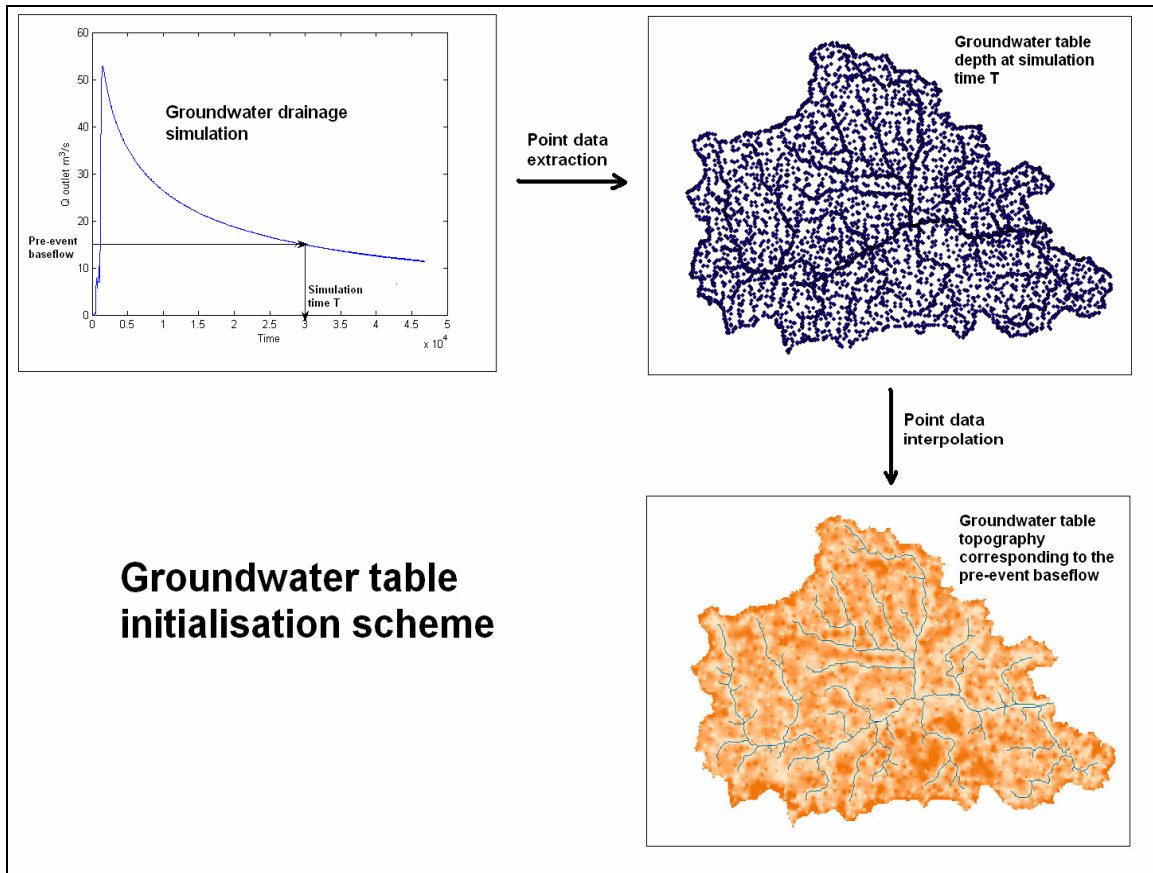


Figure 4-12 Schematic representation of the groundwater table initialisation scheme

4.2.2 Weather data

4.2.2.1 Rainfall

Rainfall is one of the main input data in rainfall-runoff modelling. It is used in both forms of gauge data and radar data during this research. As hourly rainfall data from rain gauges is not available for the catchment (only daily data is available), and as radar rainfall data is not very accurate both data have been combined to create inputs to the model.

Radar rainfall data

Radar rainfall data has been recorded by Met Eireann at Shannon Airport since 1999. The data provided is hourly intensities measured with a sensibility of 0.1mm/hr and a grid resolution of 1000x1000 meters over a 240km range. The files provided are ascii files containing a header and the data matrix as shown in Table 4-4. The header of the files is described in Table 4-5.



Figure 4-13 Met Eireann weather radars in Ireland

Table 4-4 Example of a radar rainfall data file (*.rra)

2003	4	13	12	13	5	5	1	2	480	480				
0	0	0	0	0	0	0	0	0	0	0	0	0	0	...
0	0	0	0	0	0	0	0	0	0	0	0	0	0	
0	0	0	0	0	0	0	0	0	0	0	0	0	0	
0	0	0	0	0	0	0	0	0	0	0	0	0	0	
0	0	0	0	0	0	0	0	0	0	0	0	0	0	
0	0	0	0	0	0	0	0	0	0	0	0	0	0	
0	0	0	0	0	0	0	0	0	0	0	0	0	0	
0	0	0	0	0	0	0	0	0	0	0	0	0	0	
0	0	0	0	0	0	0	0	0	0	0	0	0	0.3	
0	0	0	0	0	0	0	0	0	0	0	0.2	0.2		
0	0	0	0	0	0	0	0	0	0	0	0.2	0.5		
...														

Table 4-5 Header structure of radar rainfall data files (*.rra)

Header structure												
YYYY	MM	DD	hh	HH	A	B	C	D	XXX	YYY		
where:	YYYY	year										
	MM	month										
	DD	day										
	hh	start hour										
	HH	end hour (in this case HH=hh+1)										
	A	number of files used										
	B	number of scans used										
	C	type (0=100km version, 1=240km version)										
	D	radar (0=Shannon, 1=Dublin)										
	XXX	number of columns										
	YYY	number of rows										

Figure 4-14 shows an example of a radar image as recorded by the rainfall radar of Met Eireann. The image is centered on the radar in Shannon Airport (Latitude 52°41'31"N, Longitude 8°55'8"W, referenced at R 380 610 in the Irish National Grid). The Blackwater catchment to Mallow is shown in black contours. The grid refers to the Irish National Grid coordinates.

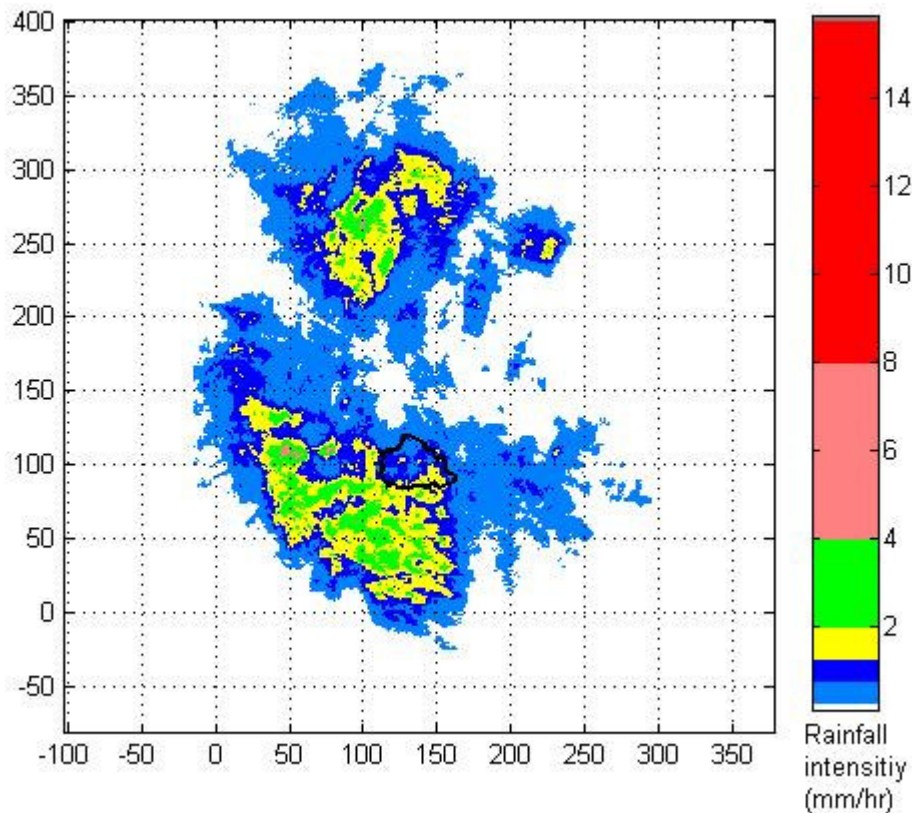


Figure 4-14 Example of a radar image

The radar data time series presents many gaps due to radar failure or maintenance. Figure 4-15 shows the radar data that is available over the period 2000-2004. Only gaps greater than 24 hours are visible on the chart. There are 4272 hours of missing radar files during that 5 years period, which represents 9.7% of the entire time series. The longest gaps occur during the year 2000 where the entire month of October is missing. The year 2004 also presents important gaps, but the rest of the time series has smaller gaps.

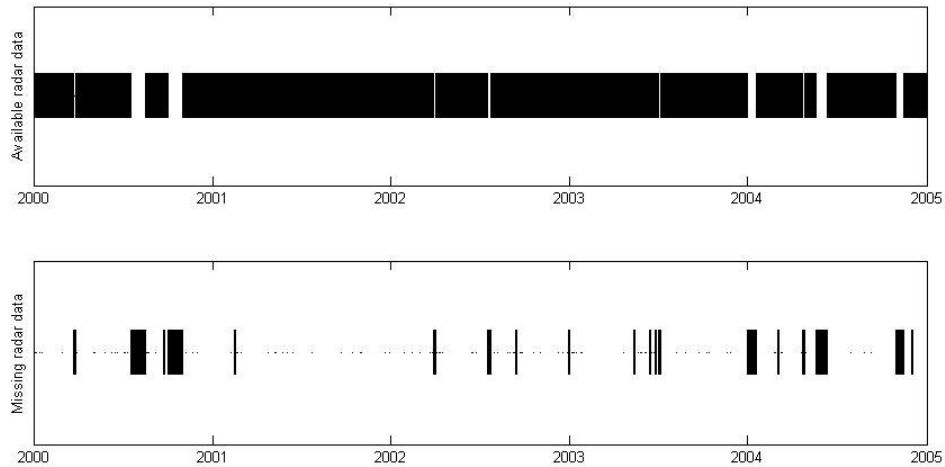


Figure 4-15 Available (top) and missing (bottom) radar data over the period 2000-2004

Weather radar measures the reflectance of raindrops (i.e. the ability of raindrop to backscatter radar waves), which is proportional to the sixth power of the size of the raindrops. The accuracy of the radar is limited by the strong dependence of the signal to drop size distribution within a rain cloud. Data accuracy is also limited by the height at which the radar samples rainfall. Due to the earth curvature the radar cannot detect rainfall below 1500m of altitude at a distance of 75km, and at 240km the limit is 4000m. Therefore the data accuracy decreases with distance to the radar. As rainfall is measured at an altitude, there also exists uncertainty concerning the spatial distribution as a droplet might fall outside the pixel where it is measure because of the wind.

There are further problems that can be encountered with radar rainfall measurements, Moore et al (2004) summarize them in Figure 4-16. These are: **1.** Radar beam overshooting shallow precipitation at long range. **2.** Low-level evaporation below radar beam **3.** Orographic enhancement over hills, which is undetected below beam. **4.** Bright-band. **5.** Underestimation of intensity of drizzle due to absence of large droplets. **6.** Bending of radar beam in presence of strong hydrolapse down to ground or sea.

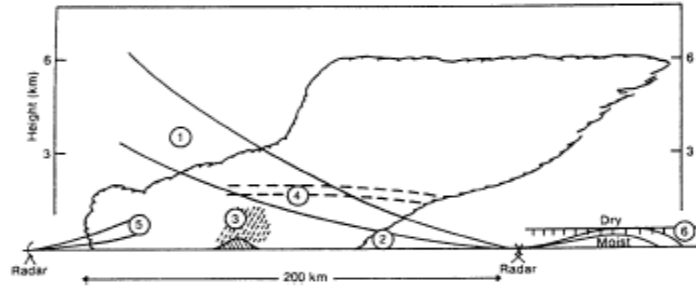


Figure 4-16 Schematic overview of problems with radar rainfall measurements [Moore et al, 2004]

The section of the Munster Blackwater study lies between 40 and 80km from the radar. The lack of accuracy due to the height of sample is therefore limited. It is assumed that the radar detects most of the rainfall in this area.

Usually weather radars are calibrated against “ground truth” raingauge measurement on the ground. However, no calibration has been done yet for the Shannon radar. The radar data is raw data and the rainfall estimation are not precise. It was therefore decided to use the radar rainfall data for its spatial distribution and correct the intensity estimation using ground raingauge measurement.

Raingauges data

There are 13 rain gauges operated by Met Eireann on the Blackwater catchment to Mallow or just around Mallow. The details and the location of the gauges is given in Table 4-6 and Figure 4-17. The data of these gauges is collected manually by Met Eireann staff. They are daily precipitation readings from 9:00 UTC of day D to 9:00 UTC of day D+1.

Table 4-6 List of the Met Eireann operated raingauges on the Blackwater catchment to Mallow

Station Number	Station Name	Latitude (North)	Longitude (West)	Grid Reference
706	MALLOW (HAZELWOOD)	52°11'25"	8°39'00"	R 556 045
1406	KANTURK	52°10'40"	8°54'00"	R 387 032
5206	NEWMARKET BALLINATONA P.H.	52°15'28"	9°02'57"	R 283 122
5706	CASTLEMAGNER	52°10'59"	8°50'27"	R 425 038
5806	FREEMOUNT PUMPING STATION	52°16'25"	8°53'20"	R 395 138
6006	BALLYDESMOND	52°10'53"	9°14'39"	R 149 040
6206	LOMBARDSTOWN (DROMPEACH)	52°05'49"	8°47'02"	W 463 942
6306	BANTEER LYRE	52°04'53"	8°51'11"	W 415 925
6506	MILLSTREET SEWAGE WORKS	52°03'58"	9°03'28"	W 275 908
6906	MILLSTREET (COOMLOGANE)	52°03'55"	9°04'45"	W 260 909
7306	NEWMARKET (NEW STREET)	52°12'55"	9°00'05"	R 314 074
7406	MALLOW (SPA HOUSE)	52°08'20"	8°38'06"	W 565 987
7506	BANTEER (GLENSOUTH)	52°04'58"	8°50'20"	W 425 926

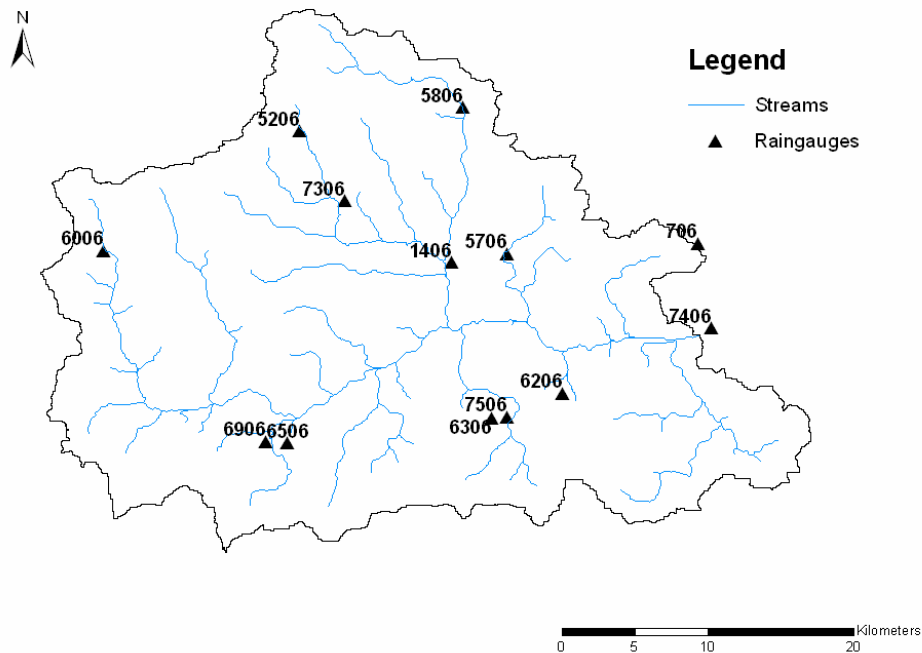


Figure 4-17 Map of the location of the Met Eireann operated raingauges on the Blackwater catchment to Mallow

The data was provided by the Met Office in tables indicating the date, the rainfall depth and an indicator code as shown in Table 4-7. The indicator code assesses the quality of the data and their description is given in Table 4-8.

Table 4-7 Example of Met Eireann raingauge data

BALLYDESMOND				
year	month	day	rain	ind
2000	1	1	0.0	4
2000	1	2	0.0	2
2000	1	3	10.5	9
2000	1	4	3.9	0
2000	1	5	10.2	0
2000	1	6	3.2	0
2000	1	7	9.1	0
2000	1	8	6.1	0
2000	1	9	1.8	0
2000	1	10	4.1	0
2000	1	11	22.4	0
2000	1	12	6.0	0
2000	1	13	1.0	0
2000	1	14	0.0	4

Table 4-8 Raingauge data indicator code description

Code	Description
0	Satisfactory
1	Estimated
2	Cumulative, no reading
3	Estimated cumulative total
4	Trace
5	Estimated trace
6	Cumulative trace
7	Estimated cumulative trace
8	Not available
9	Cumulative total

As shown in the indicator code table, there are periods of missing data and periods where rainfall depth is measured over a cumulative period of a few days. Figure 4-18 shows the availability of the data over the period 2000-2004. There are only 5 stations with continuous records over that period. All other stations show gaps in their data due to equipment failure or operator absence.

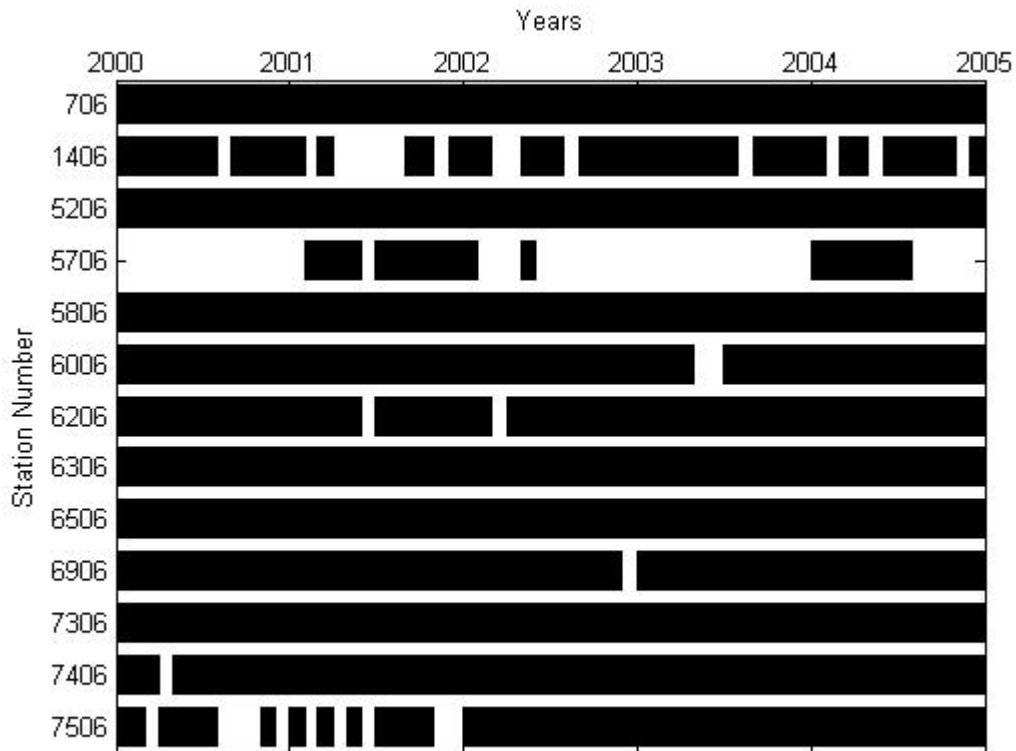


Figure 4-18 Met Eireann raingauge data availability over the period 2000-2004

The map of Figure 4-17 shows there are raingauges located close to each other: station #6506 and #6906 in Millstreet, and station #6306 and #7506 near Banteer. It was decided to use only one of each couple of station, respectively #6506 in Millstreet Sewage Works and #6306 in Banteer Lyre, for their better data consistency (see Figure 4-18). Station #5706 in Castlemagner presents very inconsistent data, with more gaps than actual values. This station was therefore not used in the study. Station #1406 in Kanturk also presents many gaps in the rainfall time series. However, the data of this station was used in the study because the missing data are mainly during summer periods and the gauge location allows denser raingauge coverage. Figure 4-19 shows the selected raingauges and their contributing area defined as the Thiessen (or Voronoi) polygon associated to each station.

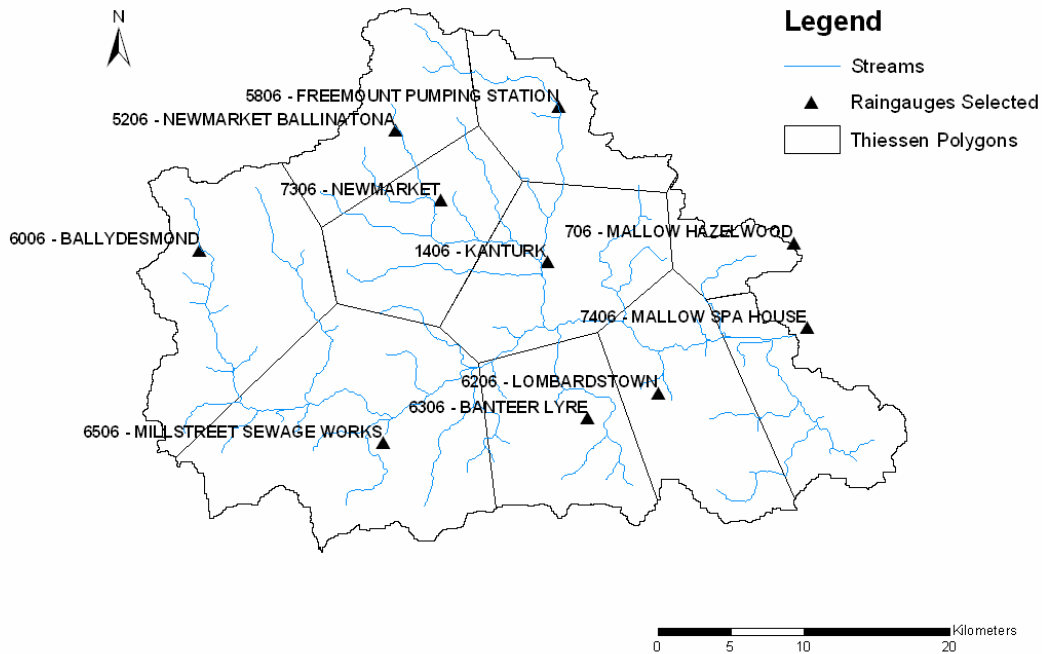


Figure 4-19 Map of the selected Met Eireann operated raingauges

Rainfall correction

Radar and raingauge data often do not match, with radar data mostly underestimating gauge data, due to the problems mentioned in section 0. It is assumed that gauge precipitation is more reliable and gives an accurate measurement of the actual rainfall. Figure 4-20 compares radar and gauge precipitation at 5 different stations on the catchment. Radar precipitation for a station is defined as the average precipitation of the pixel corresponding to the gauge location and the 9 surrounding ones, to account for the wind causing raindrops to fall outside the pixel where they are measured. It is noted that radar precipitation can underestimate actual rainfall by factor greater than 2. The example of April 2003 shows ratios of cumulative precipitation from gauge and radar measurements vary between 1.8 and 2.6 from the storm of April, 12 onwards.

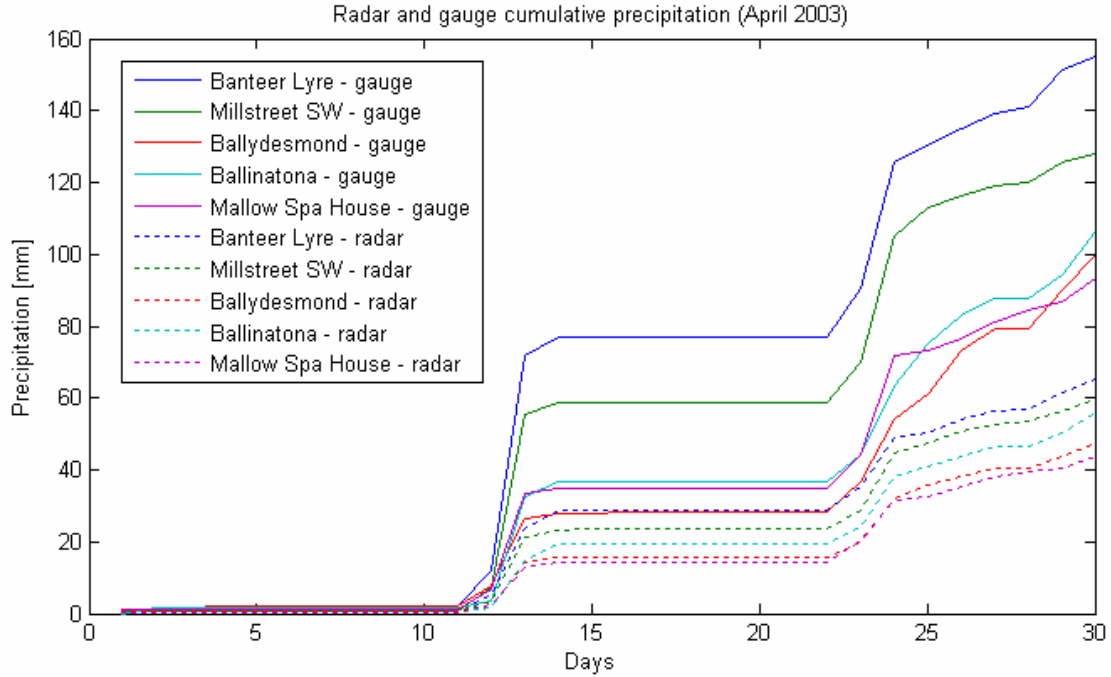


Figure 4-20 Gauge and radar cumulative precipitation comparison

It is assumed that raingauge data are more accurate than radar rainfall. However, radar data provide useful information in terms of temporal and spatial variation of precipitation. Two transformations of precipitation data have therefore been carried out to elaborate rainfall input for tRIBS: correction of radar precipitation depth and disaggregation of daily gauge measurements into hourly time series. The two types of precipitation inputs are compared in this research.

The rainfall correction undertaken for this study is not a calibration of the weather radar. Calibration of the radar would result in ‘absolute’ bias coefficients for radar data that would not be dependent on the rainfall measurements anymore. Here radar measurements are compared to raingauges measurements and corrected accounting for the depth of precipitation observed on the ground. Therefore each dataset of a period T corresponding to the time series of gauge measurements (usually one day, several days for cumulative readings) has its own bias coefficient defined as mean of the bias coefficient at every station i :

$$C(T) = \frac{1}{n} \sum_{i=1}^n C_i(T)$$

Where $n=10$ is the number of stations and:

$$C_i(T) = \frac{Pg_i(T)}{\sum_{t \in T} Pr_i(t)}$$

With $Pg_i(T)$ is the raingauge rainfall over the period T at the station i , $Pr_i(t)$ is the radar rainfall sampled at pixel corresponding to the location station i at time t and the t time series is a discretisation of the period T .

The corrected radar data then becomes:

$$\mathbf{M}^*(t \in T) = C(T)\mathbf{M}(t \in T)$$

Where $\mathbf{M}(t)$ is the original radar rainfall data matrix at time t , and $\mathbf{M}^*(t)$ is the corrected data matrix used as input.

Similarly, the desegregation produces rainfall time series Pg_i^* for each station i , at the time step of one hour corresponding to:

$$Pg_i^*(t \in T) = C_i(T)Pr_i(t \in T)$$

Figure 4-21 shows the cumulative precipitation of gauge rainfall and radar data corrected with the method described above. Corrected radar precipitation does not completely match gauge precipitation as bias coefficient applied to radar data is global, but the gaps have been significantly reduced. Ratios of cumulative gauge rainfall over corrected radar rainfall vary between 0.8 and 1.3 after the April, 12 storm.

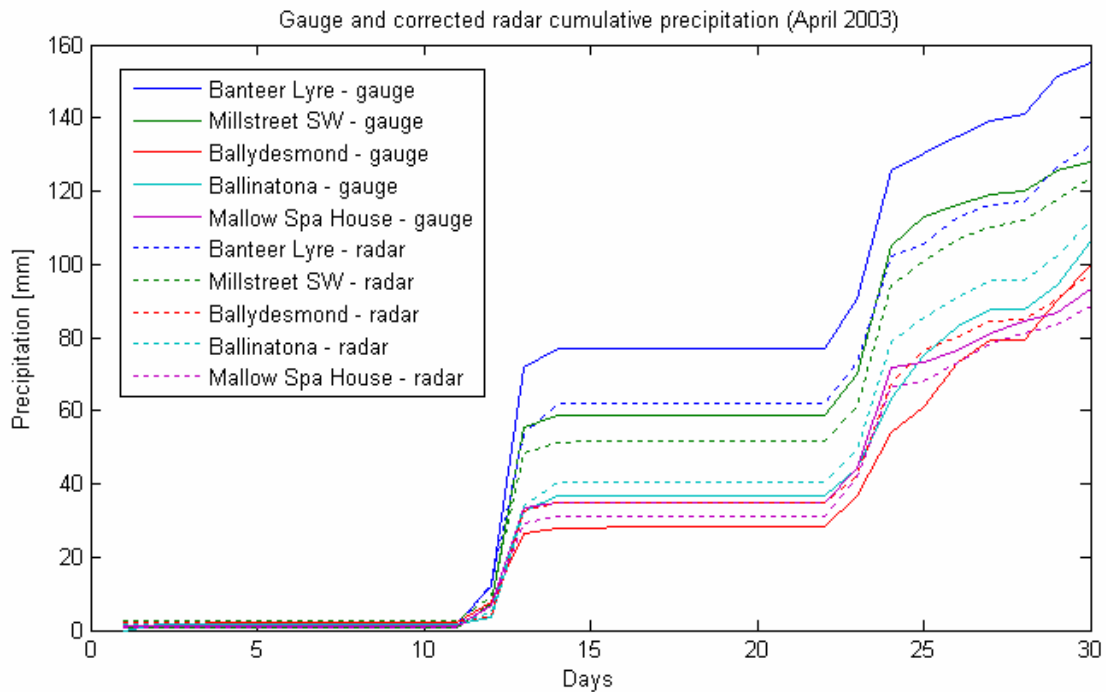


Figure 4-21 Gauge and corrected radar cumulative precipitation comparison

4.2.2.2 Meteorological data

There is no meteorological station recording continuous weather data on the catchment. Another station, operated by UCC Hydromet research group and located in Donoughmore, about 5km South of the catchment, is used for this study (Latitude 51°59'12" N, Longitude 8°45'06"W, National Grid Reference W 483 818). It is assumed that this site presents similar meteorological conditions to the Blackwater catchment. This station records most of the data necessary for the model inputs except for cloud cover since 2002. Wind speed data is however available only from 2004 onwards. The data recorded at this station is detailed in Table 4-9.

Table 4-9 Meteorological data used from Donoughmore weather station

Symbol	Data Description	Units	Available since
PA	Atmospheric Pressure	mb	1/1/2002
XR	Relative Humidity	%	1/1/2002
XC	Sky Cover	tenths	no data
US	Wind Speed	m/s	1/1/2004
TA	Air Temperature	°C	1/1/2002
TS	Soil Temperature	°C	1/1/2002
NR	Net Radiation	W/m ²	1/1/2002

4.2.3 Streamflow data

Stream flow data is used to compare the simulation output to observation and validated the model. This data is derived from river heights measured by automatic stations and transformed into flow data using rating curves (or stage/discharge curves).

4.2.3.1 River heights

There are several river gauge stations along the Blackwater River upstream of Mallow. Three of these are automatic river stations operated by the Environmental Protection Agency (EPA) on behalf of Cork County Council. They have been continuously recording river height at a time interval of 15 minutes for more than 20 years. There are also 3 stations recently installed by the Office of Public Work in Mallow town: one at the Railway Bridge, the two others directly upstream and downstream of Mallow Arch Bridge. The station at the Railway Bridge is the only location in Mallow where flows have been measured so far. This station will therefore constitute the outlet of the Blackwater catchment to Mallow. The details of the river station is given in Table 4-10 and their location is shown on the map of Figure 4-17.

Table 4-10 Automatic river station on the Blackwater River upstream of Mallow

Station No.	Station Name	River	NGR	Body resp.	Area [km ²]	Records Begin
18006	Mallow Sugar Factory	Blackwater	W 525 973	Greencore	1041	1977
18048	Dromcummer	Blackwater	W 398 993	Cork Co Co	867	1981
18050	Duarrigle	Blackwater	W 249 943	Cork Co Co	250	1981
90701	Mallow Rail Bridge	Blackwater	W 550 980	OPW	1177	2001

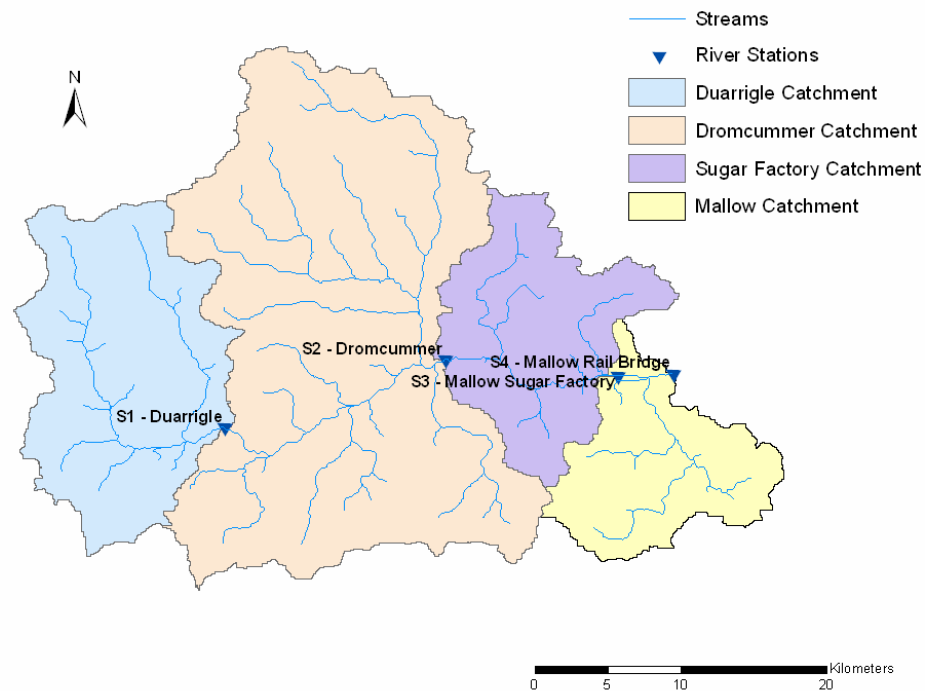


Figure 4-22 Map of the river stations and their sub-catchments

4.2.3.2 River flows

The EPA and the OPW have undertaken some flow measurements at those stations for different river heights. Rating curves have been elaborated by extrapolation of the measured data using an equation of the type:

$$Q = ah^b$$

Where Q is the stream flow in m³/s, h the river height in metres, and a and b interpolation coefficients. The rating curves for the 4 different stations are shown in Figure 4-23.

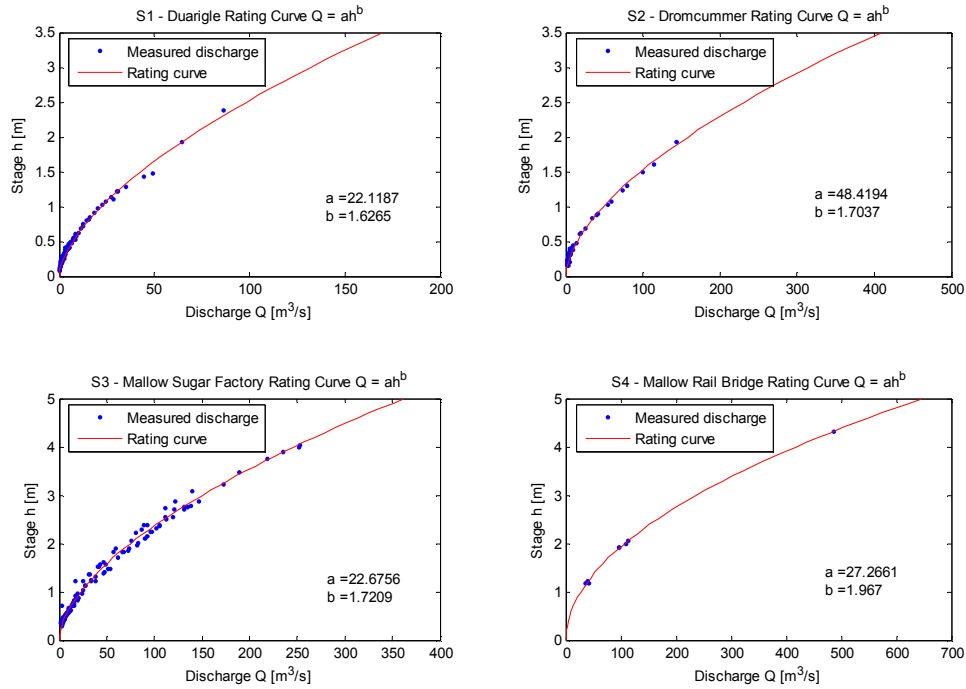


Figure 4-23 Rating curves

There is a long history of flow measurements at the stations S1, S2 and S3, as can be seen if Figure 4-23, but high flows corresponding to flood flows (stage greater than 2.5m at S1 and S2, greater than 4m at S3) have never been measured. The rating curve for those stations can therefore be considered accurate for low flow, but necessarily unreliable for flood flow. However extrapolated data are used in order to visualize flow peaks, bearing in mind that the flow magnitude might be inaccurate. Station S4 has only been installed in 2001 and there are therefore only few flow measurements. However, high flows have measured at that location, which gives more consistency to flood flow values.

Chapter 5

Results: Calibration and Validation

5.1 Model calibration

5.1.1 Model sensitivity

A model sensitivity assessment was carried out with a uniform soil and land use texture to evaluate the influence of the different parameters (e.g. hydraulic conductivity, channel roughness) on the output hydrograph. As the focus of this study is flood flows, only the impact of parameters on the outlet stream flow hydrograph is considered here. Parameter values have been changed within the range of physically realistic values and their impact on the outlet hydrograph was observed. Information about model sensitivity and calibration can also be found in Ivanov et al (2004).

5.1.1.1 Soil hydraulic properties

Soil hydraulic properties (K_{on} , f , a_r , θ_s , θ_r , n , λ , and ψ_b) control the timing and magnitude of runoff production. These are the key parameters of the model since they determine the state variables of the system. The hydraulic conductivity K_{on} and the hydraulic conductivity decay parameter f are the principal parameters controlling rainfall partitioning into runoff and infiltration. The anisotropy ratio a_r controls the magnitude of the subsurface lateral exchanges. The anisotropy ratio was considered uniform for both saturated and unsaturated subsurface flow conditions even if model inputs allow to differentiate both situations.

K_{on} and f are highly interdependent, which may result in numerous possible combinations (see Figure 5-1a-d). Hydraulic conductivity has a very important effect on the soil response to rainfall. Indeed low values of K_{on} favour runoff by infiltration excess ($K_{on} < \text{rainfall intensity}$) while high hydraulic conductivity generates runoff when the soil is saturated from below ($K_{on} > \text{rainfall intensity}$). A clear difference in the basin response from poorly conductive and well drained soils can be seen in Figure 5-1a and Figure 5-1b. In the same way higher values of f favour infiltration excess runoff and lower values of f generates more subsurface flow. As a result higher values of f and low values of K_{on} generate a fast basin response with an abrupt hydrograph, while higher subsurface flows due to low values of f and high values of K_{on} show slower basin response and with a prolonged recession limb. When subsurface flows are dominant ($K > \text{rainfall intensity}$), K and f control the timing of the production of the major runoff. Slow response corresponds to higher soil conductivity with larger depth (i.e. larger f).

The decay parameter f also controls groundwater flow and thus baseflow. High values of f essentially prohibit generation of groundwater flow and result in low baseflow while higher values of f favour higher baseflow (Figure 5-1c). The influence of f is reduced in poorly conductive soils (Figure 5-1d).

The anisotropy ratio a_r controls the magnitude of the subsurface lateral exchanges besides the direct effects of K_{0n} and f (see Figure 5-1e-f). Higher values of allow greater groundwater flow and thus baseflow for conductive soils (Figure 5-1e) but a_r has almost no influence on poorly conductive soils (Figure 5-1f). They also result in faster convergence of subsurface flows in the channel network and thus faster basin response.

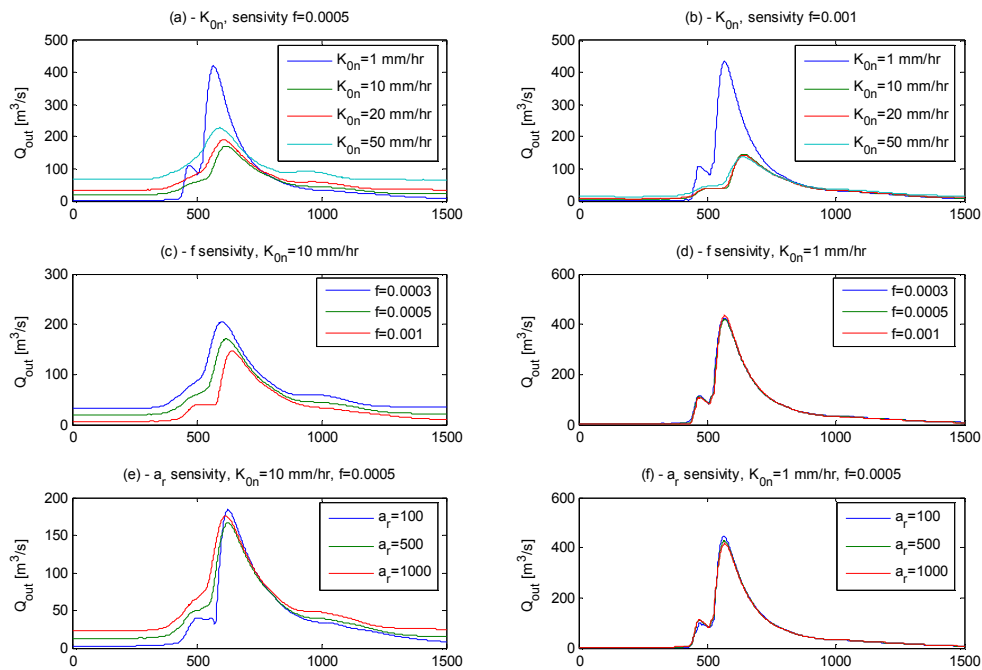


Figure 5-1 Hydraulic parameters sensitivity

The other soils parameters such as porosity n , soil moisture at saturation θ_s , or air entry bubbling pressure ψ_b , or pore distribution index λ have less direct influence on the outlet hydrograph. The soil thermal properties could not be assessed due to the problems concerning the evapotranspiration scheme.

5.1.1.2 Land use parameters

Vegetation interception parameters do not have a great influence on the shape of outlet hydrograph, as opposed to soil hydraulic properties. According to Ivanov et al (2004), the main vegetation parameters controlling the partitioning of energy fluxes are K_t , r_s , and v . However the model output revealed that the evapotranspiration scheme was not taken into account. Discussions with the model creators have not yet been able to establish the reason of the problem. Therefore, it was not possible to simulate the energy balance, and the sensitivity of the model to the relative vegetation parameters could not be assessed. However it is assumed that this problem will not affect an event-based modelling of rainfall-runoff, it would however be an issue for continuous modelling.

5.1.1.3 Routing parameters

Routing parameters c_v , r , n_e , α_B , β_B , strongly control the shape of the storm hydrograph. Channel roughness n_e , channel width-area coefficient α_B and channel width-area exponent β_B determine channel characteristics and control the speed of the wave propagation. Lower values of n_e , α_B and β_B result in faster response (see Figure 5-2). As their value increase the propagation of the flood wave travels slower and the shape of the hydrograph becomes less steep. As their influence is quite similar, various sets of parameter can potentially have the same influence.

Coefficient c_v and r controlling overland flow routing are strongly interdependent and have similar influence on the arrival of the flood wave at the outlet to previous parameters. High values of c_v and low values of r mean higher hillslope velocities for runoff waters and result in faster basin response whereas lower values of c_v and higher values of r result in slower basin response (see Figure 5-2).

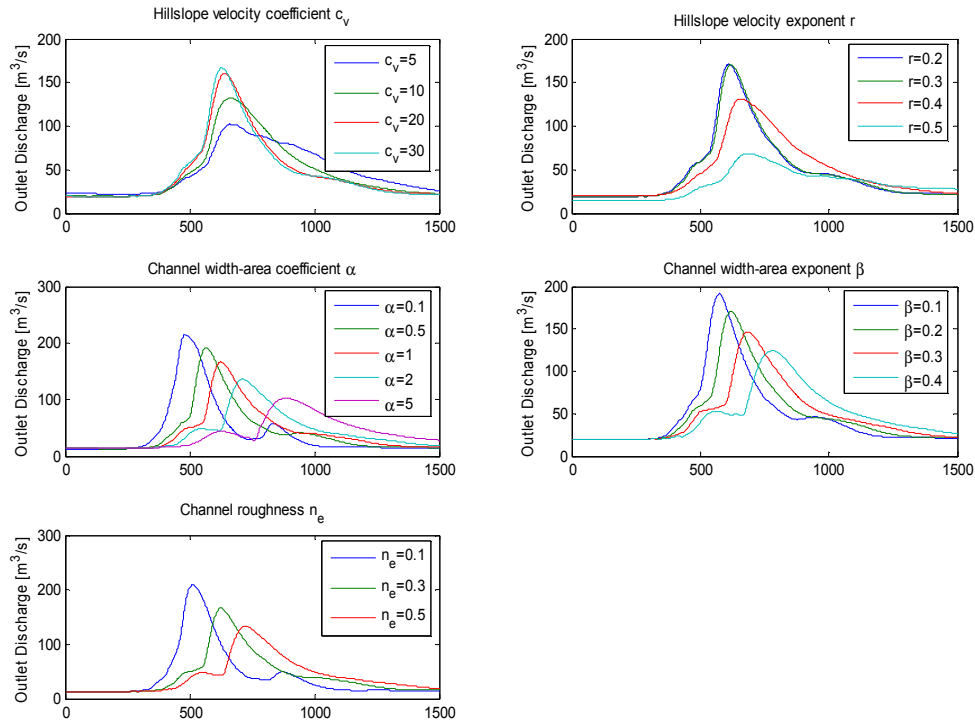


Figure 5-2 Routing parameters sensitivity

5.1.2 Calibration strategy

The calibration effort focused first on soils hydraulic properties K_{on} (soil hydraulic conductivity), f (decay parameter) and a_r (anisotropy ratio) and secondly on routing parameters c_v , r , n_e , α_B and β_B . Vegetation properties and the remaining soil parameters values were obtained from the literature. The calibrated parameters were adjusted by comparing the simulated hydrographs at the outlet and the three stations in the catchment. Stream flow observations at the outlet of the catchment (S4) and in the catchment (S1 – S3) were compared to the simulated hydrograph to calibrate the parameters.

5.1.2.1 Calibration period

The calibration period used to compare simulation hydrographs to observed stream flows was the month of April 2003. This period produced a time series of gauge rainfall without gaps. The gaps in radar data occurred for only few hours and no rain was recorded during that period. This period was also chosen for its hydrograph presenting a long initial base flow and clearly identified peaks, which makes the calibration effort easier. The hydrograph over this period at

Mallow (S4) and the three interior gauges is shown in Figure 5-3. Attention was given to the first of the two peaks.

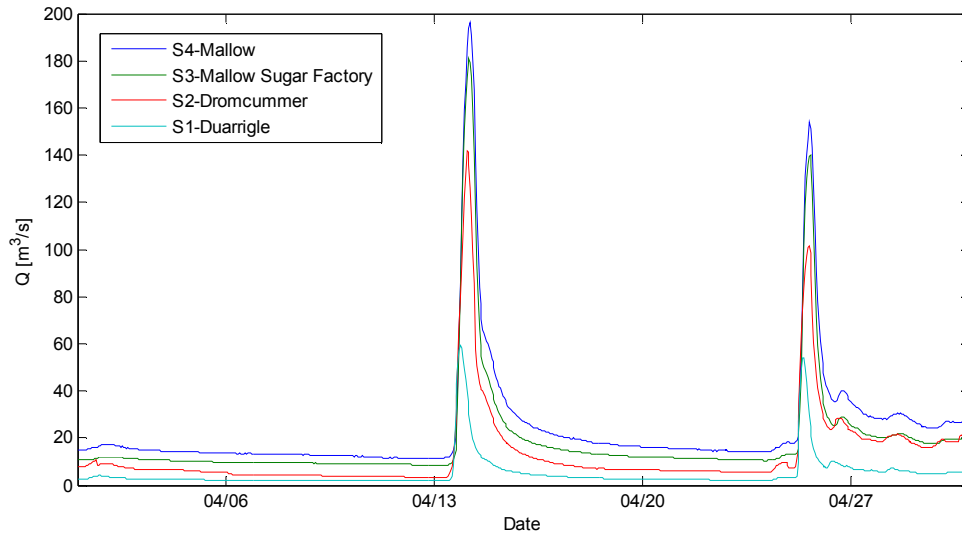


Figure 5-3 Flows at the 4 stations for the calibration period

5.1.2.2 Soil parameters

Hydraulic conductivity $K_{0n,s}$, decay parameters f and anisotropy ratio a_r were calibrated for the five different kind of soils presented in chapter 4. Soils parameters were found in the literature for the four first types of soils with reference to their texture. Peat has been treated separately as its characteristics differ from the other four one.

Initial values for saturated hydraulic conductivity for the four first soil types are derived from tables (see Table 5-1)

Table 5-1 Saturated hydraulic conductivity range

Soil ID	Soil Texture	K_{0n} range [mm/hr]*
1	Gravelly Loam	15 - 50
2	Sandy Loam	5 - 15
3	Clay Loam	0.5 - 5
4	Silty Clay Loam	5 - 15

* source: Institute of Arctic and Alpine Research, University of Colorado

Decay parameters f for each of the soils were assumed to be in accordance with the depth of the different soil layer. Thus deep well drained mineral soils and deep poorly drained mineral soils were assumed to have lower f values than shallow well drained mineral soils and alluviums. No prior assumption was made on the anisotropy ratios from soil texture information. Their values were however assumed to range between 100 and 1000 approximately according to Ivanov et al (2004).

Peat soils were assumed to have a low conductivity and high decay parameter alongside with a low anisotropy ratio, as peat land observations show that this type of soils is poorly drained and retains most the water it absorbs.

These three parameters were calibrated focusing mainly on shape of the hydrograph, the magnitude of the peak discharge and baseflow. The other soils parameters were obtained from the literature and were assigned the values described in Table 5-2.

Table 5-2 Uncalibrated soil parameter values

ID	Soil Texture	θ_s *	θ_r	ψ_b [mm]*	n	λ^{**}	k_s [J/msK]**	C_s [J/m ³ K]**
1	Gravelly Loam	0.40	0.04	-90	0.44	0.4	0.5	1,200,000
2	Sandy Loam	0.44	0.04	-90	0.48	0.4	0.5	1,200,000
3	Clay Loam	0.48	0.04	-480	0.52	0.3	0.5	1,200,000
4	Silty Clay Loam	0.48	0.04	-200	0.52	0.3	0.5	1,200,000
5	Peat	0.80	0.04	-100	0.85	0.5	0.5	1,200,000

* source: Clapp and Hornberger (1978) for soils 1-4

** source: Ivanov et al (2004) for soils 1-4

5.1.2.3 Vegetation parameters

Vegetation parameters were adapted from vegetation from Ivanov et al (2004) and the data available on the tRIBS website. The parameters were assigned the values described in Table 5-3.

Table 5-3 Uncalibrated land use parameters

ID	Land use	p	S [mm]	K [mm/hr]	g [mm ⁻¹]	a	H_v [m]	Kt	r_s [s/m]	v
1	Artificial Surfaces	0.90	1.0	0.10	4.0	0.13	0.1	0.8	100	0.10
2	Agricultural areas	0.65	0.8	0.10	3.2	0.20	0.3	0.75	70	0.65
3	Forests	0.30	1.1	0.20	4.1	0.15	12.0	0.60	100	0.60
4	Wetlands	0.50	0.9	0.15	3.8	0.20	0.1	0.70	80	0.50

Source: New Mexico Tech - tRIBS

5.1.2.4 Routing parameters

The five routing parameters were calibrated to adjust the timing of the peak discharges. The first effort was made on the hillslope velocity coefficient and exponent c_v , and r . Channel roughness n_e usually takes values around 0.3 for river beds. Calibration of this parameter was sought around that value.

Channel width-area coefficient and exponent can be obtained from cross-section measurements. These parameters link channel width W to the contributing area A in the equation $Y = \alpha A^\beta$. Cross sections were measured on 1:5000 scale digital maps at the four stations S1 to S4 on the basin (see) to approximate initial values of α_B and β_B .

Table 5-4 River cross sections

Station	Location	Cross section W [m]	Contributing area A [km ²]
S1	Duarrigle	25	250
S2	Dromcummer	35	867
S3	Mallow Sugar Factory	37	1041
S4	Mallow	42	1177

Interpolation of these measurements and the contributing areas lead to the values $\alpha_B=0.05$ and $\beta_B=0.3$. As the measurements of cross-section could not be precise, these values were only used as a reference for initial simulations and were subject to further calibration.

5.1.3 Calibration results

The resulting simulation hydrographs are shown in Figure 5-4. As the focus was mainly on the first of the two peaks, good performance was attained for this one at the 4 different stations. Peak timing, peak discharge and baseflow match quite well at Duarrigle (S1), Mallow Sugar Factory (S3) and Mallow (S4), and peak discharge at Dromcummer is slightly over estimated. The second peak flow is over estimated at the four locations but timing and baseflow match reasonably well. The hydraulic and routing parameters resulting from this calibration are listed in Table 5-5 and Table 5-6 respectively.

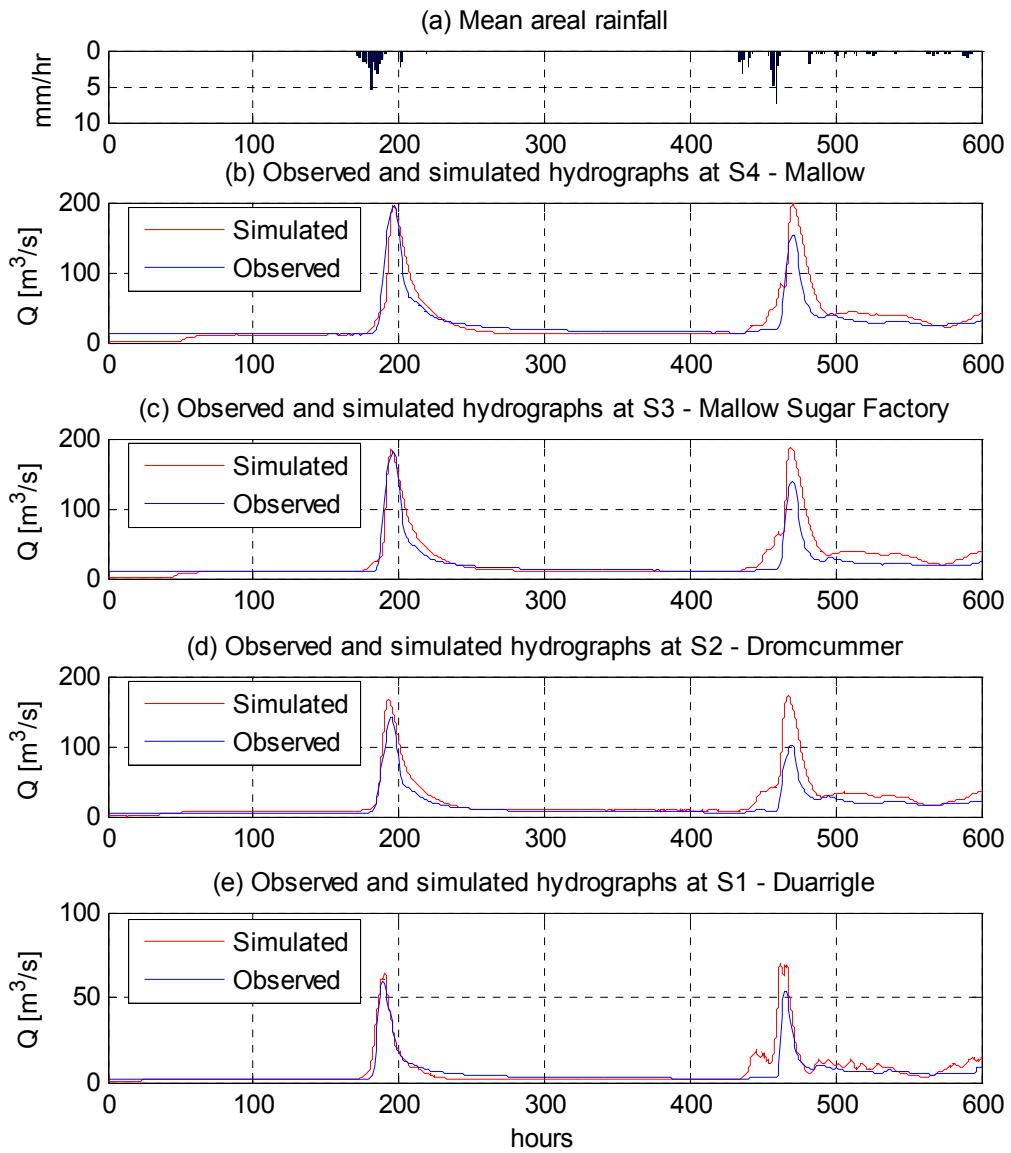


Figure 5-4 Calibration simulations output hydrographs

Table 5-5 Calibrated hydraulic parameters

Soil ID	Soil Type	K_{0n} [mm/hr]	f	a_r
1	Gravelly Loam	30	0.0005	800
2	Sandy Loam	10	0.001	800
3	Clay Loam	1	0.0005	400
4	Silty Clay Loam	5	0.001	600
5	Peat	0.5	0.001	50

Table 5-6 Calibrated routing parameters

Parameters	Calibration value
c_v	12
r	0.3
α_B	0.9
β_B	2.0
n_e	0.3

5.2 Model evaluation -Water Balance

A water balance was calculated for a simulation running for a period of 720 hours (30 days) from January, 10th at 00:00 to February 9th at 00:00.

5.2.1 Water balance equation

The equation for the water balance is the equation of mass conservation of water in the lumped catchment:

$$P = R + E + \Delta S + \Delta G$$

Where: P : precipitation

R : stream runoff

E : evapotranspiration

ΔS : change in soil moisture status

ΔG : change in groundwater status

All the variables are here expressed in mm.

5.2.2 Precipitation

The precipitation P is obtained directly from the model output by the summation of the mean areal rainfall

$$P = \sum_i MAP_i \Delta t$$

Where MAP_i : mean areal precipitation at time step i [mm/hr]

Δt : output time step [hrs]

5.2.3 Stream runoff

The stream runoff is obtained from the output hydrograph by integration of the streamflow over the simulation period and dividing it by the catchment area.

$$R = \frac{\sum_i \frac{Q_i + Q_{i+1}}{2} \Delta t}{A}$$

Where Q_i : streamflow at time step i [m^3/s]

Δt : output time step [s]

A : catchment area [m^2]

5.2.4 Evapotranspiration

The evapotranspiration scheme in the model was turned off. Therefore there is no evapotranspiration taking place in the simulation and $E=0$.

5.2.5 Soil moisture status

The change in soil moisture is evaluated using the spatially distributed state variable data for the total soil moisture in the unsaturated zone, which outputted by the model at the start and at the end of the simulation. Total soil moisture in the unsaturated zone is calculated by the model for each node of the TIN mesh (except for stream nodes) in mm. The volume of water retained in the unsaturated zone is calculated for each Voronoi cell and the total amount is divided by the catchment area.

$$\Delta S = \frac{\sum_i moist_{end,i} a_i - \sum_i moist_{init,i} a_i}{A}$$

Where $moist_{init,i}$: soil moisture of the Voronoi cell i at the start of the simulation [mm]

$moist_{end,i}$: soil moisture of the Voronoi cell i at the end of the simulation [mm]

a_i : area of the Voronoi cell i [m^2]

A : total area of the catchment [m^2]

5.2.6 Groundwater

The change in the groundwater status is estimated in using the spatially distributed state variable data for water table depth, which outputted by the model at the start and at the end of the simulation. The variation of volume of the groundwater is calculated for each Voronoi cell, integrated over the whole catchment and divided by the catchment area.

$$\Delta G = -\frac{\sum_i WTd_{end,i} a_i - \sum_i WTd_{init,i} a_i}{A}$$

Where $WTd_{init,i}$: water table depth of the Voronoi cell i at the start of the simulation [mm]

$WTd_{end,i}$: water table depth of the Voronoi cell i at the end of the simulation [mm]

a_i : area of the Voronoi cell i [m²]

A : total area of the catchment [m²]

5.2.7 Results

The computation carried out as described above gave the following results:

$$P = 265 \text{ mm}$$

$$R = 175 \text{ mm}$$

$$\Delta S = 90 \text{ mm}$$

$$\Delta G = -14 \text{ mm}$$

$$\text{Hence } R + \Delta S + \Delta G = 251 \text{ mm}$$

$$\text{And } P - (R + \Delta S + \Delta G) = 14 \text{ mm}$$

Hence a difference of 5.3%

5.3 Model assessment for flood forecasting

5.3.1 Model validation on flood event

Accuracy of the flow predictions is the essential part of a flood forecasting model. The accuracy of flow estimation by tRIBS using the inputs details in chapter 4 and the calibrated parameters of 5.1 was tested on different flood events that occurred in Mallow between 2002 and 2005.

5.3.1.1 Flood events

There were 6 major flood events recording river levels higher than 3.50m (or a discharge of 320m³/s) between 2002 and the beginning of 2005. The details of the flood events are shown in Table 5-7.

Table 5-7 Major flood events between 2002 and 2005

Flood Event	Year	Flood period	Peak date	Peak time	Peak height [m]	Peak discharge [m ³ /s]
1	2002	23-Jan to 24-Jan	23-Jan	23:00	3.50	320
2	2002	01-Feb to 02-Feb	02-Feb	00:00	3.93	403
3	2003	13-Nov to 15-Nov	15-Nov	06:00	3.63	342
4	2004	27-Oct to 30-Oct	28-Oct	13:00	4.37	496
5	2004	18-Dec to 20-Dec	19-Dec	14:00	3.68	354
6	2005	07-Jan to 08-Jan	08-Jan	13:00	3.86	389

Rainfall-runoff simulations were performed for 5 of the 6 flood events mentioned in Table 5-7 as validation for the calibrated parameters and the assessment of the model to forecast flood flows. No simulation was performed for the flood event No.5 due to missing radar rainfall data during the event which lead to erroneous disaggregation of daily rainfall data with the algorithm described in chapter 4. Some radar files were missing for the other flood events. However these missing files were replaced by zero rainfall data since rainfall data in the previous and following hours showed little or no rainfall, or because they did not influence the flood discharge as they were recorded at least two days after the flood peak. The floods No.1 and No.2 of January and February 2002 were simulated together as there was only a few days between both events. Details of the simulation periods are given in Table 5-8.

Table 5-8 Flood events simulations

Flood Simulation	Flood Event	Simulation Period	Simulation Length [hrs]	Missing radar files
1	1 & 2	10-Jan-02 to 9-Feb-02	720	2
2	3	01-Nov-03 to 21-Nov-03	480	1
3	5	05-Dec-04 to 25-Dec-04	480	0
4	6	26-Dec-04 to 15-Jan-05	480	4

5.3.1.2 Simulation results

The output hydrograph at the catchment outlet are presented in Figure 5-5 to Figure 5-8. The shapes of the simulated hydrographs follow the shapes of the observed ones. However, simulated flows tend to underestimate the actual flows, especially for high discharges. The volumes of water in the simulated hydrograph are smaller than the observed ones. The simulation seems slightly late for small peak discharges but ahead of the observed peaks for high discharges. It can also be noted that when two consecutive peaks occur, the second peak is mostly underestimated.

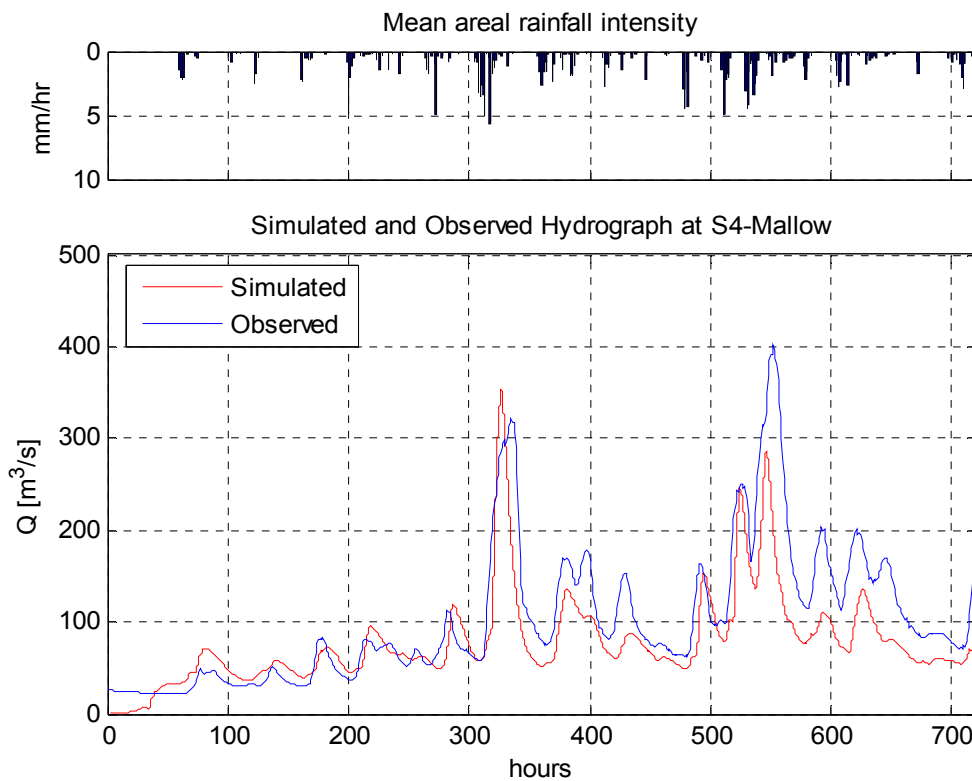


Figure 5-5 Simulation 1 - Flood events 1&2 - 10-Jan-02 to 09-Feb-02

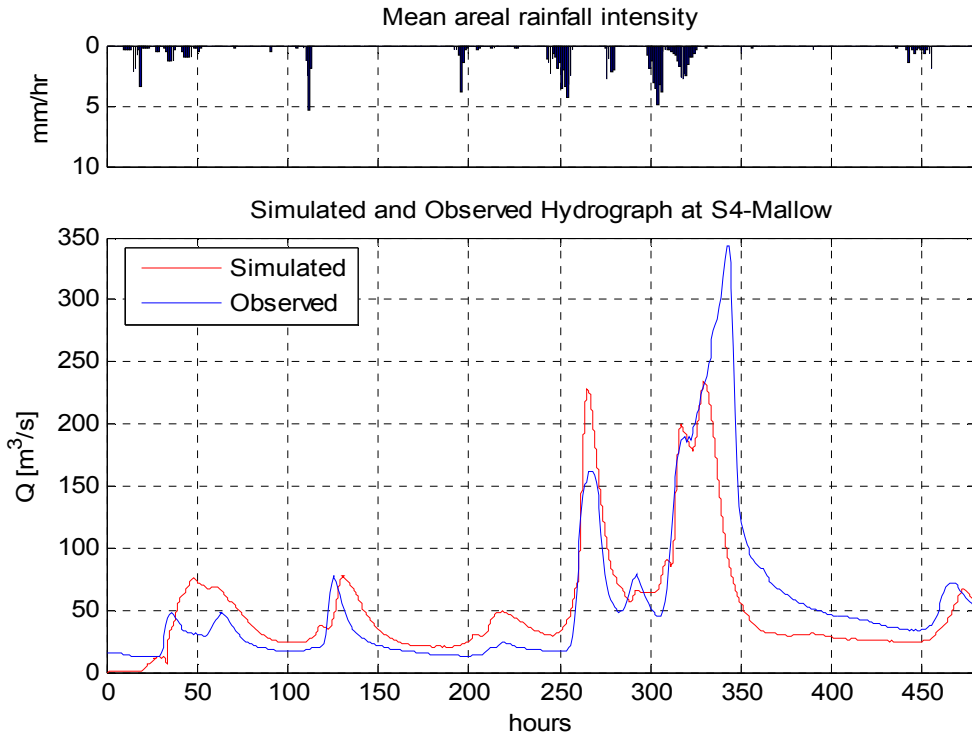


Figure 5-6 Simulation 2 - Flood event 3 - 01-Nov-03 to 21-Nov-03

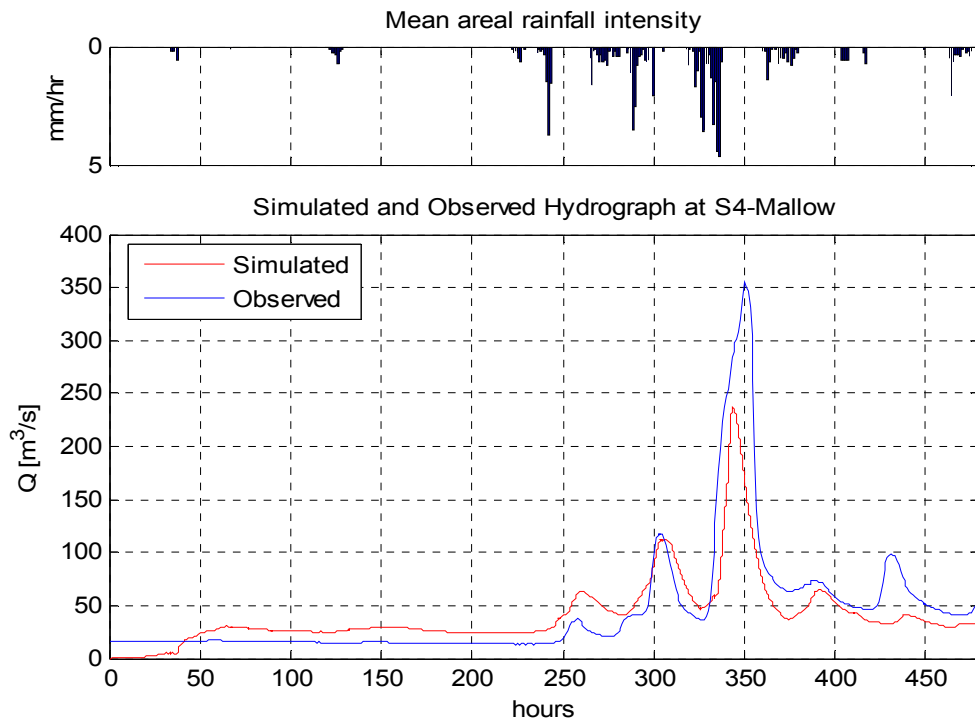


Figure 5-7 Simulation 3 - Flood event 5 - 05-Dec-04 to 25-Dec-04

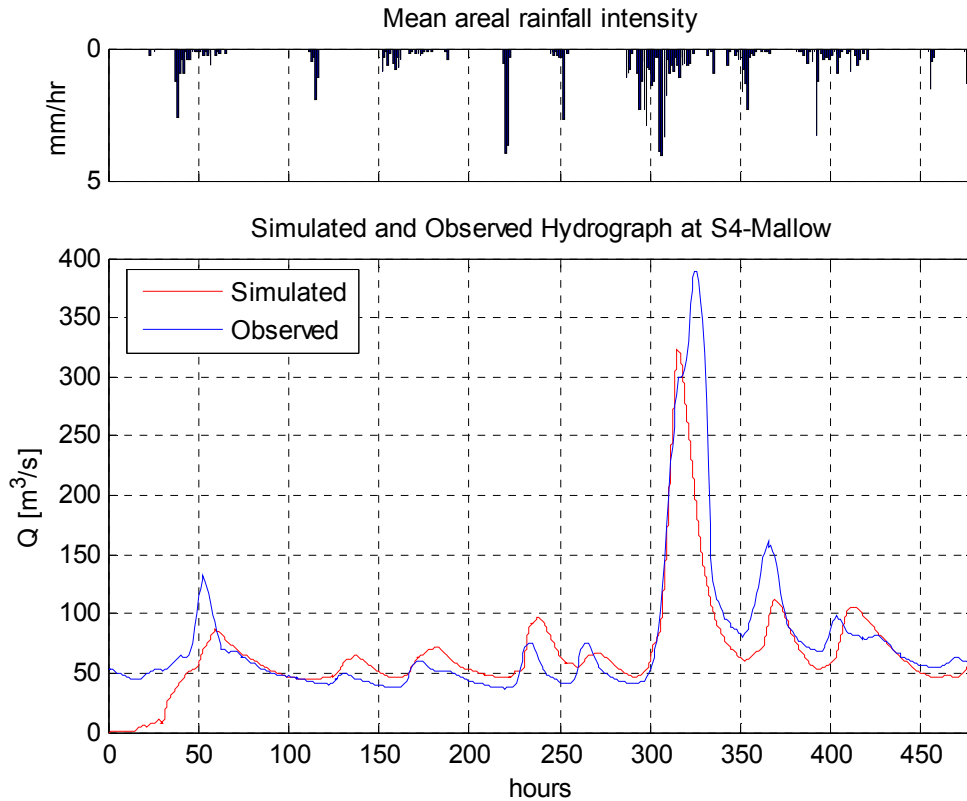


Figure 5-8 Simulation 4 - Flood event 6 - 26-Dec-04 to 15-Jan-05

The timing and magnitude of the peak discharges for the four simulations were examined in order to assess its potential use for flood forecasting and flood warning. The comparison of peak discharge is detailed in Table 5-9, and peak timing comparison is shown in

Table 5-10. Except for the first flood event where the peak discharge is overestimated by a mere 11%, the four other peaks are underestimated, and three of them by about 30%. As far as timing is concerned, the peaks arrive slightly before the observed ones with an advance ranging from 5h30min to 12h.

Table 5-9 Observed and simulated peak discharge

Flood event	Flood simulation	Observed peak flow [m ³ /s]	Simulation peak flow [m ³ /s]	Error (Sim-Obs)	Error % (Err/Obs)
1	1	320	354	+34	+11%
2	1	403	286	-117	-29%
3	2	342	234	-108	-32%
5	3	354	238	-116	-33%
6	4	389	324	-65	-17%

Table 5-10 Observed and simulated peak times

Flood event	Flood simulation	Observed peak flow time	Simulated peak flow time	Error (Obs-Sim)
1	1	23-Jan 23:00	23-Jan 14:30	08:30
2	1	02-Feb 00:00	01-Feb 18:30	05:30
3	2	15-Nov 06:00	14-Nov 18:00	12:00
5	3	19-Dec 14:00	19-Dec 08:00	06:00
6	4	08-Jan 13:00	08-Jan 03:30	09:30

5.3.1.3 Discussion

Applied in a flood forecasting system with a the threshold discharge for a flood in Mallow of 250m³/s (or 4m at Mallow Sugar Factory, according to Steinmann (2004)), the model would have warned for 3 floods, slightly overestimating the level of the event No.1 (by 11%), underestimating slightly the event No.5 (by 17%) but largely underestimating No.2 (by 29%), which was the highest of the five. It would have missed the flood events No.3 and No.4 as the predicted flood peak discharges were only of 234 and 238 m³/s respectively. It seems in this situation not suitable for flood forecasting. The main concern raised by these simulations is about the calculated discharge volumes which are underestimated by the model simulations.

One of the reasons could be the overestimation of the storage capacity of the basin, which means that the calibration parameters are not optimum or that the initial water table depth did not match the actual. The underestimation of the second of two consecutive peaks and the difference in the timing of small peak discharges and high peak discharges also questions the reliability of the calibration parameters.

However baseflows are underestimated as well. Baseflows would be expected to raise in the case of the slower release from a groundwater system with more storage capacity. Therefore another reason for the underestimation of the river flows could be the accuracy of the rainfall data. These might be underestimated because of the underestimation of their measurements, or the correcting algorithm which does not compensate enough for it.

A third reason of the underestimation of peak flows and flow volumes could lie in the reliability of the rating curves used to evaluate flows from stage measurements. Flows measurements in Mallow were indeed very limited as the station was installed only four years ago (i.e. in 2001). There are indeed no flow measurements for river stages between 2m and 4.3m, and thus no flow measurements between 115m³/s and 480m³/s, which is the range of the studied flood

peaks. It might be that the rating curve equation used to interpolate flows is not good enough for this gauge.

5.3.2 Radar – raingauges comparison

5.3.2.1 Simulations

As radar rainfall data seem to underestimate actual rainfall (by comparison with the raingauges) it was considered to use raingauge measurements to compare the two types of inputs. The gauge data used is daily data disaggregated into hourly data using the radar data as in the algorithm described in chapter 4.

The hydrographs comparing the flood simulations described in 5.3.1.1 using disaggregated raingauge data and corrected radar data are shown in Figure 5-9 to Figure 5-12.

Simulated flows with raingauge data input tend to be lower than those simulated with corrected radar rainfall, both in low and peak flows. Simulation 3 however show better results with raingauge input than with radar rainfall, mainly in the timing and the magnitude of the flood peak, but is still below the observed one.

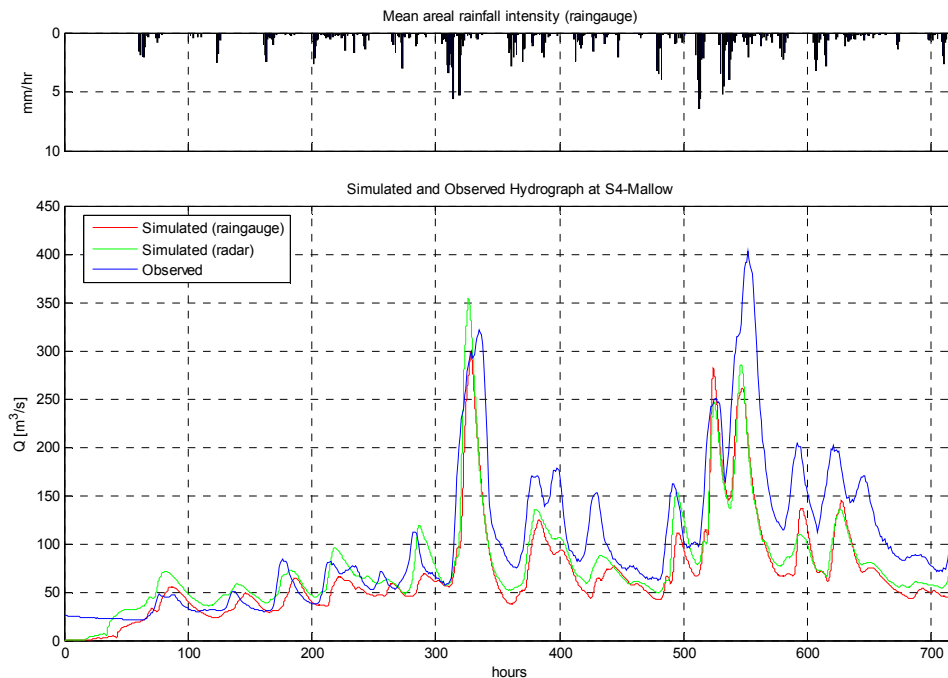


Figure 5-9 Simulation 1 (with raingauges) - Flood event 1& 2 - 10-Jan-02 to 09-Feb-02

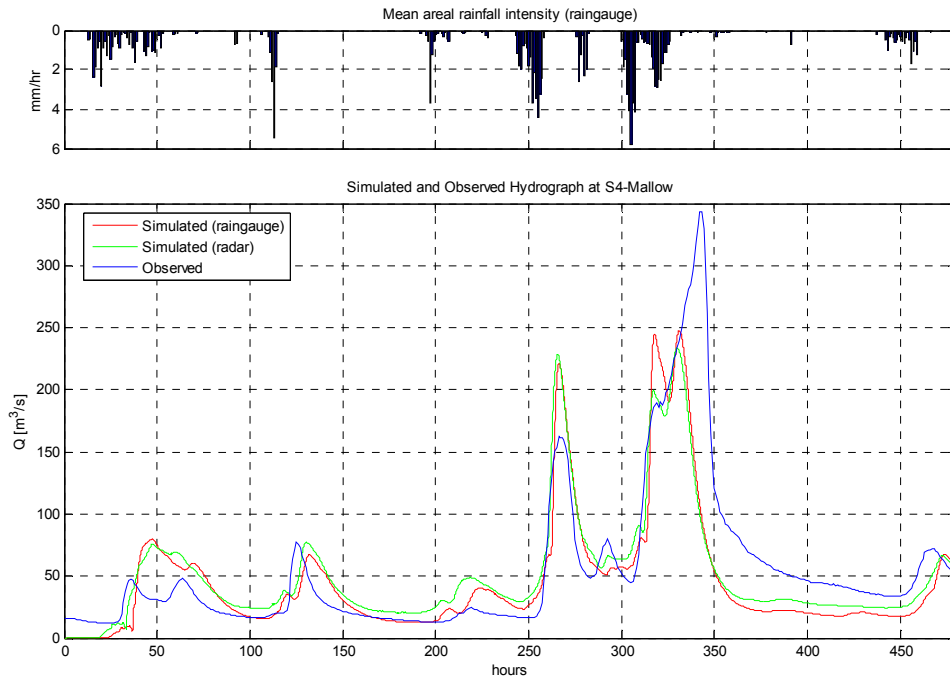


Figure 5-10 Simulation 2 (with raingauges) - Flood event 3 - 01-Nov-03 to 21-Nov-03

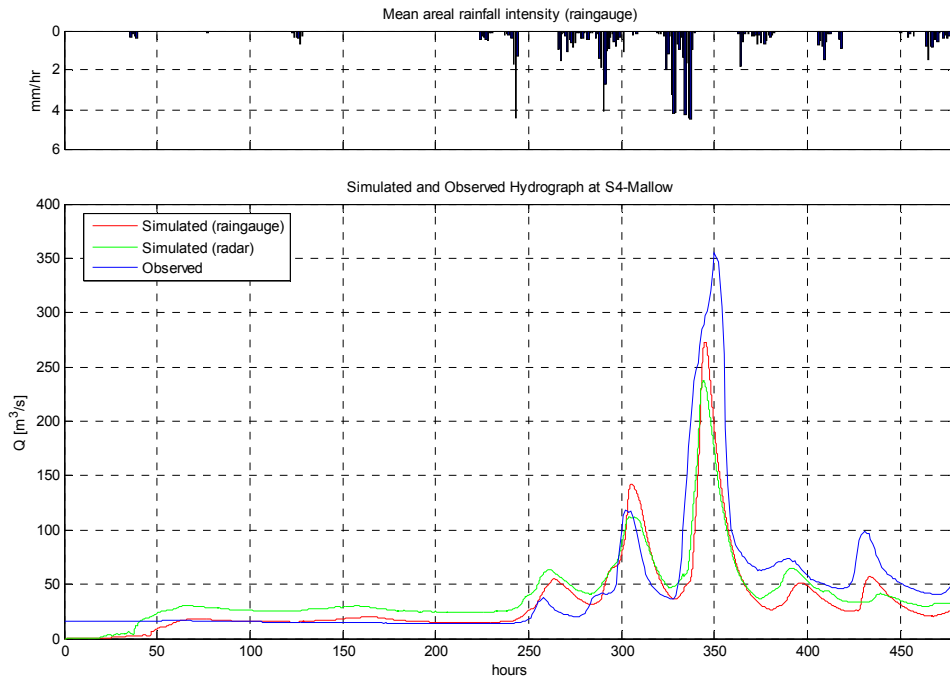


Figure 5-11 Simulation 3 (with raingauges) - Flood event 5 - 05-Dec-04 to 25-Dec-04

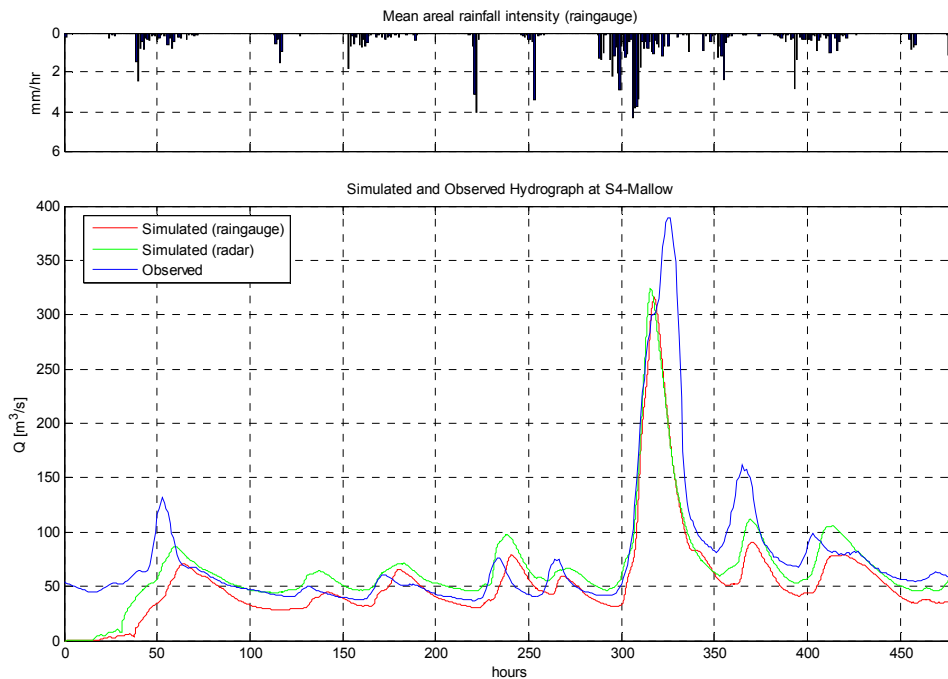


Figure 5-12 Simulation 4 (with raingauges) - Flood event 6 - 26-Dec-04 to 15-Jan-05

5.3.2.2 Discussion

Simulations using disaggregated radar data do not show better results than simulations using corrected radar data, and the issue about flow volume still remains. Raingauge rainfall is believed to be more accurate than radar measurements, thus point rainfall depth might be better represented, but it does not allow representation of the spatial variability of a rainfall event. The data is indeed resampled into uniform values over the Thiessen polygons associated with each raingauge. It is therefore possible that raingauges miss the place of high or on the opposite low precipitation intensities. On the other hand, radar data better represents spatial rainfall variations but the algorithm used to correct the data applies a uniform bias for the whole catchment and, in a way, averages the data instead of accounting for local variation due to elevation or distance from radar. These results shows that radar rainfall is more relevant than raingauge as model input.

However the small difference in flow volumes between the two types of simulation questions even more the calibration parameters and the consistency of the rating curves used to estimate flood flows. These results also show that calibration is even more difficult as it depends on the rainfall input.

5.3.3 Potential warning time

Besides the accuracy of the forecasting, the other important factor in flood forecast is how long ahead the forecast is issued, and thus how much time it allows to respond to the flood.

5.3.3.1 Simulation

The 5 flood events were simulated at different dates from $T=T_f-24$ to $t=T_f$, where T_f is the time of the simulated flood peak. Each simulation takes into account the radar precipitation from the start of the simulation $t=0$ of the simulation to simulation date $t=T$ and considers zero rainfall over the catchment for the rest of the simulation from $t=T$ to $t=T_{end}$. This allows us to see how rainfall actually measured transforms into river flow at Mallow.

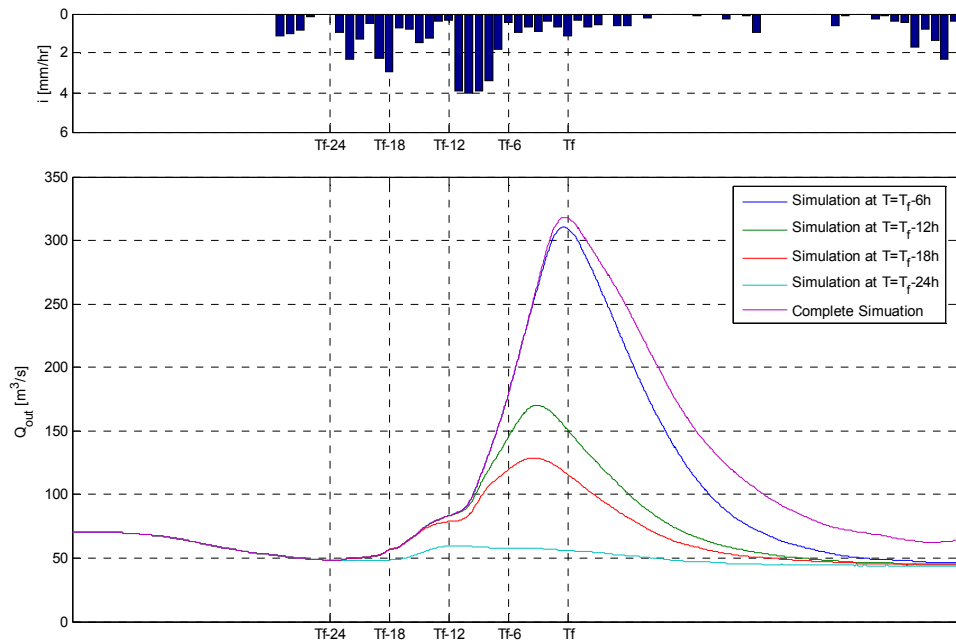


Figure 5-13 Flood forecast simulation - Flood event 1

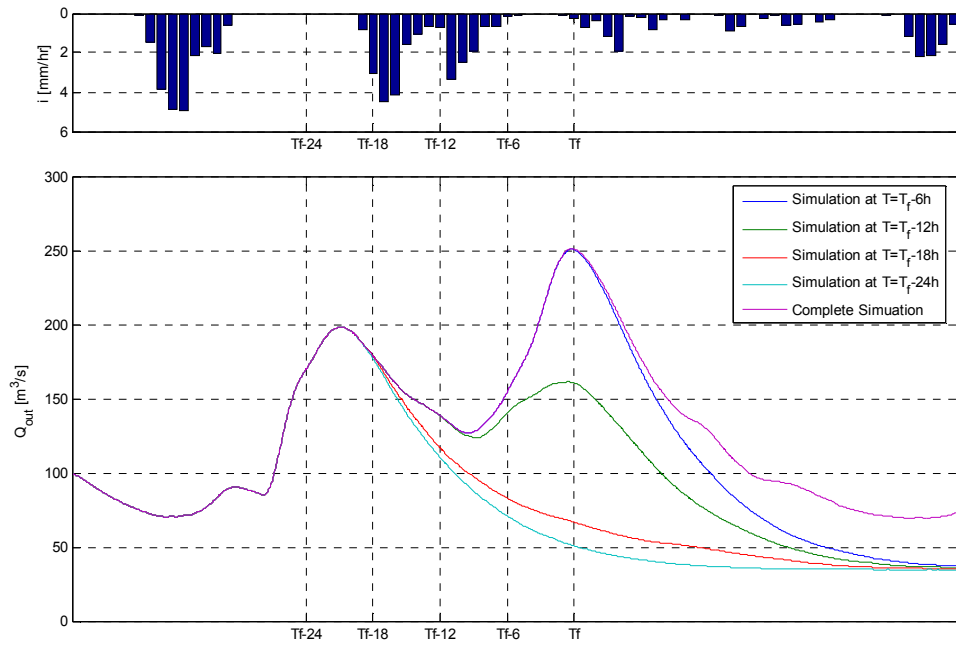


Figure 5-14 Flood forecast simulation - Flood event 2

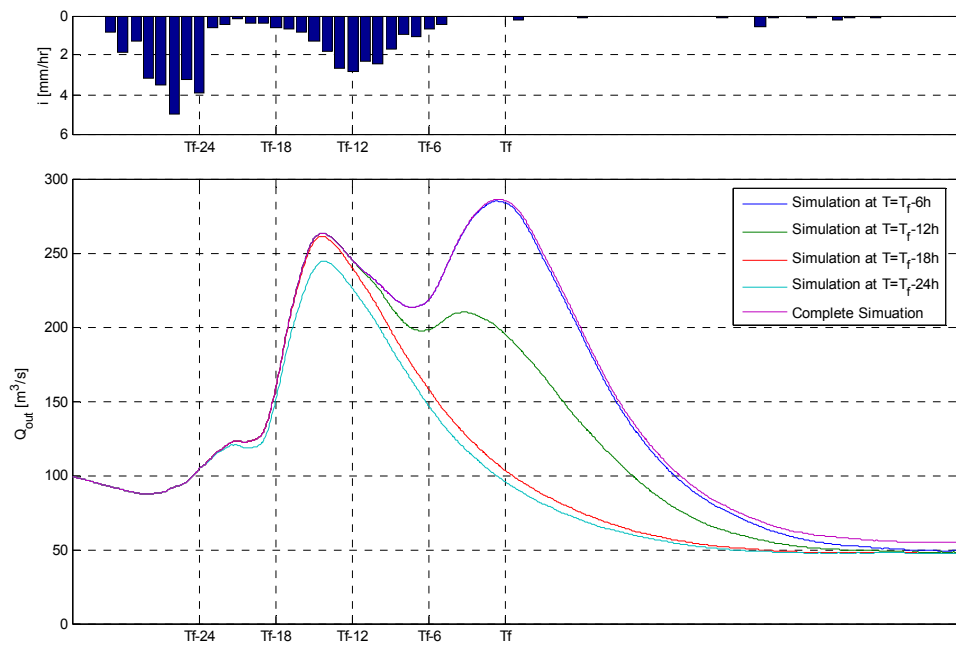


Figure 5-15 Flood forecast simulation - Flood event 3

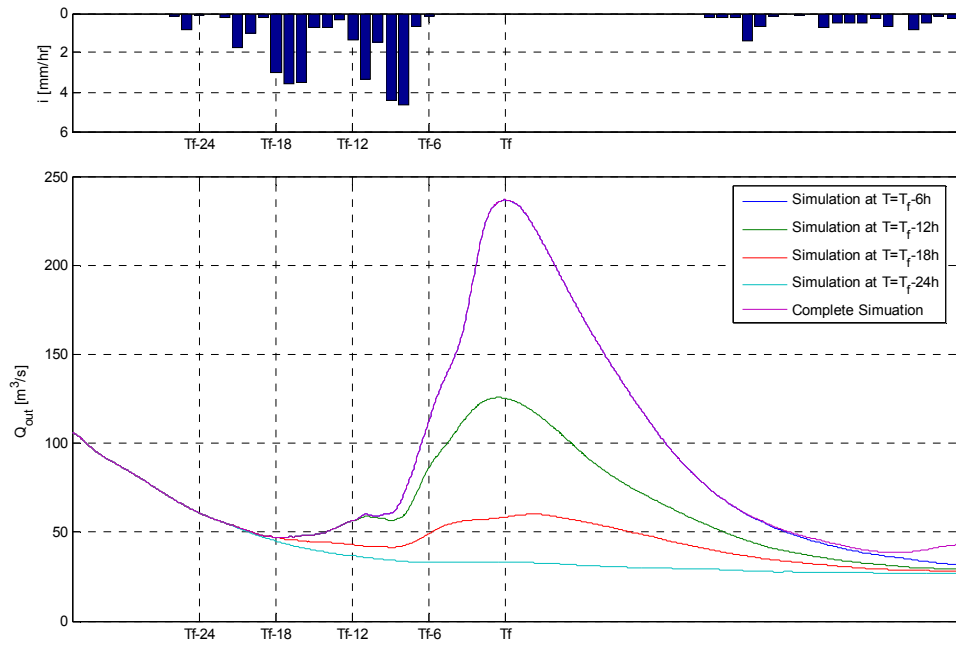


Figure 5-16 Flood forecast simulation - Flood event 5

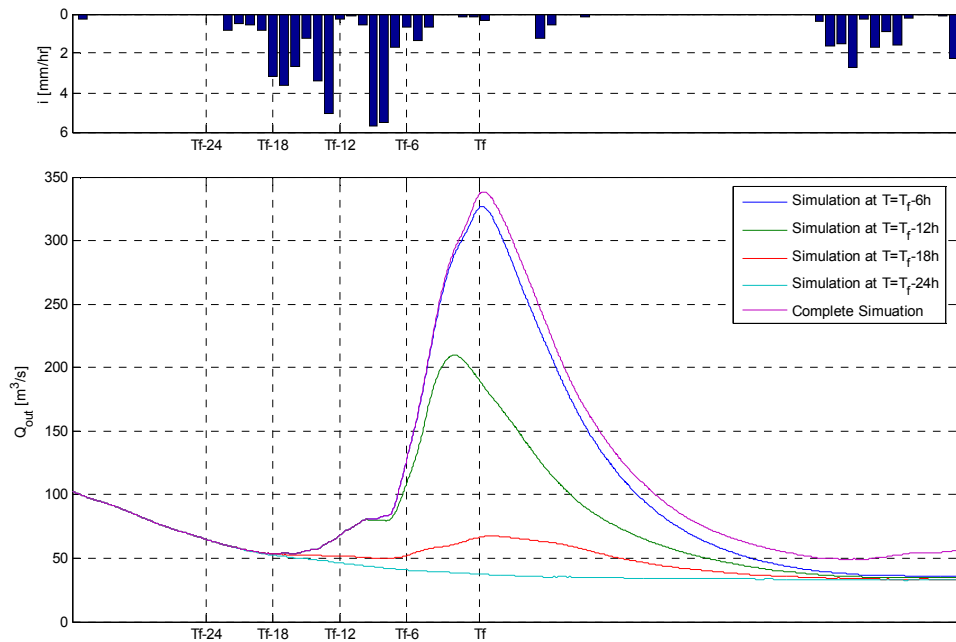


Figure 5-17 Flood forecast simulation - Flood event 6

Figure 5-13 to Figure 5-17 show that for all flood events there was about 24 hours between the start of the rainfall and the flood peak. This also applies for the flood events No.2 and No.3 if we consider it as the combination of 2 separated events. For all events the majority of the rainfall occurred between T_f-18h and T_f-6h , starting with small intensities and reaching a maximum of intensity between T_f-12h and T_f-6h . The magnitude of the peak discharge is well estimated at $T_f=6$ for both floods. The timing of the peak discharge shifts slightly as the forecast is closer to the actual simulation, but of generally less than 4 hours

5.3.3.2 Discussion

The forecast simulation show that the magnitude and the timing of the peak discharge can be forecasted between 6 and 12 hours ahead. This time interval would constitute the time of reaction of the basin, as it represents the time between the rain reaching the soils and arriving at Mallow. If we add to that the error in timing of the model as seen in 5.3.1 , which is greater than 6 hours on average, this could lead to a potential forecasting lead time of 12 to 18 hours, providing the accuracy is improved. Furthermore, adding precipitation forecast could even increase the warning time.

Chapter 6

Conclusion

6.1 Conclusion

The validation of the tRIBS model using the calibrated parameters revealed that the model could predict accurately the floods that occurred in Mallow between 2002 and 2005 in only one out of five cases. In this case, it slightly overestimated the flood peak discharge by 11% and its timing by 8h30. Potential warning would have been issued in two other cases but the magnitude of the peak flows were underestimated by 17% and 29%. It would have failed in the two other as estimated flows were too low by 31% and 33%. The model, as it was currently calibrated, is not suitable for implementation in a flood warning system. Inaccuracies of the model lie mainly in the underestimation of the river flow which is mostly the case for high flows.

The field of investigation for the reasons of the inaccuracies of the model is large. The first could be the calibration parameters which are not reliable enough and could be improved through a longer calibration effort. Model inputs can also be questioned for their reliability. This is the case for the initial water table depth which controls the initial soils moisture and the storage capacity of the catchment. It is also the case of rainfall inputs which could be improved through the calibration of the rainfall radar. Another field of investigation would be the reliability of the flow values which are estimated from rating curves developed from a small amount of data.

However, if the accuracy of the model is improved it could lead to a potential 12 to 18 hours forecast lead time. This is the result of the calculation of the transformation of rainfall into streamflow at Mallow using the calibrated model, while considering the error in timing revealed during the validation of the model. This warning time could even be increased by using rainfall forecasts.

The tRIBS model is not yet ready to be used as a flood forecasting model on the Blackwater River, but shows promising results. Further work on the model and its inputs will undoubtedly improve its accuracy.

6.2 Recommendation for further research

- 1) The modelling results can be enhanced by extending the calibration effort. Timing and magnitude of flood events were not accurate enough and can be improved. This task consists in the adjustment of the parameters calibrated for this study. Improvement can be made on the parameters but this is a time consuming task as the computational effort required is important.

- 2) The update of the stage/discharge measurements at Mallow and the other gauges should be done as often as possible as they determine the values of the observed streamflows which are used to assess the validity of the model.
- 3) Investigation of the soil water storage issue could reveal beneficial as well. The initial water table depth, which is a boundary condition of the model, has a great influence on the storage capacity of the simulated catchment. Ivanov (2002) proposes another approach in quantifying the initial groundwater table depth, based on the assumption of quasi steady state conditions of the groundwater system.
- 4) The calibration of the rainfall radar seems another important issue for the implementation of tRIBS in a flood warning system. Radar data indeed are suitable as model input as it accounts for the spatial distribution of rainfall. Radar data also presents the advantage of coming from one source whereas multiple raingauges are more difficult to maintain and more expensive in the downloading of data. However, radar rainfall measurements suffer from a lack of accuracy and mainly underestimate precipitation. Calibration of the rainfall radar would mean affecting bias coefficient to the radar data, dependant on space or magnitude of rainfall but independent of time. Calibration would then allow to use radar rainfall data without checking it against ground measurement. Cooperation with the Irish Met service could prove therefore very useful, not only for the latter issue but as well as for the provision of precipitation forecasts which would allow to increase the warning lead time.
- 5) Finally, the investigation of conceptual and statistical model should not be dismissed in the perspective of flood warning. Conceptual models currently make up the majority of the models used in flood forecasting and their implementation would be easier than tRIBS's. Combinations of statistical and conceptual approaches are currently developing taking into account prediction uncertainty which is an important parameter in decision making. This type of model should not be ignored.

References

- Abbott, M.B., Bathurst, J.C., Cunge, J.A., O'Connell, P.E. and Rasmussen, J., 1986. An introduction to the European Hydrological System -- Systeme Hydrologique Europeen, "SHE", 1: History and philosophy of a physically-based, distributed modelling system. *Journal of Hydrology*, 87(1-2): 45-59.
- Beven, K., 1989. Changing ideas in hydrology -- The case of physically-based models. *Journal of Hydrology*, 105(1-2): 157-172.
- Beven, K.J., 1982. On subsurface stormflows: An analysis of response times. *Hydrological Sciences Journal*, 27: 55-521.
- Beven, K.J., 1984. Infiltration into a class of vertically non-uniform soils. *Hydrological Sciences Journal*, 29(4): 425-434.
- Beven, K.J., 2001. *Rainfall-runoff modelling - The Primer*. John Wiley & Sons, Chichester, 360 pp.
- Beven, K.J. and Kirkby, M.J., 1979. A physically based, variable contributing area model of basin hydrology. *Hydrological Sciences Bulletin*, 24(1): 43-69.
- Beven, K.J., Kirkby, M.J., Schofield, N. and Tagg, A.F., 1984. Testing a physically-based flood forecasting model (TOPMODEL) for three U.K. catchments. *Journal of Hydrology*, 69(1-4): 119-143.
- Bras, R.L., 1990. *Hydrology: an introduction to hydrologic science*. Addison-Wesley-Longman, Reading, Mass.
- Brooks, R.H. and Corey, A.T., 1964. Hydraulic properties of porous media. *Hydrol. Pap. 3*. Colo. State University, Fort Collins.
- Burdine, N.T., 1953. Relative permeability calculations from pore-size distribution data. *Trans. AIME*.
- Cabral, M.C., Garrote, L., Bras, R.L. and Entekhabi, D., 1992. Kinematic model of infiltration and runoff generation in layered and sloped soils. *Advances in Water Resources*, 15(5): 311-324.
- Coles, N.A., Sivapalan, M.K., Larsen, J.E., Linnet, P.E. and Fahrner, C.K., 1997. Modelling runoff generation on small agricultural catchments: can real world runoff responses be captured? *Hydrological Processes*, 11(2): 111-136.
- Corcoran, G., 2004. Development and examination of flood warning systems for the Munster Blackwater at Mallow. M.Eng.Sc Thesis, University College Cork, Cork, 145 pp.
- Deardorff, J.M., 1978. Efficient prediction of ground surface temperature and moisture with inclusion of a layer of vegetation. *Journal of Geophysical Research*, 82: 1889-1903.
- Doheny, J., 1997. Flooding of the Munster Blackwater Catchment. Higher Diploma Environmental Engineering Thesis, University College Cork, Cork.

- Elshorbagy, A., Simonovic, S.P. and Panu, U.S., 2000. Performance Evaluation of Artificial Neural Networks for Runoff Prediction. *Journal of Hydrologic Engineering*, 5(4): 424-427.
- Eltahir, E.A.B. and Bras, R.L., 1993. A Description of Rainfall Interception over Large Areas. *Journal of Climate*, 6(6): 1002-1008.
- Famiglietti, J.S. and Wood, E.F., 1991. Evapotranspiration and runoff from large land areas, Land surface-atmosphere interaction: Observations, models and analysis. Kluwer Acad., Norwell, Mass.
- Garrote, L. and Bras, R.L., 1995. A distributed model for real-time flood forecasting using digital elevation models. *Journal of Hydrology*, 167(1-4): 279-306.
- Goodrich, D.C., Woolhiser, D.A. and Keefer, T.O., 1991. Kinematic routing using finite elements on a triangular irregular network. *Water Resources Research*, 27(6): 995-1003.
- Green, W.H. and Ampt, G.A., 1911. Studies in soils physics. *Journal of Agricultural Science*, 4: 1-24.
- Hu, Z. and Islam, S., 1995. Prediction of ground surface temperature and soil moisture content by the force-restore method. *Water Resources Research*, 31(10): 2531-2539.
- Ivanov, V.Y., 2002. A continuous real-time interactive basin simulator (RIBS). M.Sc Thesis, Massachusetts Institute of Technology, 158 pp.
- Ivanov, V.Y., Vivoni, E.R., Bras, R.L. and Entekhabi, D., 2004. Catchment hydrologic response with a fully distributed triangulated irregular network model. *Water Resources Research*, 40.
- Ivanov, V.Y., Vivoni, E.R., Bras, R.L. and Entekhabi, D., 2004. Preserving high-resolution surface and rainfall data in operational-scale basin hydrology: a fully-distributed physically-based approach. *Journal of Hydrology*, 298(1-4): 80-111.
- Kiely, G., 1998. *Environmental Engineering*. McGraw-Hill, Boston, Mass.
- Kirkby, M.J., 1975. Hydrograph modelling strategies. In: R. Peel, M. Chisholm and P. Hagget (Editors), *Processes in Physical and Human Geography*. Heinemann, London, pp. 69-90.
- Kisi, O., 2004. River Flow Modeling Using Artificial Neural Networks. *Journal of Hydrologic Engineering*, 9(1): 60-63.
- Krzysztofowicz, R., 2001. The case for probabilistic forecasting in hydrology. *Journal of Hydrology*, 249(1-4): 2-9.
- Kuchment, L.S., Demidov, V.N. and Motovilov, Y.G., 1983. River runoff generation: physically based models. Nauka, Moscow.
- Leahy, P., Corcoran, G. and Kiely, G., Short-term flood forecasting using artificial neural networks. in preparation.

- Leopold, L.B. and Maddock, T., 1953. The hydraulic geometry of stream channels and some physiographic implications, U.S Geol. Surv. Prof. Pap., 252.
- Lin, J.D., 1980. On the force-restore method for prediction of ground surface temperature. *Journal of Geophysical Research*, 85: 3251-3254.
- Miller, E.E. and Miller, R.D., 1956. Physical Theory for Capillary Flow Phenomena. *Journal of Applied Physics*, 27(4): 324-332.
- Monteith, J.L., 1965. Evaporation and environment. *Symp. Soc. Exp. Biol.*, 19: 205-230.
- Moore, R.J., Bell, V.A. and Carrington, D.S., 2000. Intercomparison of rainfall-runoff models for flood forecasting. In: M. Lees and P. Walsh (Editors), *Flood forecasting: what does current research offer the practitioner?* Occasional paper No 12. British Hydrological Society, pp. 69-76.
- Moore, R.J., Bell, V.A. and Jones, D.A., 2005. Forecasting for flood warning. *Comptes Rendus Geosciences*, 337(1-2): 203-217.
- Morel-Seytoux, H.J. and Khanji, J., 1974. Derivation of an equation of infiltration. *Water Resources Research*, 10: 795-800.
- Neumann, S.P., 1976. Wetting front pressure head in the infiltration model of Green and Ampt. *Water Resources Research*, 12: 564-565.
- Orlandini, S. and Rosso, R., 1998. Parameterization of stream channel geometry and the distributed modeling of catchment dynamics. *Water Resources Research*, 10: 1971-1986.
- Penman, H.L., 1948. Natural evaporation from open water, bare soil and grass, *Proceedings of the Royal Society of London*.
- Porporato, A. and Ridolfi, L., 2001. Multivariate nonlinear prediction of river flows. *Journal of Hydrology*, 248(1-4): 109-122.
- Press, W.H., Teukolsky, S.A., Vetterling, W.T. and Flannery, B.P., 1999. *Numerical recipes in C: the art of scientific computing*. Cambridge Univ. Press, New York.
- Reed, S. et al., 2004. Overall distributed model intercomparison project results. *Journal of Hydrology*, 298(1-4): 27-60.
- Restrepo-Posada, P.J. and Eagleson, P.S., 1982. Identification of independent rainstorms. *Journal of Hydrology*, 55(1-4): 303-319.
- Rodriguez-Iturbe, I. and Valdes, J., 1979. The geomorphologic structure of hydrologic response. *Water Resources Research*, 15: 1409-1420.
- Rogers, R.R. and Yau, M.K., 1989. *A short course of cloud physics*. Butterworth-Heinemann, Woburn, Mass.

- Rutter, A.J., Kershaw, K.A., Robins, P.C. and Morton, A.J., 1971. A predictive model of rainfall interception in forests, 1. Derivation of the model from observations in a plantation of Corsican pine. *Agricultural Meteorology*, 9: 367-384.
- Salvucci, G.D., 1993. An approximate solution for steady vertical flux of moisture through an unsaturated homogeneous soil. *Water Resources Research*, 29(11): 3749-3754.
- Salvucci, G.D. and Entekhabi, D., 1994. Equivalent steady soil moisture profile and the time compression approximation in water balance modeling. *Water Resources Research*, 30(10): 2737-2750.
- Selker, J.S., Duan, J. and Parlange, J.-Y., 1999. Green and Ampt infiltration into soils of variable pore size with depth. *Water Resources Research*, 35(5): 1685-1688.
- Shuttleworth, W.J., 1979. Evaporation. Rep. 56, Institute of Hydrology, Wallingford, U.K.
- Shuttleworth, W.J., 1992. Evaporation. In: D.R. Maidment (Editor), *Handbook of hydrology*. McGraw-Hill, New York, pp. 4.11-4.18.
- Siccardi, F., Boni, L., Ferraris, L. and Rudari, R., 2005. A hydrometeorological approach for probabilistic flood forecast. *Geophysical research*, 110.
- Singh, V.P., 1996. Kinematic wave modeling in water resources: Surface water hydrology. John Wiley, Hoboken, N.J.
- Sivapalan, M.K. and Wood, E.F., 1987. On hydrologic similarity: 2. A scaled model of storm runoff production. *Water Resources Research*, 23: 2266-2278.
- Smith, M.B. et al., 2004. The distributed model intercomparison project (DMIP): motivation and experiment design. *Journal of Hydrology*, 298(1-4): 4-26.
- Smith, R.E., Corradini, C. and Melone, F., 1993. Modeling Infiltration for Multistorm Runoff Events. *Water Resources Research*, 29(1): 133-144.
- Steinmann, E., 2004. Flood warning for Mallow, Cork County Council.
- Tamea, S., Laio, F. and Ridolfi, L., 2005. Probabilistic nonlinear prediction of river flows. *Water Resources Research*, 41.
- Todini, E., 1988. Rainfall-runoff modeling -- Past, present and future. *Journal of Hydrology*, 100(1-3): 341-352.
- Toth, E., Montanari, A. and Brath, A., 1999. Real-time flood forecasting via combined use of conceptual and stochastic models. *Physics and Chemistry of the Earth, Part B: Hydrology, Oceans and Atmosphere*, 24(7): 793-798.
- Troch, P.A., De Troch, F.P. and Brutsaert, W., 1993. Effective water table depth to describe initial conditions prior to storm rainfall in humid regions. *Water Resources Research*, 29(2): 427-434.

- Tucker, G.E., Lancaster, N.M., Gasparini, N.M. and Bras, R.L., 2001. The Channel-Hillslope Integrated Landscape Development (CHILD) model. In: R.S. Harmon and W.W. Doe (Editors), Landscape erosion and sedimentation modeling. Kluwer Acad., Norwell, Mass., pp. 349-388.
- Vieux, B.E., Cui, Z. and Gaur, A., 2004. Evaluation of a physics-based distributed hydrologic model for flood forecasting. *Journal of Hydrology*, 298(1-4): 155-177.
- Vivoni, E.R., Ivanov, V.Y., Bras, R.L. and Entekhabi, D., 2004. Generation of Triangulated Irregular Networks Based on Hydrological Similarity. *Journal of Hydrologic Engineering*, 9(4): 288-302.
- Wagener, T. and Wheater, H.S., 2004. Rainfall-runoff Modelling in gauged and ungauged catchments. Imperial College Press, London, 306 pp.
- Wasserman, P.D., 1989. Neural computing. Van Nostrand Reinhold, New York, USA, 230 pp.
- Wheater, H.S., Jakeman, A.J. and Beven, K.J., 1993. Progress and direction in rainfall-runoff modelling. In: A.J. Jakeman, M.B. Beck and M.J. McAleer (Editors), Modelling change in environmental systems. John Wiley & Sons, pp. 101-132.
- Wigmosta, M.S., Vail, L.W. and Lettenmaier, D.P., 1994. A distributed hydrology-vegetation model for complex terrain. *Water Resources Research*, 30(6): 1665-1680.
- Wilson, J.P. and Gallant, J.C., 2000. Terrain analysis: principles and applications. John Wiley, Hoboken, N. J.
- World Meteorological Organisation, 1992. Simulated real-time intercomparison of hydrological models. Operational Hydrology Report No. 38, Geneva, Switzerland.
- Young, P.C., 1992. Parallel processes in hydrology and water quality: a unified time series approach. *Institution of Water and Environmental Management*, 6: 598-612.

Appendix A
Example of a tRIBS input file

```
#####
##
##
##          TIN-based Real-time Integrated Basin Simulator
##          Ralph M. Parsons Laboratory
##          Massachusetts Institute of Technology
##
##
## mall.in          Mallow Railway Bridge Simulation
##
#####
```

```
##=====
##
##
##          Section 1: Model Run Parameters
##
##
##=====
```

```
## Time Variables
## -----
##
##
```

```
STARTDATE: Starting time          (#MM/DD/YYYY/HH#)
01/28/2002/00
```

```
RUNTIME:      Run duration          (#hours#)
240
```

```
TIMESTEP:     Unsaturated zone computational time step (#mins#)
3.75
```

```
GWSTEP:      Saturated zone computational time step  (#mins#)
30
```

```
METSTEP:     Meteorological data time step          (#mins#)
60
```

```
RAININTRVL:  Time interval in rainfall input        (#hours#)
1
```

```
OPINTRVL:    Output interval          (#hours#)
1
```

```
SPOPINTRVL:  Spatial Output interval          (#hours#)
12
```

```
INTSTORMMAX: Interstorm interval          (#hours#)
120
```

```
RAINSEARCH:  Rainfall search interval (hours)
24
```

```
## Routing Variables
## -----
```

```
BASEFLOW:      Baseflow discharge          (#m3/s#)
15
```

```
VELOCITYCOEF:  Discharge-velocity coefficient      (#m/s#)
3
```

```
VELOCITYRATIO: Stream to hillslope velocity coefficient (#D/L#)
30
```

```
KINEMVELCOEF:  Coefficient in power law for non-linear routing
12
```

```
FLOWEXP:       Nonlinear discharge coefficient      (#D/L#)
0.3
```

```
CHANNELROUGHNESS: Uniform channel roughness value      (#D/L#)
0.3
```

```
CHANNELWIDTH:  Uniform channel width              (# m #)
10
```

```
CHANNELWIDTHCOEFF: Coefficient in width-area relationship
0.9
```

```
CHANNELWIDTHEXPNT: Exponent in width-area relationship
0.2
```

```
CHANNELWIDTHFILE: Filename that contains channel widths
NaN
```

```
##=====
```

```
##
##
```

```
##          Section 2: Model Run Options
```

```
##
##
```

```
## OPTMESHINPUT:  1  tMesh data          5  Arc/Info *.net
##                2  Point file          6  Arc/Info *.lin,*.pnt
##                3  ArcGrid (random)    7  Scratch
##                4  ArcGrid (hex)      8  Point file using Tipper
```

```
##
```

```
## RAINSOURCE:    1  Stage III radar
##                2  WSI radar
##                3  Rain gauges
```

```
##
```

```
## OPTEVAPOTRANS: 0  Inactive evapotranspiration
##                1  Penman-Monteith method
##                2  Deardorff method
##                3  Priestley-Taylor method
##                4  Pan evaporation measurements
```

```
##
```

```
## OPTINTERCEPT: 0  Inactive interception
```

```

##          1  Canopy storage method
##          2  Canopy water balance method
##
##  GFLUXOPTION:  0  Sensible heat method
##                1  Temperature gradient method
##
##  METDATAOPTION: 0  Inactive meteorological data
##                1  Weather station point data
##                2  Gridded meteorological data
##
##  CONVERTDATA:  0  Inactive met data preprocessing
##                1  Active met data preprocessing
##
##  OPTBEDROCK:   0  A uniform value used (DEPTHTOBEDROCK)
##                1  Input grid file of bedrock depth is expected
##
##=====

OPTMESHINPUT:  Mesh input data option
1

INPUTTIME:     Time slice which is searched by tListInputData
0

RAINSOURCE:   Rainfall data source option
2

OPTEVAPOTRANS: Option for evapoTranspiration scheme
1

OPTINTERCEPT: Option for interception scheme
2

GFLUXOPTION:  Option for ground heat flux
2

METDATAOPTION: Option for meteorological data
1

CONVERTDATA:  Option to convert met data format
0

OPTBEDROCK:   Option to read bedrock depth
0

WIDTHINTERPOLATION: Option for interpolating width values
0

##=====
##
##
##          Section 3: Model Input Files and Pathnames
##
##
##=====

```

```

## Mesh Generation
## -----

INPUTDATAFILE:    tMesh input file base name *.nodes, *.edges, *.tri: Opt 1
Output/voronoi/mall2

POINTFILENAME:    tMesh input file base name *.points: Opt 2
Input/mall2.points

ARCINFOFILENAME:  tMesh input file base name *.net, *.lin, *.pnt: Opt 5, 6
input/terrain/mall2net

## Soil Variables
## -----

DEPTHTOBEDROCK:   Uniform depth to bedrock          (#mm#)
10000

## Resampling Grids
## -----

BEDROCKFILE:      Bedrock depth file
Input/

SOILTABlename:    Soil parameter reference table (*.sdt)
Input/mall.sdt

SOILMAPNAME:      Soil texture ASCII grid (*.soi)
Input/soil.soi

LANDTABlename:    Land use parameter reference table (*.ldt)
Input/mall.ldt

LANDMAPNAME:      Land use ASCII grid (*.lan)
Input/land.lan

GWATERFILE:       Ground water ASCII grid (*.iwt)
Input/bf25mall.iwt

RAINFILe:         Base name of the radar ASCII grid
rain/radar/pb

RAINEXTENSION:    Extension for the radar ASCII grid
txt

## Meterological Data
## -----

HYDROMETSTATIONS: Hydrometeorological station file (*.sdf)
Weather/donoughmore.sdf

HYDROMETGRID:     Hydrometeorological ASCII grid (*.gdf)
Weather/

```

```

HYDROMETCONVERT:  Hydrometeorological data input file (*.mdi)
Weather/

HYDROMETBASENAME: Hydrometeorological data file (*.mdf)
Weather/donoughmore.mdf

GAUGESTATIONS:    Rain Gauge station file (*.sdf)
Rain/Gauges/MORaingauges.sdf

## Output Data
## -----

OUTFILENAME:      Base name of the tMesh and dynamic variable output
Output/voronoi/mall

OUTHYDROFILENAME: Base name for hydrograph output
Output/hyd/hyd_mall

OUTHYDROEXTENSION: Extension for hydrograph output
mrf

RIBSHYDOUTPUT:
0

NODEOUTPUTLIST
Input/Nodes/pNodes.dat

HYDRONODELIST
Input/Nodes/hNodes.dat

OUTLETNODELIST
Input/Nodes/oNodes.dat

## Stochastic Climate Forcing
## -----

STOCHASTICMODE:   Stochastic Climate Mode Option
0

PMEAN:           Mean rainfall intensity (mm/hr)
2.2438

STDUR:           Mean storm duration (hours)
5.2854

ISTDUR:          Mean time interval between storms (hours)
93.3346

SEED:            Random seed
400

PERIOD:          Period of variation (hours)
0

```

```

MAXPMEAN:      Maximum value of mean rainfall intensity (mm/hr)
0

MAXSTDURMN:    Maximum value of mean storm duration (hours)
0

MAXISTDURMN:   Maximum value of mean interstorm period (hours)
0

WEATHERTABLENAME:
Input/

## Rainfall Forecasting
## -----

FORECASTMODE:  Rainfall Forecasting Mode Option
0

FORECASTTIME:  Single Forecast Time (hours from start)
0

FORECASTLEADTIME: Forecast Lead Time (hour interval)
0

FORECASTLENGTH: Forecast Window Length (hours)
0

FORECASTFILE:  Base name of the radar QPF grids
Rain/

CLIMATOLOGY:   Rainfall climatology (mm/hr)
0

RAINDISTRIBUTION: Distributed or MAP radar rainfall
0

##=====
##
##
##      End of mall.in
##
##
##=====

```

Appendix B
Matlab Code for creating tRIBS radar rainfall
input files

```

% tRIBS_corrected_radar_inputfiles.m
% ES 09.08.2005
% Disaggregates daily rainfall data into hourly data using radar rainfall
% time series and creates biased radar files as inputs for tRIBS.
%

clear

% SELECT TIME PERIOD
dstart='10/01/2002'
dend='20/01/2002'

dstart=datenum(dstart, 'dd/mm/yyyy');
dend=datenum(dend, 'dd/mm/yyyy');

% SELECT STATIONS
station(1).name='Banteer_lyre';
station(2).name='Millstreet_sewage_works';
station(3).name='Ballydesmond';
station(4).name='Newmarket_ballinatona';
station(5).name='Mallow_hazelwood';
station(6).name='Kanturk_voc_school';
station(7).name='Freemount_pumping_station';
station(8).name='Lombardstown';
station(9).name='Newmarket_new_street';
station(10).name='Mallow_spa_house';

Nstations=length(station);

% LOAD DATA
for i=1:length(station)
filename=['c:\work\rainfall\gauges\raw_data\MetOffice_stations\' ,station(i)
.name, '.dat'];
    if exist(filename)<1
        station(i).exist=0;
        display(['data not available for ', (i).name]);
    else
        station(i).exist=1;
        data=dlmread(filename);
        station(i).date=data(:,1);
        station(i).rain=data(:,2);
        station(i).index=data(:,3);
    end
end

% radar data
data=dlmread('c:\work\rainfall\radar\radar2gauge3.dat'); % read radar
point data sampled at the gauge locations
radar.date=data(:,1);
radar.rain=data(:, [7:10,12:15,17:18]); % CHECK THAT COLUMNS CORRESPOND TO
GAUGE STATIONS

% -----
% DISAGGREGATE DAILY RAINFALL DATA
% -----
datelist=dstart:dend;

```

```

calendar=dstart:1/24:dend+2;
rain=zeros(length(calendar),Nstations);

for i=1:Nstations
    disp(['station: ',station(i).name])
    if station(i).exist==1
        count2s=0;
        for j=1:length(datelist)
            day=datelist(j);
            n_station=find(station(i).date==day);
            index=station(i).index(n_station);

            if isempty(n_station) | index==8 % No data available
                rain(n_calendar:m_calendar,i)=NaN;

            elseif index==0 | index==1 |index==4 |index==5 %Good reading
                n_radar=find(abs(radar.date-(day+9/24))<0.001);
                m_radar=find(abs(radar.date-(day+1+8/24))<0.001);
                n_calendar=find(abs(calendar-(day+9/24))<0.001);
                m_calendar=find(abs(calendar-(day+1+8/24))<0.001);

                gauge_data=station(i).rain(n_station);
                radar_data=radar.rain(n_radar:m_radar,i);
                ratio=gauge_data/sum(radar_data);
                if isnan(ratio) | ratio==Inf
                    ratio=1;
                end

                radar_data=ratio*radar_data;
                rain(n_calendar:m_calendar,i)=radar_data;

            elseif index==2 % Cumulative rain, no reading, add up days to
cumulative reading (index 3 or 9)
                count2s=count2s+1;

            elseif index==3 | index==9 % Cumulative rain data (add index=2
data)
                n_radar=find(abs(radar.date-(day+9/24-count2s))<0.001);
                m_radar=find(abs(radar.date-(day+1+8/24))<0.001);
                n_calendar=find(abs(calendar-(day+9/24-count2s))<0.001);
                m_calendar=find(abs(calendar-(day+1+8/24))<0.001);
                count2s=0;

                gauge_data=station(i).rain(n_station);
                radar_data=radar.rain(n_radar:m_radar,i);
                ratio=gauge_data/sum(radar_data);
                if isnan(ratio) | ratio==Inf
                    ratio=1;
                end

                radar_data=ratio*radar_data;
                rain(n_calendar:m_calendar,i)=radar_data;
            end
        end
    end
end
end
end

```

```

% Write result data into file
%
dlmwrite('rainfall_disaggregated.dat',[calendar',rain'],'precision','%.10f'
)

% Create biased radar files
for i=i:length(calendar)
    date=calendar(i);
    n_rain=find(rain(:,1)==date);
    n_radar=find(radar.date==date);
%     calculate bias coefficient
    bias(i)=nanmean(rain(i,2:end)'./radar.rain(n_radar,2:end)');
end

% -----
% CREATE tRIBS RAINFALL INPUT FILES
% -----
% Destination Directory
DestinationDirectory='c:\cygwin\home\emmanuel\blackwater\rain\';
tRIBS_filename_type='pb'; %stands for precipitation biased

% header information
ncols=60;
nrows=41;
xllcorner=100000;
yllcorner=80000;
cellsize=1000;
nodata_value=-9999;

% Define the part of the radar matrix (sub-matrix) to consider
type=240;
pstart=grid2mat(type,xllcorner/1000,yllcorner/1000);
pend=grid2mat(type,xllcorner/1000+ncols-1,yllcorner/1000+nrows-1);
Rstart=pstart(1,1);
Rend=pstart(1,1);
Cstart=pstart(1,2);
Cend=pstart(1,2);

% Create biased radar data
for i=i:length(calendar)
    date=calendar(i);
    tribs_filename=[tRIBS_filename_type,datestr(date,'mddyYYHH')];
    radarfile=read_rra(date);
    data=bias(i)*flipud(radarfile.data(Rstart:Rend,Cstart:Cend));

% Write file
    file=[DestinationDirectory,tribs_filename,'.txt'];
    fid=fopen(file,'w');

%     Write header
    fprintf(fid,'%12s %2d\n%12s %2d\n%12s %12f\n%12s %12f\n%12s%12f\n
%12s%5d\n','ncols',ncols,'nrows',nrows,'xllcorner',xllcorner,'yllcorner',y
llcorner,'cellsize',cellsize,'NODATA_value',nodata_value);

```

```
% Write matrix data
for k=1:size(data,1)
    fprintf(fid,'%3.1f ',data(k,:));
    fprintf(fid,'\n');
end
fclose(fid);
end
```